ARO 26301.1-EL-S

②

JC-2053-A

AD-A222 995

STUDIES OF ECCM IMPROVEMENTS
FOR FREQUENCY-HOPPING
CPFSK SYSTEMS

DTIC
ELECTE
JUN 15 1990
S D D

FINAL REPORT
May 30, 1990

PREPARED FOR

U. S. ARMY RESEARCH OFFICE

CONTRACT
DAAL03-89-C-0010

The views, opinions, and/or findings contained in this report are those of the authors and should not be construed as an official Department of the Army position, policy, or decision unless so designated by other documentation.

J. S. LEE ASSOCIATES, INC.

**2001 JEFFERSON DAVIS HIGHWAY, SUITE 601
ARLINGTON, VIRGINIA 22202**

90 06 14 176

REPORT DOCUMENTATION PAGE

1a. REPORT SECURITY CLASSIFICATION		1b. RESTRICTIVE MARKINGS
Unclassified		

2a. SECURITY CLASSIFICATION AUTHORITY	3. DISTRIBUTION/AVAILABILITY OF REPORT
2b. DECLASSIFICATION / DOWNGRADING SCHEDULE	Approved for public release; distribution unlimited.

4. PERFORMING ORGANIZATION REPORT NUMBER(S)	5. MONITORING ORGANIZATION REPORT NUMBER(S)
JC-2053-A	ARO 26301.1-EL-S

6a. NAME OF PERFORMING ORGANIZATION	6b. OFFICE SYMBOL (If applicable)	7a. NAME OF MONITORING ORGANIZATION
J. S. Lee Associates, Inc.		U. S. Army Research Office

6c. ADDRESS (City, State, and ZIP Code)	7b. ADDRESS (City, State, and ZIP Code)
2001 Jefferson Davis Highway, Suite 601 Arlington, Virginia 22202	P. O. Box 12211 Research Triangle Park, NC 27709-2211

8a. NAME OF FUNDING/SPONSORING ORGANIZATION	8b. OFFICE SYMBOL (If applicable)	9. PROCUREMENT INSTRUMENT IDENTIFICATION NUMBER
U. S. Army Research Office		DAAL03-89-C-0010

8c. ADDRESS (City, State, and ZIP Code)	10. SOURCE OF FUNDING NUMBERS			
	PROGRAM ELEMENT NO.	PROJECT NO.	TASK NO.	WORK UNIT ACCESSION NO.
P. O. Box 12211 Research Triangle Park, NC 27709-2211				

11. TITLE (Include Security Classification)
Studies of ECCM Improvements for Frequency-Hopping CPFSK Systems

12. PERSONAL AUTHOR(S)
J. S. Lee, L. E. Miller, R. H. French

13a. TYPE OF REPORT	13b. TIME COVERED	14. DATE OF REPORT (Year, Month, Day)	15. PAGE COUNT
Final	FROM 4/1/89 TO 3/31/90	90 May 30	122 + viii

16. SUPPLEMENTARY NOTATION
The view, opinions and/or findings contained in this report are those of the author(s) and should not be construed as an official Department of the Army position, policy, or decision, unless so designated by other documentation.

17. COSATI CODES			18. SUBJECT TERMS (Continue on reverse if necessary and identify by block number)
FIELD	GROUP	SUB-GROUP	Frequency hopping, digital FM radio, ECCM, jamming, statistical communication theory, phase distributions, coding, synthesizers, diversity combining

19. ABSTRACT (Continue on reverse if necessary and identify by block number)

The performance of frequency-hopping CPFSK modulations (such as used in several Army radio systems) in the presence of worst-case partial-band noise jamming (WCPBNJ) is derived for both limiter-discriminator and differential detector forms of receiver. The transmitter is assumed to repeat the data L times on different hops, and the receiver combines the L chips for each data symbol in a way to mitigate the effects of the jamming. Hard-decision combining simply makes a binary decision on each chip, then a majority decision on the whole symbol; this limits a jammed chip to one vote. AGC combining weights each analog chip sample in inverse proportion to the received noise power and decides on the basis of the sum of weighted chip samples; jammed chips tend to be weighed less. Analysis and computations show that either form of ECCM combining can produce a 27 dB gain against WCPBNJ, and with error-control coding, a 31-33 dB gain. Coding alone can give a 28-29 dB gain. Soft decoding of hard-decision diversity combining gives 1.4 dB more gain than hard decoding. (continued)

20. DISTRIBUTION/AVAILABILITY OF ABSTRACT	21. ABSTRACT SECURITY CLASSIFICATION
☐ UNCLASSIFIED/UNLIMITED ☒ SAME AS RPT. ☐ DTIC USERS	Unclassified

22a. NAME OF RESPONSIBLE INDIVIDUAL	22b. TELEPHONE (Include Area Code)	22c. OFFICE SYMBOL
Dr. James W. Gault	(919) 549-0641	SLCRO-EL

DD FORM 1473, 84 MAR　　83 APR edition may be used until exhausted.　　SECURITY CLASSIFICATION OF THIS PAGE
All other editions are obsolete.　　UNCLASSIFIED

19. ABSTRACT (continued)

It is also shown that, due to the spectral attenuation characteristics of the receiver's IF filter, the effects of the transient phase difference between the incoming hopping waveform and the receiver's synthesizer are primarily confined to an interval of duration $T + ts + tau$, where T is the symbol duration (inverse of IF bandwidth), ts is the synthesizer switching time, and tau is the offset in synchronization between the received signal and the receiver's synthesizer. Therefore a one-symbol guard time is sufficient to avoid effects of the transient on the data; normally, a considerably larger guard time is used for the purpose of emission control. Therefore, emission control has more of an influence on the amount of data per hop than do transients.

STUDIES OF ECCM IMPROVEMENTS
FOR FREQUENCY-HOPPING
CPFSK SYSTEMS

FINAL REPORT

May 30, 1990

PREPARED FOR

U. S. ARMY RESEARCH OFFICE

CONTRACT

DAAL03-89-C-0010

J. S. LEE ASSOCIATES, INC.
2001 JEFFERSON DAVIS HIGHWAY, SUITE 601
ARLINGTON, VIRGINIA 22202

TABLE OF CONTENTS

LIST OF FIGURES

LIST OF FIGURES (continued)

TABLES

1.0 INTRODUCTION

State-of-the-art Army tactical radios, such as JTIDS (Joint Tactical Information Distribution System), EPLRS (Enhanced Position Location Reporting System), and SINCGARS (Single Channel Ground and Airborne Radio System), employ frequency hopping to render their transmissions "spread spectrum" and therefore more difficult for an opponent to intercept and to degrade through intentional electromagnetic interference (jamming). The modulation used by these communications systems to transmit data while dwelling at a particular carrier frequency is a form of binary frequency modulation (FM) known as continuous phase-shift modulation (CPSM) or minimum-shift keying (MSK), which is a special case of continuous-phase frequency-shift keying or CPFSK. The combination of frequency hopping and this modulation is denoted by FH/CPFSK.

1.1 CURRENT WORK RELATED TO FH/CPFSK SYSTEMS

CPFSK is the modulation of choice for many systems, as opposed to other modulations such as M-ary noncoherent frequency-shift keying (MFSK), because of its efficient use of the available spectrum, that is, for the same data rate, the bandwidth required by CPFSK to support the reception of the data with acceptable quality in terms of bit error probability is relatively small. Also, in the case of limiter-discriminator detection of the hopped CPFSK waveform, it has been estimated that CPFSK enjoys a 4 dB advantage in performance over MFSK in the presence of noise jamming [1].

In a previous report submitted to the Army Research Office [8], the authors studied the performance of FH/CPFSK when subjected to worst-case partial-band noise jamming. Partial-band noise jamming, as the name implies, features the placement of the jammer's effective available power, J, in a fraction of the bandwidth, W, over which the signal is hopping. Rather than spreading the jamming noise power over the entire hopping bandwidth, with a noise spectral power density of

$$\mathcal{N}_J \triangleq J/W, \tag{1-1}$$

by concentrating the power in a smaller bandwidth γW, where $\gamma \leq 1$, the spectral power density in the jammed portions of the band is $\mathcal{N}_J/\gamma$, a higher value which can be expected to be more effective in degrading the signal. However, now the signal is not always jammed, so that there is a tradeoff involving the choice of γ which results in the maximum (worst-case) value of the average bit error probability at the receiver.

1

Worst-case partial-band noise jamming can be very effective in degrading the FH/CPFSK system's performance, as illustrated in Figure 1-1, which is excerpted from [8] for the case of a receiver using differential detection to demodulate the data. The figure shows the bit error probability (P_e), as a function of the ratio of signal bit energy to average jamming noise spectral power density, E_b/N_J, assuming that the signal energy-to-noise density ratio prior to the onset of jamming is $E_b/N_0 = 15\,dB$ (which gives a $P_e \ll 10^{-5}$), and parametric in different values of γ, the jamming fraction. It is clear from the figure that if the worst-case value of γ is always chosen, the dependence of P_e on E_b/N_J, rather than being exponential (as is approximately the case for wideband noise), is "inverse linear," that is,

$$P_e \propto (E_b/N_J)^{-1}, \quad \text{worst-case } \gamma \text{ used.} \tag{1-2}$$

Note that the concept of worst-case jamming through selection of the jamming fraction γ is a theoretical concept: whether or not it is practical to implement such worst-case jamming[1], it is of interest to calculate the worst-case performance and ways for improving it.

A general model of an advanced slow-hopping FH/CPFSK communications system is shown in Figure 1-2. The advanced features, intended to improved the system performance while under jamming, include error control coding, interleaving, L hops per bit diversity, and electronic counter-countermeasures (ECCM) diversity combining. In [8], a "baseline" version of the system was evaluated. For this baseline system, at the receiver the L analog data sample values for each bit are summed, and the bit decision is given by the polarity of this sum. Our analysis and computations included a rigorous treatment of background noise, intersymbol interference, and FM noise "clicks." The evaluation, summarized in [15], determined that linear combining or summing the diversity components (chips) of each bit does not improve system performance in worst-case partial-band noise jamming. This conclusion holds for both limiter-discriminator and differential detection demodulation techniques.

1.2 RATIONALE FOR FURTHER STUDIES OF ECCM COMBINING

The diversity sum method for combining the L chips for a given FH/CPFSK bit can be regarded as implementing a form of "soft-decision metric." Note that the summing operation does not utilize any "side information" on whether a particular chip has been jammed, or how strongly it was jammed. Since there is no mechanism for excluding or otherwise treating jammed chips differently, when one or more chips is

---

[1]See, for example, [20] and [29] for discussions of jammer implementation.
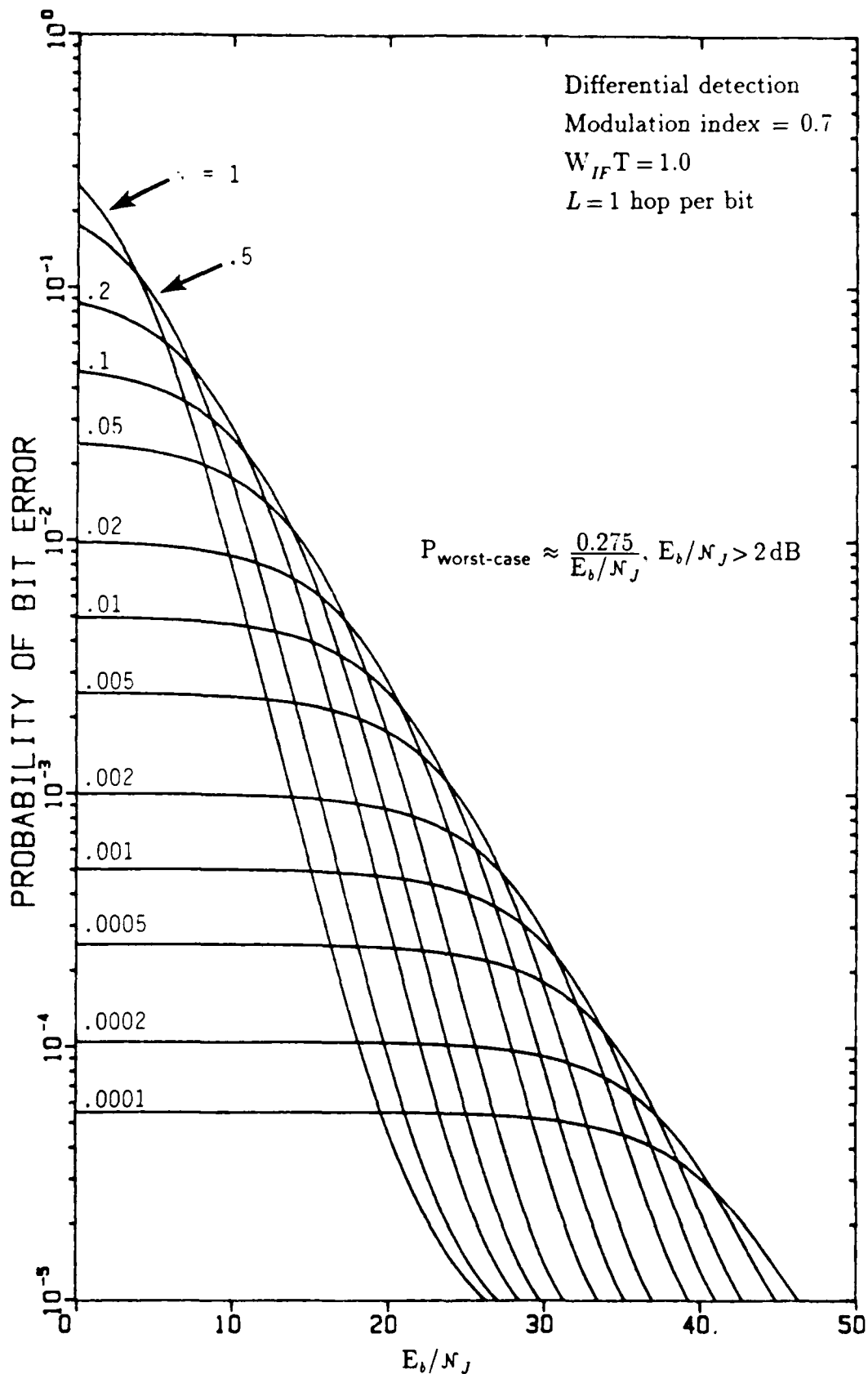
FIGURE 1-1 FH/CPFSK PERFORMANCE IN PARTIAL-BAND NOISE JAMMING

The chart is labeled with the axis title PROBABILITY OF BIT ERROR on the vertical axis and $E_b/\mathcal{N}_J$ on the horizontal axis.

Annotations within the plot:

Differential detection
Modulation index = 0.7
$W_{IF}T = 1.0$
$L = 1$ hop per bit

$$P_{\text{worst-case}} \approx \frac{0.275}{E_b/\mathcal{N}_J}, \quad E_b/\mathcal{N}_J > 2\,\text{dB}$$

Curve labels: = 1, .5, .2, .1, .05, .02, .01, .005, .002, .001, .0005, .0002, .0001
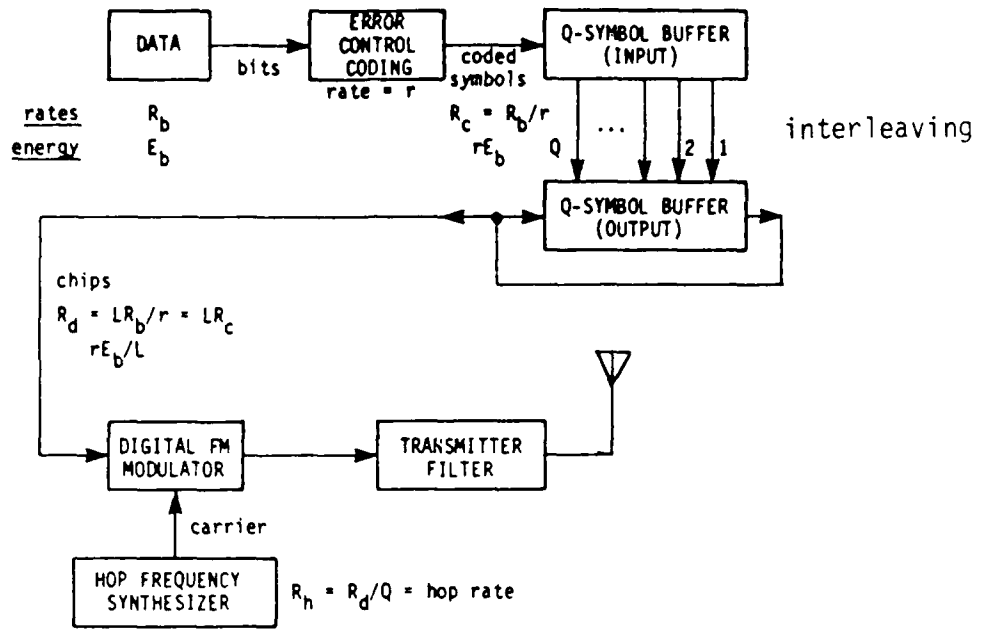
(a) Transmission scheme
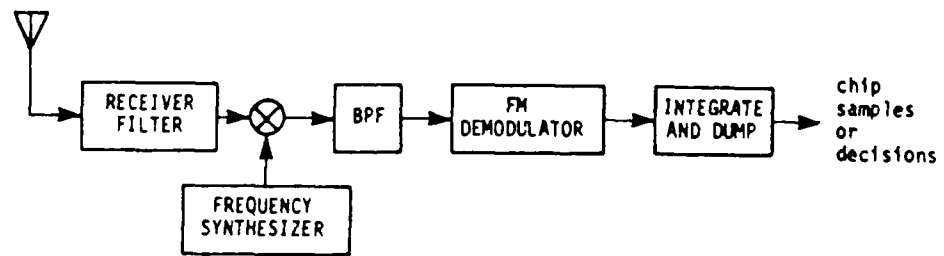
Chip Sampling

Diversity Combining and Decoding

(b) Reception scheme

FIGURE 1-2 FH/CPFSK SYSTEM MODEL

4

subject to jamming, the entire sum is corrupted; this accounts for the failure of the sum metric to provide a diversity improvement.

Now, for hopped MFSK systems, it has been shown [21] that if, instead of soft-decision combining of the chips, we combine hard decisions on each chip, the result is that for high E_b/N_0 (15 dB or more) there is a diversity gain, in the sense that for a particular J/S ratio, more than one hop per bit may yield a lower bit error probability. The improvement is due to the hard decision's limiting a jammed chip to "one vote" in the sum of hard decisions. Since no side information is required, this simple ECCM scheme is very attractive to consider for FH/CPFSK also, except for the fact that noncoherent combining losses are high for hard-decision metrics, relative to soft decisions, in general.

In [8] it was also shown that a diversity gain would result from using a "perfect side information" soft-decision diversity combining scheme for FH/CPFSK which includes only unjammed chips in the diversity sum, unless all chips happen to have been jammed. Figure 1-3 illustrates the theoretical performance of FH/CPFSK using such a scheme in the absence of any thermal noise ($E_b/N_0 \rightarrow \infty$). The error probability under these assumptions is such that for higher values of E_b/N_J,

$$P_\epsilon \propto (E_b/N_J)^{-L}; \tag{1-3}$$

in the figure it is evident that the different curves for different values of L are related such that there is an "optimum diversity" which is a function of E_b/N_J.

The implication of the theoretical results shown in Figure 1-3 is that it is likely that some practical method exists for combining the analog chip samples or soft decisions into a metric that will result in an FH/CPFSK performance in worst-case partial-band noise jamming that is better than the one obtained using the sum of hard decisions. Such metrics have been found for noncoherent FH/BFSK, including a "self-normalizing" technique that does not require side information [22, 23].

Based on all these previous findings, in the work summarized in this report we have developed and evaluated soft-decision schemes for combining FH/CPFSK diversity transmissions which produce a diversity improvement against worst-case partial-band noise jamming. An analysis by Torrieri [1] suggested that a concatenation of a convolutional "outer code" with hard-decision diversity combining (an "inner code") would yield an FH/CPFSK performance that improves as L, the number of hops per bit, increases. provided that soft decoding is used. Therefore. in this report we also include calculations of coded performance in combination with diversity combining.
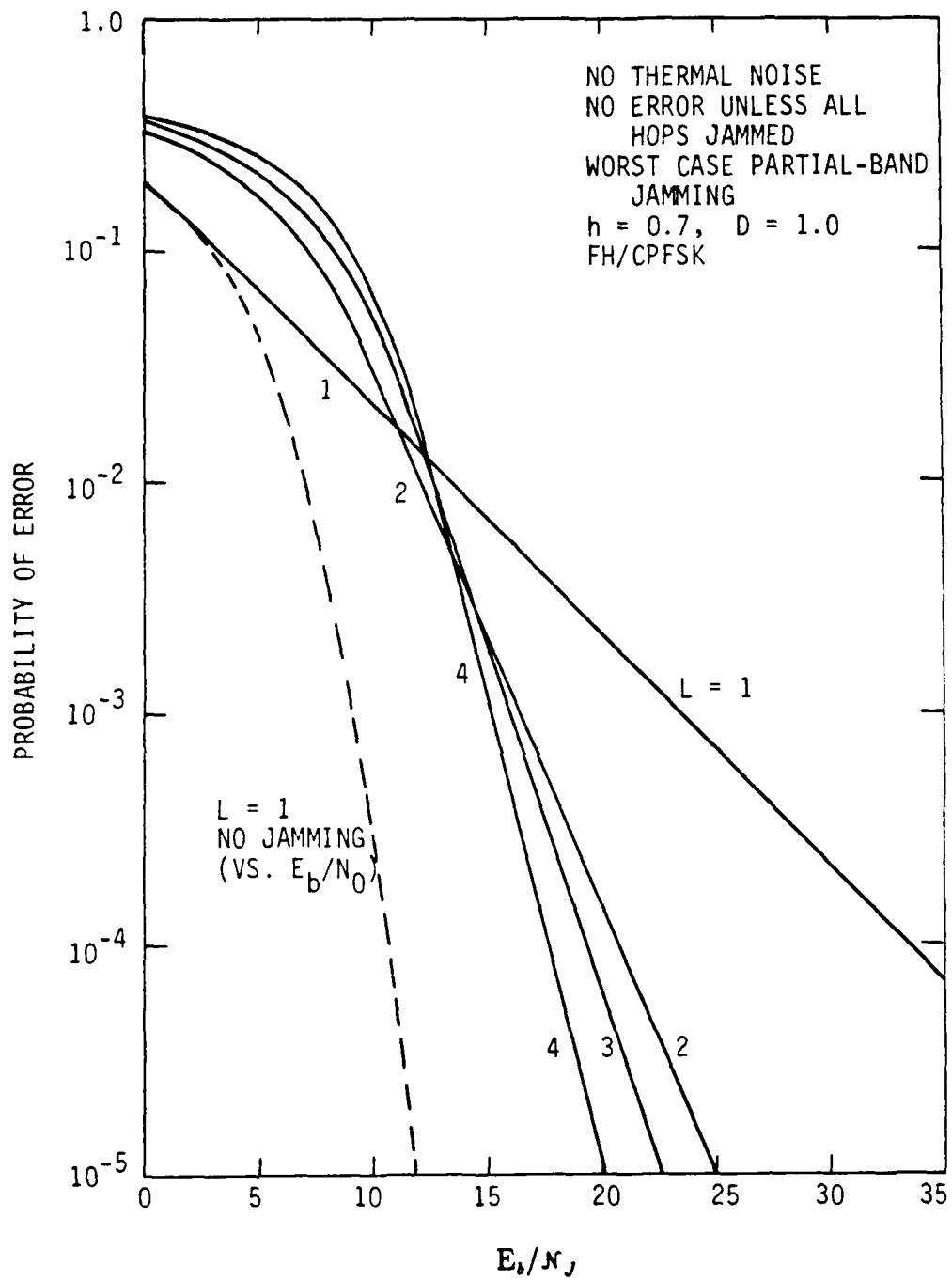
FIGURE 1-3 FH/CPFSK DIVERSITY SUM PERFORMANCE ASSUMING
PERFECT SIDE INFORMATION AND NO THERMAL NOISE

6

1.3 FH/CPFSK RECEIVER IMPLEMENTATION ISSUES

It has been maintained [5] that a loss in performance is experienced, in terms of theoretical error probability, by using a differential detector instead of a limiter-discriminator for reception of CPFSK, either in Gaussian noise or, when hopped, in worst-case partial-band noise jamming. However, this conclusion was based on comparing the performances of the two receiver implementations (parametric in the modulation index and in the receiver filter's bandwidth-time product) on the basis of the same differential delay time, one bit (or chip) period. Ekanayake [4] has shown that the differential detector's performance can be made very competitive with that of the limiter-discriminator by using a differential delay value less than a bit period. In this report, we do not emphasize the improvement in differential detector performance that can be obtained by selection of the delay, but do develop the performance of both receiver implementations when hard or soft decision ECCM combining is used for demodulating multiple hops per bit transmissions.

Another implementation issue concerns the phase transients or discontinuities experienced by an FH/CPFSK receiver during and just following the hop transitions to different carrier frequencies. If the signalling rate is increased slightly to allow for a dwell time between hops, there will be a performance degradation due to the loss of energy per bit, assuming the same carrier power and average bit rate. Therefore. it is important to calculate the amount of dwell time needed in order to preclude significant transient interference effects on the initial bits or chips on each hop.

1.4 ORGANIZATION OF THE REPORT

The report is organized as follows: following this introductory section, which includes a summary of findings, the modelling and methodologies used in the report are summarized in Section 2. Then, in Section 3, we summarize our studies of FH/CPFSK implementation issues, including hop transients.

In Section 4, the major part of our work is presented: analysis and calculations showing the uncoded performance of FH/CPFSK against worst-case partial-band noise jamming when combining of the L chips transmitted per bit on different hops takes place according to an "automatic gain control" scheme.

In Section 5, the performance of the system using a particular error-control code in addition to ECCM diversity combining is evaluated through calculations.

1.5 SUMMARY OF FINDINGS

The analysis and computations described in this report support the following conclusions regarding frequency-hopped CPFSK communications systems.

Regarding FH/CPFSK implementation issues (Section 3), it is shown that due to the spectral attenuation characteristics of the receiver's IF filter, the effects of the transient phase difference between the incoming hopping waveform and the receiver's synthesizer are primarily confined to the time interval $(0, T_c + t_s + \tau)$, referenced to the input waveform, with $t=0$ at the instant that the incoming signal begins to switch frequencies and using

$$T_c = \text{CPFSK modulation symbol duration} \approx (\text{IF bandwidth})^{-1}$$

$$t_s = \text{synthesizer switching time}$$

$$\tau = \text{offset in receiver synthesizer switching time}.$$

Therefore, a one-symbol guard time is advisable before resuming the transmission of data. Typically, the amplitude shaping and other emissions control procedures used by hopping radios dictate a larger off time, so that these factors determine what fraction of the dwell time may be used to transmit data, rather than switching transient effects.

Regarding ECCM combining techniques (Section 4), for both limiter-discriminator (LD) and differential detection (DD) types of FH/CPFSK receiver, it is shown that

• With no coding or ECCM diversity combining, the effect of worst-case partial-band noise jamming (WCPBNJ) is to require the value of the bit-energy-to-jamming-noise-spectral-density ratio E_b/N_J to be 43 or 44 dB, rather than about 12 or 15 dB in fullband jamming for the LD and DD, respectively.

• Using the optimum value of L, the diversity or number of hops per symbol, it is possible to achieve a 27 dB gain against WCPBNJ, using either hard-decision combining or AGC combining. Relative to the DD, the LD receiver tends to suffer a loss in performance when AGC combining is used, due to the effects of FM noise clicks, but otherwise retains its usual advantage.

• Coding alone can produce a 28 or 29 dB gain against the WCPBNJ.

• Coding plus optimum diversity can provide 31–33 dB gain. Soft-decision decoding gives about 1.4 dB more gain than hard-decision decoding.

Several of the analytical results are new. These include the use of a truncated Gaussian or a Gaussian-uniform mixture distribution to approximate the modulo-2π probability distribution of the differential phase, and expressions for its characteristic function which include the effects of FM noise clicks on the distribution.

2.0 ANALYSIS MODELS AND METHODOLOGY

Our studies concern the jammed performance of hopped binary FM communications, particularly under the assumption of partial-band noise jamming and the use of (time) diversity and various diversity combining techniques to mitigate the jamming. In this section, we present the analysis models used to formulate measures of system performance, and outline the methodology employed in calculating the performance measures.

2.1 MODELS FOR THE SYSTEM STUDIED AND ITS PARAMETERS

In the following, models for the outputs of the several system components are discussed individually.

2.1.1 Encoding and Transmission Schemes

Figure 2-1 gives a block diagram of the transmission scheme for the system studied. Binary data, after error-control coding and possibly encryption, are to be transmitted using slow-frequency-hopping digital FM, or CPFSK. The coded symbols are to be repeated on L different hops in order to increase the likelihood that some of the symbols are free of jamming. The figure suggests one of many possible ways to accomplish this objective. According to the version shown in the figure, the coded symbols are first read into a Q-bit shift register (Q-symbol buffer), where Q is the number of symbols that can be transmitted in one hop period. For example, if the channels allotted to the system support 20 kbps digital FM signalling, and the hop rate is 100 hops/sec, then Q could be as high as 200.

When the Q symbols have all been generated at rate R_c and stored in the input buffer, they are then transferred to a second (output) buffer. The transmitter logic reads this buffer L times at the rate LR_c, and this stream of data "chips" is used to frequency-modulate the selected carrier frequency, which is changed (hopped) to a new, pseudorandomly-selected value after Q chips have been transmitted. In this manner, L copies of the Q-symbol sequence have been transmitted on L different, successive hops. Although Figure 2-1 suggests that the Q symbols are repeated in the same order on each hop, it is of course possible with a more sophisticated system to permute the symbols or otherwise scramble them so that the order of appearance of the symbols is different on each hop.

9
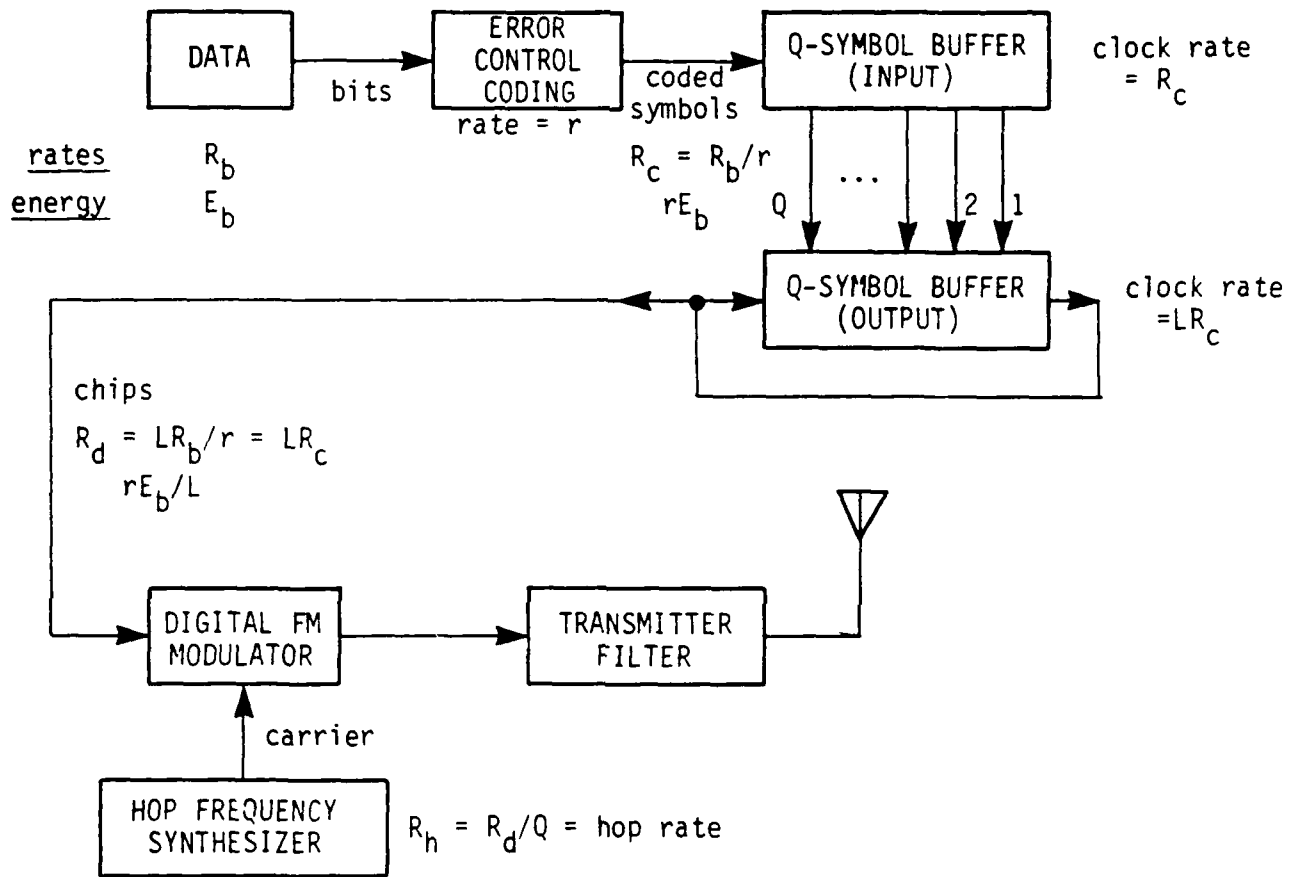
FIGURE 2-1   TRANSMISSION SCHEME

We note that certain fundamental relationships exist among the digital rates at various points in the transmission logic, and among the energies in the transmitted waveform which correspond to each rate. The symbols actually transmitted are keyed at the rate R_d which, as we have already noted, is a basic specification of the communications channel being used for hopping. The original symbol rate is $R_c = R_d/L$, on account of the repetitions. Viewed another way, the energy transmitted per chip is the fraction $1/L$ of the coded symbol energy. If the error control code rate is r, then the original bit rate is

$$R_b = R_c r = rR_d/L. \tag{2-1}$$

For example, for $R_d = 20\,\text{kbps}$, $r = \frac{1}{2}$, and $L = 5$, the equivalent coded symbol and bit rates are $R_c = 4\,\text{kbps}$ and $R_b = 2\,\text{kbps}$; between the coding and the repetitions, the bit energy gets split into ten pieces in this example.

Having briefly gone over the overall transmission scheme, we now discuss certain of its aspects in greater detail.

2.1.1.1 Error control coding

It has been suggested in [1] that concatenation of a convolutional "outer" forward-error-control code with an "inner" repetition code will yield an FH/CPFSK performance in worst-case partial-band noise jamming which improves with the number of hops per bit, L, when soft-decision outer decoding and hard-decision inner decoding are used. These terms will be discussed further below; here we note the effect that use of L hops/bit has on the input data rate. If the maximum channel data rate R_d is 20 kbps using CPFSK, then the maximum coded symbol rate is $R_c = 20\,\text{kbps}/L$ and the maximum input data rate is $R_b = 20\,\text{kbps} \cdot r/L$. For example, with $r = \frac{1}{2}$ and $L = 4$, the system can accommodate a bit rate no higher than 2.5 kbps. The practical effect of this limitation is that the coding cannot be used for most voice transmissions, since the bit rate needed to support voice data is commonly regarded to be 16 kbps, although in some situations an acceptable digital voice quality may be achieved with a significantly lower data rate. Therefore, when we speak of coded results, including diversity transmissions, necessarily we are considering data other than voice data. Encryption (scrambling) can be used for voice transmissions, since the data rate is not affected; such a procedure provides a measure of transmission security but does not offer any improvement in system performance against jamming.

For this study, it is assumed that the error control code used is a convolutional code with rate $r = \frac{1}{2}$ and constraint length 7.

11

2.1.1.2 Inter-hop switching time

Another practical consideration which relates to the transmission scheme is the fact that the transmitted data rate during the hop dwell times is not R_d, as depicted in our simplified diagrams. Rather, R_d is the average channel data rate since usually between hops (that is, while the synthesizer frequency is changing) the transmitter's power is smoothly turned off and then restored in order to avoid generating spurious harmonics or splatter. During this interhop switching period, some buffering of the channel data chips is required, since they are being produced during this period when there is no output. It also follows that the actual transmission of the chips must be "bursted" at a slightly higher rate, $R_d' > R_d$.

In our analysis, for the most part it is permissible to overlook this implementation detail. However, in Section 3 we shall be studying the issues connected with the inter-hop switching time in detail, in order to assess the effects it has on the system's performance.

2.1.1.3 Transmitted waveform and its parameters

The coded symbol chip stream $\{d_k\}$ going into the modulator in Figure 2-1 is assumed to be representable by the bipolar data waveform

$$\mathrm{d}(t) = \sum_k d_k \,\mathrm{p}(t-kT), \; d_k = \pm 1, \tag{2-2}$$

where the pulse function $\mathrm{p}(t)$ is assumed to be rectangular:

$$\mathrm{p}(t) = \mathrm{u}(t) - \mathrm{u}(t-T) \triangleq \mathrm{rect}(t-\tfrac{1}{2}T), \tag{2-3}$$

with $\mathrm{u}(t)$ being the unit step function. The interval T is the symbol duration, so that the data rate is $R_d = 1/T$. Although much attention has been given to reducing the transmitted bandwidth of binary FM signals by employing non-rectangular $\mathrm{p}(t)$ pulse shapes and by correlative coding or trellis coding of the data, here we will assume the $\mathrm{p}(t)$ as given and will treat the d_k symbol values as having been generated independently. The resulting modulated carrier frequency is given by

$$f(t) = f_h + f_d \cdot \mathrm{d}(t), \tag{2-4}$$

and the commonly accepted measure of relative frequency deviation is the modulation index h, defined by normalizing the deviation by the data rate:

$$h \triangleq 2f_d/R_d = 2f_d T. \tag{2-5}$$

The frequency modulation of the carrier frequency f_h by the data waveform $\mathrm{d}(t)$ results in the constant envelope signal

$$s_0(t) = const. \times \cos[\omega_h t + \theta_m(t)], \tag{2-6a}$$

where the data-modulated phase $\theta_m(t)$ is

$$\theta_m(t) = 2\pi f_d \int_{-\infty}^{t} d\xi \, d(\xi). \tag{2-6b}$$

Some filtering of the transmitted signal may be done in order to contain the output spectrum; however, this would introduce amplitude and phase distortion. Therefore, only the broadest type of filtering is used on the transmitter output, such as may be needed to reject modulation products, etc. The preferred way to control the bandwidth of the emitted spectrum is to smooth the data waveform, as in "tamed FM" [2], in such a way that the resulting intersymbol interference is predictable. In our analysis, any effects of transmitter filtering are neglected, and for convenience all intersymbol interference and signal distortion effects are considered as resulting from the receiver processing.

2.1.2 Reception Scheme and Received Waveform

Figure 2-2 provides an overview of the FH/CPFSK reception scheme. Basically, the processes involved are the reverse of those for the transmission scheme. The receiver must accurately synthesize local oscillator frequencies in order to dehop the signal at the proper times, and must then be capable of sampling the demodulator output at the end of each chip interval. These sample, QL of them for L complete hops, are buffered so that the receiver logic can in some manner combine the L chips belonging to a particular code symbol.

As the figure suggests, binary decisions can be made on each chip as it is received. The resulting logic and buffering for such a "hard decision" procedure is simpler than that required for a "soft decision" scheme, which involves A/D conversion of the samples and storing the resulting QL multibit words, one per chip. With either hard or soft chip processing, after diversity combining there is the option to perform binary decoding of code symbol decisions or else soft-decision decoding using code symbol metrics produced by the combining.

2.1.2.1 Received signal waveform

Waveform selection in the receiver is accomplished using a hopping local oscillator (synthesizer), assumed to be in synchronism with the hopping pattern of the received signal waveform, and a bandpass filter centered at the IF (intermediate frequency) of the receiver. Ideally, the signal portion of the IF waveform out of this bandpass filter is
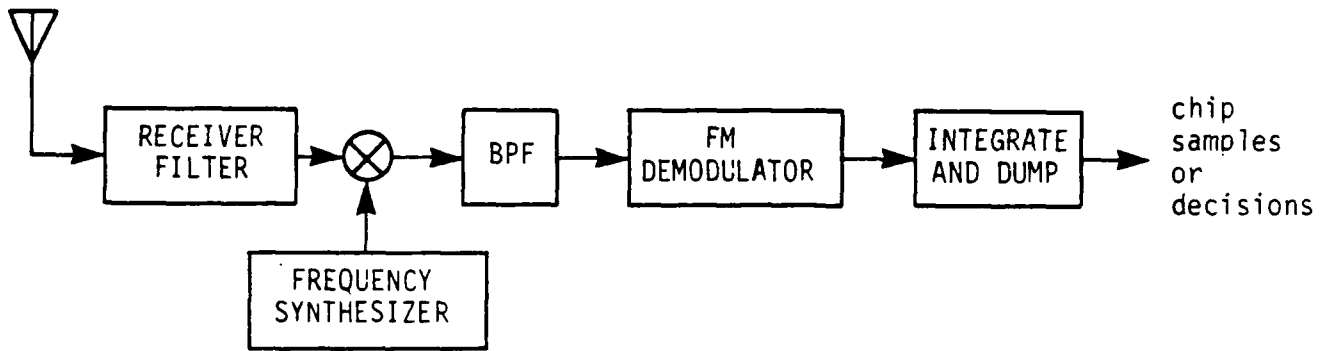
(a) Chip Sampling

(b) Diversity Combining and Decoding

FIGURE 2-2   RECEPTION SCHEME

equivalent to that for a system whose carrier frequency is fixed, not hopping:

$$s(t) = a(t) A \cos[\omega_{IF} t + \phi(t)], \qquad (2\text{-}7)$$

where $f_{IF} = \omega_{IF}/2\pi$ is the IF center frequency and A is the received signal amplitude, assumed constant. The amplitude modulation $a(t)$ and the distortion of the transmitted phase modulation $\theta_m(t)$ into the phase function $\phi(t)$ are effects induced by the IF filter. These quantities are given by

$$a(t) = \sqrt{u^2(t) + v^2(t)} \qquad (2\text{-}8a)$$

and

$$\phi(t) = \tan^{-1}\left[\frac{u(t)}{v(t)}\right], \qquad (2\text{-}8b)$$

where

$$u(t) \triangleq h_0(t) * \sin\theta_m(t) \qquad (2\text{-}9a)$$

and

$$v(t) \triangleq h_0(t) * \cos\theta_m(t) \qquad (2\text{-}9b)$$

are the quadrature and in-phase components, respectively, of the IF filter output. In these expressions, $(*)$ denotes convolution, and $h_0(t)$ is the equivalent lowpass impulse response of the IF filter, that is, that filter is modelled by

$$h_{IF}(t) = 2 h_0(t) \cos\omega_{IF} t \qquad (2\text{-}10a)$$

or, in the frequency domain,

$$H_{IF}(f) = H_0(f - f_{IF}) + H_0(f + f_{IF}). \qquad (2\text{-}10b)$$

For example, if the lowpass filter has the Gaussian shape

$$H_0(f) = e^{-\pi f^2 / 8 B_0^2}, \qquad (2\text{-}11)$$

then the 3 dB bandwidth B_3 is 0.9294 times the lowpass noise bandwidth $B_0 = \frac{1}{2} W_{IF}$. For an n-pole Butterworth filter with transfer function

$$|H_0(f)|^2 = \frac{1}{1 + (f/B_3)^{2n}}, \qquad (2\text{-}12a)$$

the noise bandwidth is related to the 3 dB bandwidth by

$$B_0 = B_3 \times \left(\frac{\pi}{2n}\right) / \sin\left(\frac{\pi}{2n}\right) \qquad (2\text{-}12b)$$

$$= 1.5708 B_3, \quad n = 1$$
$$= 1.1107 B_3, \quad n = 2$$
$$= 1.0472 B_3, \quad n = 3$$
$$= 1.0262 B_3, \quad n = 4.$$

Now since theoretically the FM signal waveform has infinite bandwidth, the IF filtering rejects not only unwanted signals but also portions of the desired signal. Therefore the filtering introduces distortion in the form of amplitude modulation and phase distortion, as shown above. For the common modelling assumptions we are making, in effect the distortion caused by the finite IF bandwidth represents all the distortion suffered by the waveform—at least all distortion due to filtering—just as the noise at IF represents all noise present.

2.1.2.2 Noise and jamming

The total IF waveform x(t) noted in Figure 2-2 is assumed to consist of the signal term given by (2-7) plus stationary, additive Gaussian noise: $x(t) = s(t) + n(t)$. When partial-band noise jamming is present, covering the fraction γW of the total hopping bandwidth W, with $0 \leq \gamma \leq 1$, the noise power in the IF bandwidth is modelled as random on account of the signal's hopping around in the total bandwidth, and has a two-valued distribution:

$$E\{n^2(t)\} = \sigma_N^2 \qquad \text{with probability } 1-\gamma \qquad (2\text{-}12a)$$

$$= \sigma_N^2 + \sigma_J^2 \equiv \sigma_T^2 \qquad \text{with probability } \gamma. \qquad (2\text{-}12b)$$

Assuming both types of input noise—the combined background and receiver input noise, represented by σ_N^2, and the jamming noise, represented by σ_J^2—have flat spectral power density functions going into the IF filter, the respective noise powers are

$$\sigma_N^2 = \mathcal{N}_0 W_{IF} \qquad (2\text{-}13a)$$

and

$$\sigma_J^2 = \mathcal{N}_J W_{IF}/\gamma. \qquad (2\text{-}13b)$$

In (2-13b), the spectral level $\mathcal{N}_J$ is the average jammer noise spectral power density referred to the total bandwidth, that is,

$$\mathcal{N}_J \triangleq J/W, \qquad (2\text{-}13c)$$

where J is the total jammer power at the receiver location.

The signal-to-noise power ratio (SNR) at the output of the IF filter without and with jamming are time-varying due to the amplitude distortion $a(t)$ as a function of the data modulation. For $a(t) = 1$, we define the SNR's

$$\rho_N \triangleq \frac{A^2}{2\sigma_N^2} = \frac{1}{W_{IF}T} \cdot \frac{E_d}{\mathcal{N}_0} = \frac{1}{D} \cdot \frac{r}{L} \cdot \frac{E_b}{\mathcal{N}_0} \qquad (2\text{-}14)$$

and

$$\rho_J \triangleq \frac{A^2}{2\sigma_J^2} = \frac{\gamma}{W_{IF}T} \cdot \frac{E_d}{\mathcal{N}_J} = \frac{\gamma}{D} \cdot \frac{r}{L} \cdot \frac{E_b}{\mathcal{N}_J}. \qquad (2\text{-}15)$$

16

In (2-14) and (2-15) for convenience we use the symbol D to denote the IF filter's bandwidth-time product:

$$D \triangleq W_{IF}T. \tag{2-16}$$

How the phase of the total waveform $x(t)$ is affected by the noise can be seen by combining signal and noise terms at the output of the IF filter to obtain

$$x(t) = a(t)A\cos[\omega_{IF}t + \phi(t)] + n(t)$$

$$= [v(t) + n_c(t)]\cos\omega_{IF}t - [u(t) + n_s(t)]\sin\omega_{IF}t$$

$$= R(t)\cos[\omega_{IF}t + \Phi(t)], \tag{2-17a}$$

in which $R(t)$ and $\Phi(t)$ are envelope and phase of the total waveform, and we have utilized the quadrature or Rician decomposition of bandpass noise:

$$n(t) = n_c(t)\cos\omega_{IF}t - n_s(t)\sin\omega_{IF}t. \tag{2-17b}$$

We may define a phase noise term by writing

$$\tan\Phi(t) = \frac{u(t) + n_s(t)}{v(t) + n_c(t)} \triangleq \tan[\phi(t) + \eta(t)]; \tag{2-18}$$

the phase noise term thus defined is

$$\eta(t) = \tan^{-1}\left[\frac{\tan\Phi - \tan\phi}{1 + \tan\Phi\tan\phi}\right]$$

$$= \tan^{-1}\left[\frac{n_s v - n_c u}{u^2 + v^2 + n_c v + n_s u}\right]$$

$$= \tan^{-1}\left[\frac{\nu_s(t)}{a(t)\sqrt{2\rho} + \nu_c(t)}\right]. \tag{2-19}$$

in which ρ is the SNR, and ν_c and ν_s at the same time instant are the independent, zero-mean, unit-variance Gaussian random variables given by

$$\sigma\nu_s(t) = n_s(t)\cos\phi(t) - n_c(t)\sin\phi(t) \tag{2-20a}$$

$$\sigma\nu_c(t) = n_s(t)\sin\phi(t) + n_c(t)\cos\phi(t). \tag{2-20b}$$

From observation of (2-19) we may state that for low SNR, η tends to be uniformly distributed, since for this case η is approximately the random phase of the noise. For high SNR, the distribution of η tends toward a truncated or "aliased" modulo-2π Gaussian distribution, since $\tan^{-1}x \approx x$ for $x \ll 1$. We also observe from (2-19) that this additive phase noise is signal-dependent.

17

2.1.3   Demodulator Options

Two types of FM demodulator are considered in this study: limiter-discriminator and differential detector, as illustrated in Figure 2-3.

Essentially the limiter-discriminator extracts the instantaneous frequency deviation from the carrier (or IF center frequency), $\dot{\Phi}(t)$, and is followed by an integrate-and-dump lowpass filter. The receiver output produced is given by the differential phase sample value at $t_k = kT + t_0$

$$\Delta\Phi(t_k) = \Phi(t_k) - \Phi(t_k - T). \tag{2-21}$$

The differential detector's output is, when the delay τ equals T,

$$\Big[R(t_k) R(t_k - T) \cos[\omega_{IF} t_k + \Phi(t_k)] \sin[\omega_{IF}(t_k - T) + \Phi(t_k - T)] \Big]_{\text{lowpass}}$$

$$= \tfrac{1}{2} R(t_k) R(t_k - T) \sin[\Delta\Phi(t_k) + \omega_{IF} T]$$

$$= \tfrac{1}{2} R(t_k) R(t_k - T) \sin[\Delta\Phi(t_k)], \quad \omega_{IF} T = 2n\pi. \tag{2-22}$$

Ekanayake [4] indicates that differential detector performance in terms of the probability of correct chip decisions can be made comparable with that of the limiter-discriminator by choosing $\tau < T$. For $\tau = T$, it has been shown [5] that the differential detector achieves about the same performance as the limiter-discriminator receiver when the modulation index $h \leq 0.5$, but is degraded significantly for larger values of h.

2.1.3.1   Differential phase in the absence of noise

The choice of the sampling time t_k is based on sampling when the differential phase in the absence of noise,

$$\Delta\phi(t) \triangleq \phi(t) - \phi(t - T), \tag{2-23}$$

has a positive or negative peak value. In general, the best sampling time for the distorted phase is different than that for the original, undistorted phase modulation.

The undistorted signal phase waveform, $\theta_m(t)$, at the particular instant $t_1 = k_1 T + \epsilon$, can be written as

$$\theta_m(t_1) = \pi h \sum_{k < k_1} d_k + d_{k_1} \epsilon; \tag{2-24a}$$

its differential value is

$$\Delta\theta_m(t_1) = \theta_m(t_1) - \theta_m(t_1 - T)$$

$$= \pi h \big[d_{k_1 - 1} + \tfrac{\epsilon}{T}(d_{k_1} - d_{k_1 - 1}) \big]. \tag{2-24b}$$

It is evident that when successive data bit values are different $(d_{k_1} \neq d_{k_1 - 1})$, a maximum

18

Data Samples

$x(t)$ → LIMITER → DISCRIMINATOR → $y(t)$ → INTEGRATE AND DUMP FILTER → $z(t)$

$t_k = kT + t_0$
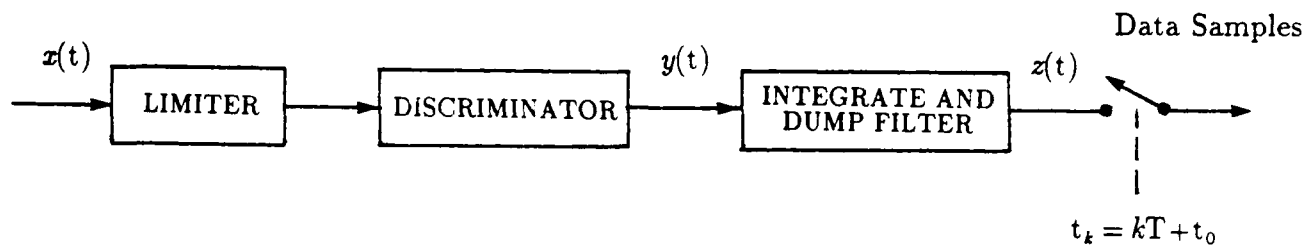
(a) Limiter-discriminator followed by an integrate-and-dump filter

$x(t)$ → ⊗ → ZONAL LPF → $z(t)$ → Data Samples

τ delay — $\frac{1}{2}\pi$ phase shift

$t_k = kT + t_0$
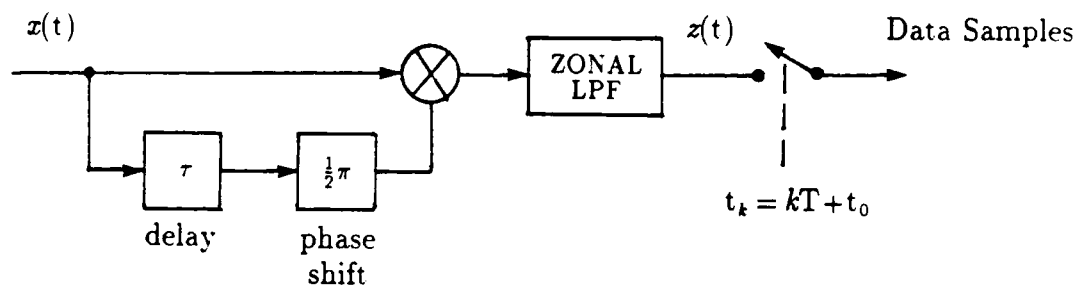
(b) Differential detector for narrowband FM

FIGURE 2-3 DEMODULATOR OPTIONS

19

deflection of $\pm \pi h$ would be achieved the undistorted phase using a sampling time at the end of the data symbol interval (i. e., $\epsilon = T$).

As shown in Appendix A, the effect of the IF filter is to produce the distorted and delayed differential phase waveform $\Delta\phi(t)$. The delay causes the maximum deflection of $\Delta\phi$ to occur at the sampling time offset $\epsilon = T + t_d > T$, where t_d is the delay, and also causes the magnitude of the deflection to be smaller than πh. The distortion induces a dependence of the sampled $\Delta\phi$ value on the data sequence, due to intersymbol interference (ISI). For the cases of practical interest, only ISI from immediately adjacent chips is significant [6].

2.1.3.2 Probability density function for the limiter-discriminator receiver output

It is assumed that the discriminator output $y(t)$ illustrated in Figure 2-3 is the derivative of the signal's instantaneous phase with respect to the center frequency, f_{IF}:

$$
\begin{aligned}
y(t) &= \dot{\Phi}(t) \\
&= \frac{d}{dt} \tan^{-1}\left[\frac{A\, a(t)\sin\phi(t) + n_s(t)}{A\, a(t)\cos\phi(t) + n_c(t)} \right] \\
&= \frac{1}{R^2(t)}\left\{ \dot{\phi}(t)\, A\, a(t)[A\, a(t) + n_c(t)\cos\phi(t) + n_s(t)\sin\phi(t)] \right. \\
&\qquad\qquad + A\, \dot{a}(t)[n_c(t)\sin\phi(t) - n_s(t)\cos\phi(t)] \\
&\qquad\qquad \left. + n_c(t)\dot{n}_s(t) - \dot{n}_c(t)n_s(t) \right\}.
\end{aligned}
$$
(2-25)

Because of the presence of the Gaussian noise terms, from these expressions we recognize the fact that the discriminator output is a random variable which can take any value on $(-\infty, +\infty)$.

The receiver further integrates the discriminator output over a symbol interval to obtain the receiver output

$$
z(t) = \int_{t-T}^{t} d\xi\, y(\xi) \tag{2-26a}
$$

$$
= \Phi(t) - \Phi(t-T) \equiv \Delta\Phi(t), \tag{2-26b}
$$

where $\Delta\Phi$ is the total differential phase. Note that this differential phase can take values on $(-\infty, +\infty)$, as observed in [7]; however, since the phases are expressible only indirectly via the arctangent function, for example,

$$
\Delta\Phi = \tan^{-1}\left\{ \frac{\tan\Phi(t) - \tan\Phi(t-T)}{1 + \tan\Phi(t)\tan\Phi(t-T)} \right\}, \tag{2-27a}
$$

20

it is customary to resolve the ambiguity of this function by writing

$$\Delta\Phi = \psi + 2\pi(N_+ - N_-), \tag{2-27b}$$

where the first term

$$\psi \equiv (\Delta\Phi)\,\text{modulo}\,2\pi \tag{2-27c}$$

is the principal value of the arctangent, and N_+ and N_- are positive and negative "click numbers," respectively.

Click statistics. For moderate and high values of SNR, it has been shown [8, 9] that the distribution of the difference of click numbers, $N_+ - N_-$, is well-represented by that of the random variable N_c whose absolute value is a Poisson random variable and whose mean tends to be of the opposite sign of $\Delta\phi$, the differential phase in the absence of noise. That is,

$$\Pr\{|N_c| = n\} = \frac{|\alpha|^n}{n!}\exp\{-|\alpha|\}, \quad n=0, 1, 2, \ldots \tag{2-28a}$$

where

$$\alpha \triangleq \overline{N_c} = -\int_{t-T}^{t} d\xi\,\frac{\dot{\phi}(\xi)}{2\pi}\,e^{-\rho a^2(\xi)}. \tag{2-28b}$$

This click average is consistent with the fact that the mean value of the discriminator output is [10]

$$E\{y(t)\} = \dot{\phi}(t)[1 - e^{-\rho a^2(t)}]; \tag{2-28c}$$

exchanging the order of integration and expectation yields the following mean value for $\Delta\Phi(t)$:

$$E\{z\} = \int_{t-T}^{t} d\xi\,\dot{\phi}(\xi) - \int_{t-T}^{t} d\xi\,\dot{\phi}(\xi)e^{-\rho a^2(\xi)}$$

$$= \Delta\phi(t) + 2\pi\,\overline{N_c}. \tag{2-28d}$$

Distribution of principal value. The probability density function for ψ has been found to be [11-13]

$$p_\psi(x) \equiv p_\psi(x;\,\Delta\phi,\,\text{r},\,\lambda,\,\text{U},\,\text{V},\,\text{W})$$

$$= \frac{1-\text{r}^2-\lambda^2}{4\pi}\int_{-\pi/2}^{\pi/2} d\alpha\,\frac{e^{-g(x,\alpha)}\cos\alpha}{[1-(\text{r}\cos x + \lambda\sin x)\cos\alpha]^2}$$

$$\times\left[1 - g(x,\alpha) + 2\frac{\text{U}-\text{W}(\text{r}\cos\Delta\phi + \lambda\,\sin\Delta\phi)}{1-\text{r}^2-\lambda^2}\right] \tag{2-29a}$$

in which

$$g(x, \alpha) = \frac{\text{U}-\text{V}\sin\alpha - \text{W}\cos(x-\Delta\phi)\cos\alpha}{1-(\text{r}\cos x + \lambda\sin x)\cos\alpha}, \tag{2-29b}$$

21

$$U = \tfrac{1}{2}\rho\left[a^2(t) + a^2(t-T)\right], \tag{2-29c}$$

$$V = \tfrac{1}{2}\rho\left[a^2(t) - a^2(t-T)\right], \tag{2-29d}$$

$$W = \sqrt{U^2 - V^2} = \rho\sqrt{a(t)\,a(t-T)} \tag{2-29e}$$

$$r = \sigma^{-2}E\{n_c(t)\,n_c(t-T)\} = \sigma^{-2}E\{n_s(t)\,n_s(t-T)\}, \tag{2-29f}$$

and
$$\lambda = \sigma^{-2}E\{n_c(t)\,n_s(t-T)\} = -\sigma^{-2}E\{n_s(t)\,n_c(t-T)\}. \tag{2-29g}$$

The domain over which (2-29a) is valid is usually taken to be $|x - \Delta\phi| < \pi$. The quantities U and W can be seen as the arithmetic and geometric averages, respectively, of the SNR's at times t and $t-T$. The parameters r and λ are the in-phase and quadrature correlation coefficients of the noise at the output of the IF filter, and are a function of that filter, assuming a flat noise spectrum going into the filter. For example, if the filter has a symmetric passband about the IF frequency, a result is that $\lambda = 0$.

The total differential phase for the output of the limiter-discriminator receiver has the probability density function

$$p_{\Delta\phi}(x) = \exp\{-|\alpha|\}\sum_{n=0}^{\infty}\frac{|\alpha|^n}{n!}\,p_\psi(x \pm 2n\pi), \tag{2-30}$$

where α is the click number average given in (2-28b) and the sign taken is the same as that of $\Delta\phi$. Figure 2-4 illustrates the multi-model character of $p_{\Delta\phi}(x)$.

When the receiver is subject to partial-band jamming with probability γ, by extension (2-30) becomes, for $\Delta\phi > 0$,

$$p_{\Delta\phi}(x;\,\gamma) = (1-\gamma)e^{-\alpha_0}\sum_{n=0}^{\infty}\frac{\alpha_0^n}{n!}\,p_\psi(x+2n\pi;\,\rho_N)$$

$$+ \gamma e^{-\alpha_1}\sum_{n=0}^{\infty}\frac{\alpha_1^n}{n!}\,p_\psi(x+2n\pi;\,\rho_T), \tag{2-31}$$

using α_0 and α_1 to denote the absolute values of click number averages under no jamming and jamming conditions, respectively. The SNR in the absence of jamming, ρ_N, was defined in (2-14); the jammed SNR, ρ_T, is given by

$$\rho_T \triangleq \frac{A^2}{2\sigma_T^2} = \frac{A^2}{2(\sigma_N^2 + \sigma_J^2)} \tag{2-32a}$$

$$= \frac{\rho_N\rho_J}{\rho_N + \rho_J} = \frac{1}{D}\cdot\frac{r}{L}\cdot\frac{\dfrac{E_b}{N_0}\cdot\gamma\dfrac{E_b}{N_J}}{\dfrac{E_b}{N_0} + \gamma\dfrac{E_b}{N_J}}. \tag{2-32b}$$

22
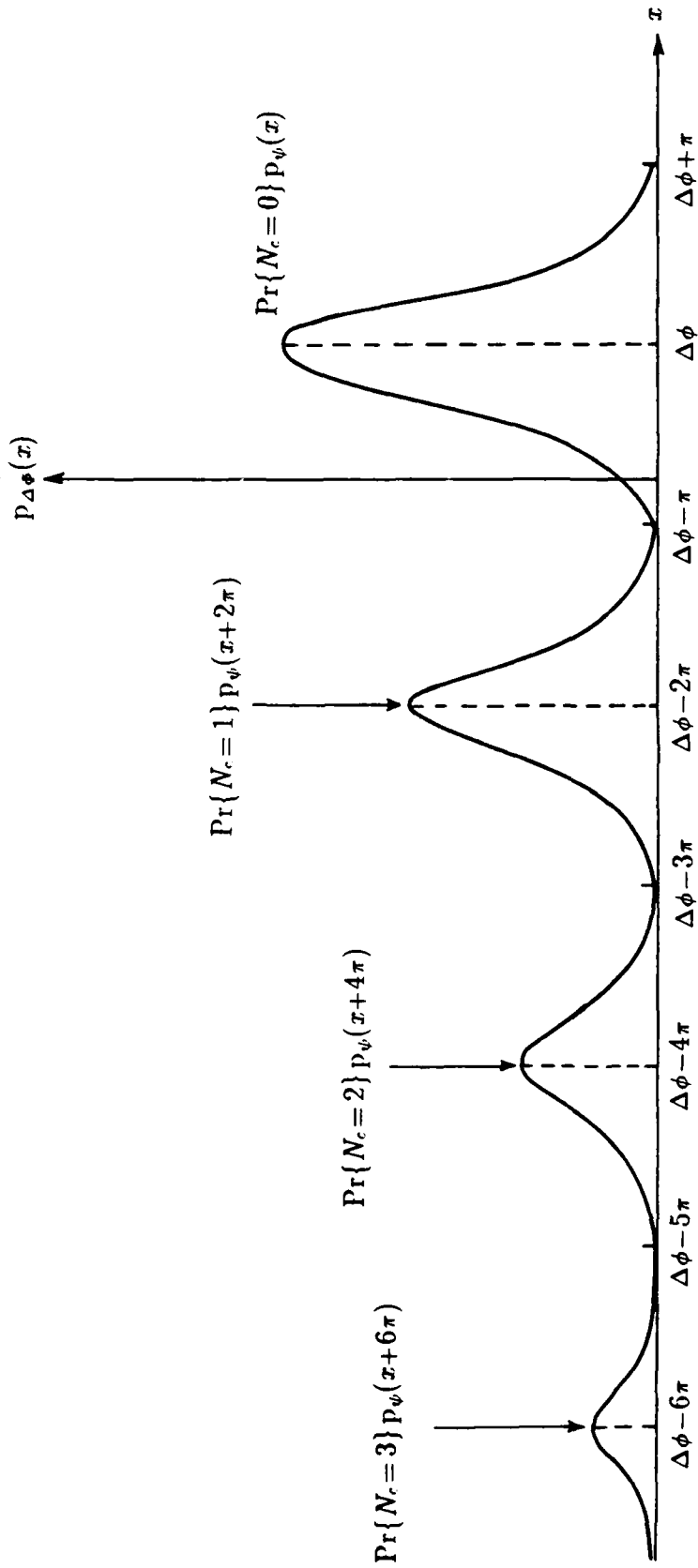
FIGURE 2-4 PROBABILITY DENSITY FUNCTION FOR DIFFERENTIAL PHASE INCLUDING FM CLICKS

23

2.1.3.3 Probability distribution for the output of a differential detector

The output of the differential detector shown in Figure 2-3(b) is

$$z(t) = \tfrac{1}{2} R(t) R(t-T) \sin [\Phi(t) - \Phi(t-T)], \quad \omega_{IF} T = 2n\pi. \tag{2-33}$$

It was shown in [8] that the output of a differential detector at the sampling time is equivalent to the difference between two independent, scaled noncentral chi-squared random variables, each with two degrees of freedom. We denote this equivalence by

$$z \sim c_1 \chi^2(2; d_1) - c_2 \chi^2(2; d_2), \tag{2-34a}$$

where the scale factors are

$$c_{1,2} = \tfrac{1}{4}\sigma^2 (\sqrt{1-r^2} \mp \lambda) \tag{2-34b}$$

and the noncentrality parameters are

$$d_{1,2} = \frac{2\{U - rW\cos\Delta\phi \pm \sqrt{1-r^2}\,W\sin\Delta\phi\}}{\sqrt{1-r^2}(\sqrt{1-r^2} \mp \lambda)}. \tag{2-34c}$$

Therefore, the characteristic function for the random variable z is

$$C_z(\nu) = C_{\chi^2}(c_1\nu;\, 2,\, d_1)\, C_{\chi^2}(-c_2\nu;\, 2,\, d_2)$$

$$= \frac{1}{1+4\nu^2 c_1 c_2 + 2j\nu(c_2-c_1)} \exp\left\{\frac{j\nu(c_1 d_1 - c_2 d_2) - 2\nu^2 c_1 c_2 (d_1+d_2)}{1+4\nu^2 c_1 c_2 + 2j\nu(c_2-c_1)}\right\}$$

$$= \frac{1}{1+j\nu A + \nu^2 B} \exp\left\{\frac{j\nu C - \nu^2 D}{1+j\nu A + \nu^2 B}\right\}, \tag{2-35a}$$

where for convenience we have defined

$$A \triangleq 2(c_2-c_1) = \sigma^2 \lambda \tag{2-35b}$$

$$B \triangleq 4c_1 c_2 = \tfrac{1}{4}(1-r^2-\lambda^2) \tag{2-35c}$$

$$C \triangleq c_1 d_1 - c_2 d_2 = \sigma^2 W \sin\Delta\phi \tag{2-35d}$$

and
$$D \triangleq 2c_1 c_2 (d_1+d_2) = \tfrac{1}{2}\sigma^4 (U - rW\cos\Delta\phi + \lambda W \sin\Delta\phi). \tag{2-35e}$$

The mean value of z is easily obtained from (2-34a) and is

$$E\{z\} = c_1(2+d_1) - c_2(2+d_2)$$

$$= 2(c_1-c_2) + c_1 d_1 - c_2 d_2$$

$$= \sigma^2(\lambda + W\sin\Delta\phi) \tag{2-36a}$$

$$= \tfrac{1}{2} A^2 \sqrt{a(t)\,a(t-T)} \sin\Delta\phi \quad \text{for } \sigma^2 = 0. \tag{2-36b}$$

24

Since we will be interested in the probability of error for various weighted combinations of differential detector output samples, the characteristic function is a more convenient description of the distribution than the probability density function (PDF), for reasons which will be shown in Section 4. For further developments of the PDF for the class of cross-correlators to which the differential detector belongs, the reader is referred to [14].

2.1.4 Generic Chip Combining Schemes

Our analysis efforts are focused on ways to combine the L chips belonging to a particular data symbol so as to give a diversity gain, if possible, against worst-case partial-band noise jamming. A generic formulation for the chip combining approach is to base the symbol decision on the polarity of the decision statistic or metric

$$z_k = \sum_{q=1}^{L} \zeta_{kq} = \sum_{q=1}^{L} f(z_{kq}), \qquad (2\text{-}37)$$

where $f(z_{kq})$ is some function of the qth chip belonging to the kth data symbol. For example. if hard decisions are made on each chip, then

$$\zeta_{kq} = f(z_{kq}) = 1, \quad z_{kq} > 0$$
$$= 0, \quad z_{kq} \leq 0. \qquad (2\text{-}38)$$

This nonlinear combining function is known to produce a diversity gain. In our previous study [8, 15], we investigated the combining based on $f(z_{kq}) = z_{kq}$. or linear combining. and found that this method does not yield a diversity gain.

In general, in order for a diversity gain to be realized, it is necessary for the receiver to give a lower weight in the sum (2-37) to chips which have undergone jamming as the consequence of the hop on which they were transmitted having hopped into a portion of the band which is jammed. Thus it is required that the function ζ_{kq} of the chip decision variable z_{kq} somehow discriminate against jammed chips. This concept can be expressed by

$$f(z_{kq}; \text{no jamming}) > f(z_{kq}; \text{jamming}). \qquad (2\text{-}39a)$$

In principle, this requirement can be satisfied by weighting z_{kq} by the ratio of the unjammed noise power, σ_N^2, to the noise power on its hop, σ_q^2, giving

$$\zeta_{kq} = \sigma_N^2 z_{kq}/\sigma_q^2 \equiv w_q z_{kq} \qquad (2\text{-}39b)$$

$$= z_{kq}, \qquad \text{hop } q \text{ not jammed} \qquad (2\text{-}39c)$$

$$= z_{kq}\sigma_N^2/\sigma_T^2, \qquad \text{hop } q \text{ jammed.} \qquad (2\text{-}39d)$$

Techniques for measuring the power on the hop are discussed in [24].

2.2 FORMULATIONS FOR THE PERFORMANCE MEASURES

In this report the performance of the system is measured in terms of the probability of a bit error for FH/CPFSK as a function of jammer power when the system is subjected to worst-case partial-band noise jamming, with and without error-control coding, for different diversity combining schemes and numbers of hops per transmitted symbol, L.

2.2.1 Uncoded Bit Error Probability

Conceptually, the probability distribution for the output of the combiner at a given time, z, is conditioned on the number of hops which have been jammed. Let $p(z|l)$ denote the PDF of z conditioned on there having been l out of L hops jammed. Then, averaged over the possible jamming event (i.e., the possible values of l), the probability of an error in deciding on the polarity of a transmitted binary symbol is

$$
\begin{aligned}
P_e &= \Pr\{d_k=0\}\Pr\{z_k>0 \mid d_k=0\} + \Pr\{d_k=1\}\Pr\{z_k<0 \mid d_k=1\} \\
&= \tfrac{1}{2}[\Pr\{z_k>0 \mid d_k=0\} + \Pr\{z_k<0 \mid d_k=1\}] \\
&= \Pr\{z_k<0 \mid d_k=1\} \\
&= \sum_{l=1}^{L} \Pr\{l \text{ hops jammed}\} \int_{-\infty}^{0} dz\; p(z|l).
\end{aligned}
\tag{2-40}
$$

This formulation assumes that the two possible binary symbol values are equally likely. and that the conditional probability of error is the same for both $d_k=0$ and $d_k=1$. Assuming that a fraction γ of the available hopping channels are jammed and that the pseudorandomly-selected hop frequencies are equally likely, the probability that l out of L hops are jammed is

$$
\Pr\{l \text{ hops jammed}\} = \binom{L}{l}\gamma^l(1-\gamma)^{L-l}.
\tag{2-41}
$$

Note that this expression represents the total number of jamming situations resulting in l hops jammed, irrespective of which of the hops are jammed, or in what order. Thus (2-39) is valid if the combiner output's probability distribution does not depend on the order in which the hops were jammed or not jammed.

Since the chips being combined are independent by virtue of being corrupted by noise in different frequency channels, their joint PDF is

$$
p(z_{k1}, z_{k2}, \ldots, z_{kL}) = \prod_{q=1}^{L} p_q(z_{k_q}).
\tag{2-42}
$$

For convenience, we may arbitrarily designate the first l samples as occurring on jammed hops.

26

For an unjammed hop the noise power on the hop is $\sigma^2 = \sigma_N^2$, and for jamming it is $\sigma^2 = \sigma_T^2 = \kappa \sigma_N^2$, where we adopt the notation

$$\kappa \triangleq \frac{\sigma_T^2}{\sigma_N^2} = 1 + \frac{\sigma_J^2}{\sigma_N^2} = 1 + \frac{E_b/\mathcal{N}_0}{\gamma E_b/\mathcal{N}_J}. \qquad (2\text{-}43)$$

Using this notation it is convenient also to write

$$
\begin{aligned}
p_q(z_{kq}) &\equiv p(z_{kq};\, \sigma_q^2) \\
&= p(z_{kq};\, \sigma_N^2), &&\text{hop } q \text{ unjammed;} && (2\text{-}44a) \\
&= p(z_{kq};\, \kappa\sigma_N^2), &&\text{hop } q \text{ jammed.} && (2\text{-}44b)
\end{aligned}
$$

This notation also allows us to rewrite (2-42) as

$$p(z_{k1},\, z_{k2},\, \ldots,\, z_{kL}) = \prod_{\substack{\text{unjammed} \\ L\text{-}l \text{ hops}}} p(z_{kq};\, \sigma_N^2) \prod_{\substack{\text{jammed} \\ l \text{ hops}}} p_q(z_{kq};\, \kappa\sigma_N^2). \qquad (2\text{-}45)$$

The characteristic function for the combiner output is, using a similar approach to the notation,

$$
\begin{aligned}
C_z(\nu;\, l) &= E\!\left[\exp\!\left\{ j\nu \sum_{q=1}^{L} f(z_{kq}) \right\} \right] \\
&= \left[E\!\left\{ e^{j\nu f(z_{k1})} \right\} \right]^l \left[E\!\left\{ e^{j\nu f(z_{kL})} \right\} \right]^{L-l} \\
&= \left[C_\zeta(\nu;\, \kappa\sigma_N^2) \right]^l \left[C_\zeta(\nu;\, \sigma_N^2) \right]^{L-l}, \qquad (2\text{-}46)
\end{aligned}
$$

in which $C_\zeta(\nu;\, \sigma^2)$ is the conditional characteristic function for $\zeta_{kq} = f(z_{kq})$ when the hop noise power is σ^2.

If the mathematical formulation for $C_\zeta(\nu;\, \sigma^2)$ is simple, the preferred method for obtaining the probability of error is first to obtain

$$p(z\,|\,l) = \int_{-\infty}^{\infty} d\nu\; e^{-j\nu z} C_z(\nu;\, l) \qquad (2\text{-}47)$$

for substitution in (2-45).

2.2.2   Coded Bit Error Probability

The decoding schemes we will be considering in this report include both hard-decision decoding and soft-decision decoding. By "hard" we mean that the inputs to the decoder are binary symbol decisions. "Soft" refers to a non-binary input to the decoder. For the selected constraint length seven, rate one-half convolutional code, the error probability for the decoded bits is bounded by [25]

$$P_b = P_b(L; \gamma, \text{ECCM combining scheme, decoding input})$$

$$\leq 36\,Q_{10} + 211\,Q_{12} + 1404\,Q_{14} + 11633\,Q_{16} + \cdots \qquad (2\text{-}48)$$

in which the quantities Q_{2m} are the probabilities of decoder error in comparing the correct path segment to a path segment that differs in $2m$ symbols. If the decoder is presented with hard decisions $\{\hat{d}_k\}$ on the transmitted code symbols $\{d_k\}$,—with average error probability $P_e(L) = P_e(L; \gamma, \frac{1}{2L}E_b)$—the Q_{2m} are given exactly by

$$Q_{2m} = \sum_{k=0}^{m-1}\binom{2m}{k}[P_e(L)]^{2m-k}[1-P_e(L)]^k + \tfrac{1}{2}\binom{2m}{m}\{[1-P_e(L)]\,P_e(L)\}^m \qquad (2\text{-}49a)$$

$$= \frac{(2m-1)!}{(m-1)!\,(m-1)!}\sum_{n=0}^{m-1}\binom{m-1}{n}\frac{(-1)^n}{m+n}[P_e(L)]^{m+n}, \qquad (2\text{-}49b)$$

where the form given by (2-49b) is derived in Section 4.2.1. For example,

$$Q_2 = P_e(L), \qquad (2\text{-}50a)$$

$$Q_4 = 3\,[P_e(L)]^2 - 2\,[P_e(L)]^3, \qquad (2\text{-}50b)$$

$$Q_6 = 10\,[P_e(L)]^3 - 15\,[P_e(L)]^4 + 6\,[P_e(L)]^5, \text{ etc.} \qquad (2\text{-}50c)$$

Using $\lambda = P_e(L)$, the polynomials used in (2-48) are

$$Q_{10} = 126\,\lambda^5 - 420\,\lambda^6 + 540\,\lambda^7 - 315\,\lambda^8 + 70\,\lambda^9 \qquad (2\text{-}51a)$$

$$Q_{12} = 462\,\lambda^6 - 1980\,\lambda^7 + 3465\,\lambda^8 - 3080\,\lambda^9 + 1386\,\lambda^{10} - 252\,\lambda^{11} \qquad (2\text{-}51b)$$

$$Q_{14} = 1716\,\lambda^7 - 9009\,\lambda^8 + 20020\,\lambda^9 - 24024\,\lambda^{10} + 16380\,\lambda^{11}$$

$$- 6006\,\lambda^{12} + 924\,\lambda^{13} \qquad (2\text{-}51c)$$

$$Q_{16} = 6435\,\lambda^8 - 40040\,\lambda^9 + 108108\,\lambda^{10} - 163800\,\lambda^{11} + 150150\,\lambda^{12}$$

$$- 83160\,\lambda^{13} + 25740\,\lambda^{14} - 3432\,\lambda^{15}. \qquad (2\text{-}51d)$$

Instead of presenting the hard symbol decisions $\{\hat{d}_k\}$ to the decoder, the inputs may be a soft-decision metric such as the number of the L chip decisions $\{\hat{d}_{kq}; q=1, 2, ...L\}$ which are positive (or conceptually, their unthresholded sum). In that situation, it is shown in [25] that the value of the Q_{2m} used in (2-48) are bounded by

$$Q_{2m} \leq \tfrac{1}{2}\left\{4P_e(1; \gamma, \tfrac{1}{2L}E_b)[1 - P_e(1; \gamma, \tfrac{1}{2L}E_b)]\right\}^{mL}, \qquad (2\text{-}52)$$

in which it is emphasized that each chip represents the fraction $r/L = 1/2L$ of the energy of an original encoded bit.

28

2.3 SUMMARY OF CALCULATION METHODOLOGY

In general, we have found it more convenient to use the characteristic function method in studying sums and weighted sums of L receiver samples. In the following we summarize how the probability of bit error may be calculated from the characteristic function.

2.3.1 Characteristic Function Method for Obtaining the Bit Error Probability

The cumulative probability distribution $P(Z) = \Pr\{z \leq Z\}$ for a random variable z may be written in terms of its characteristic function $C_z(\nu)$ as follows [16]:

$$\Pr\{z \leq Z\} = \tfrac{1}{2} - \tfrac{1}{\pi}\int_0^\infty \frac{d\nu}{\nu}\,\text{Im}\{C_z(\nu)e^{-j\nu Z}\}. \tag{2-53}$$

Therefore, the bit error probability for a binary system with decision statistic z is

$$P_e = \Pr\{z < 0 \mid d_k = 1\} = \tfrac{1}{2} - \tfrac{1}{\pi}\int_0^\infty \frac{d\nu}{\nu}\,\text{Im}\{C_z(\nu)\}. \tag{2-54}$$

When z is a weighted sum, that is,

$$z = \sum_{q=1}^{L} w_q z_q, \tag{2-55}$$

the probability becomes

$$P_e = \tfrac{1}{2} - \tfrac{1}{\pi}\int_0^\infty \frac{d\nu}{\nu}\left(\prod_{q=1}^{L}|\,C_{z_q}(\nu w_q)\,|\right)\sin\left(\sum_{q=1}^{L}\arg[\,C_{z_q}(\nu w_q)]\right). \tag{2-56}$$

2.3.2 Characteristic Function with FM Clicks Included

In Section 2.1, a general expression for the probability density function of the differential phase sample $\Delta\Phi$ at the output of the limiter-discriminator receiver was shown to be a weighted sum of shifted, modulo-2π PDF's, $p_\psi(\cdot)$. The corresponding characteristic function is

$$C_{\Delta\Phi}(\nu;\,\gamma) = \int_{-\infty}^{\infty} dx\, p_{\Delta\Phi}(x;\,\gamma)\, e^{j\nu x}$$

$$= (1-\gamma)e^{-\alpha_0}\sum_{n=0}^{\infty}\frac{\alpha_0^n}{n!}\int_{-\infty}^{\infty} dx\, e^{j\nu x}\, p_\psi(x+2n\pi;\,\rho_N)$$

$$+ \gamma\, e^{-\alpha_1}\sum_{n=0}^{\infty}\frac{\alpha_1^n}{n!}\int_{-\infty}^{\infty} dx\, e^{j\nu x}\, p_\psi(x+2n\pi;\,\rho_T)$$

29

$$= (1-\gamma) e^{-\alpha_0} \sum_{n=0}^{\infty} \frac{\alpha_0^n}{n!} \; e^{-j\nu 2\pi n} \; C_{\psi}(\nu; \; \rho_N)$$

$$+ \; \gamma \, e^{-\alpha_1} \sum_{n=0}^{\infty} \frac{\alpha_1^n}{n!} \; e^{-j\nu 2\pi n} \; C_{\psi}(\nu; \; \rho_T). \tag{2-57}$$

The individual characteristic functions $C_{\psi}(\nu; \; \rho)$ may be factored out of the sums, and the sums completed, to yield the closed form

$$C_{\Delta\Phi}(\nu; \; \gamma) = (1-\gamma) \exp\{-\alpha_0 + \alpha_0 \; e^{-j\nu 2\pi}\} \, C_{\psi}(\nu; \; \rho_N)$$

$$+ \; \gamma \exp\{-\alpha_1 + \alpha_1 \; e^{-j\nu 2\pi}\} \, C_{\psi}(\nu; \; \rho_T) \tag{2-58a}$$

$$= (1-\gamma) e^{-\alpha_0(1-\cos 2\pi\nu) - j\alpha_0 \sin 2\pi\nu} \, C_{\psi}(\nu; \; \rho_N)$$

$$+ \; \gamma \, e^{-\alpha_1(1-\cos 2\pi\nu) - j\alpha_1 \sin 2\pi\nu} \, C_{\psi}(\nu; \; \rho_T). \tag{2-58b}$$

2.3.3   Characteristic Function with Adaptive Weights

If a weight w_0 is given to a $\Delta\Phi$ sample from an unjammed hop, and w_1 to one from a jammed hop, the characteristic function for $\Delta\Phi$ becomes

$$C_{\Delta\Phi}(\nu; \; \gamma) = (1-\gamma) e^{-\alpha_0(1-\cos 2\pi w_0 \nu) - j\alpha_0 \sin 2\pi w_0 \nu} \, C_{\psi}(w_0\nu; \; \rho_N)$$

$$+ \; \gamma \, e^{-\alpha_1(1-\cos 2\pi w_1 \nu) - j\alpha_1 \sin 2\pi w_1 \nu} \, C_{\psi}(w_1\nu; \; \rho_T). \tag{2-59}$$

30

3.0 FH/CPFSK IMPLEMENTATION STUDIES

In this section we consider certain aspects of the implementation of frequency-hopped CPFSK systems. First, in Section 3.1, we discuss various issues affecting the implementation of current frequency-hopped systems. Then, in Section 3.2, we use models of synthesizer switching transient waveforms to analyze their effect on the emitted signal spectrum and the de-hopped receiver IF signal during the switching times between hops.

3.1 DISCUSSION OF IMPLEMENTATION ISSUES

The implementation issues that are the focus of the following discussions include factors affecting the selection of a hopping rate, emissions control measures and hop transient effects, and synchronization requirements.

3.1.1 Factors Affecting the Selection of a Hopping Rate

Certain fundamental limitations on frequency hopping rate follow from system requirements. Suppose that the maximum signalling rate which can be supported by a hopping slot or channel, in order to avoid adjacent channel interference (for example), is R_c. Also, let R_d denote the rate of the data symbols to be sent over the hopping channel, and let

$$T_h = R_h^{-1} = \text{hop duration or dwell time} \tag{3-1a}$$

$$Q = R_d T_h = \text{number of data symbols per hop} \tag{3-1b}$$

$$T_o = \text{portion of } T_h \text{ needed for overhead operations.} \tag{3-1c}$$

By "overhead operations" we refer to the various practical operations which must be implemented to support the transmission of a frequency hop; these include

- retuning the transmitter and receiver synthesizers,
- controlling the fall and rise of the transmitted power between hops to minimize spectral splatter,
- initializing the state of the receiver filters, and
- acquiring synchronization on the hop, if necessary.

During the portion of the hop interval in which the Q symbols of user data are being transmitted, the transmitted symbol rate R_s must be higher than R_d because of the overhead operations. Thus, the actual symbol rate on the hop is

31

$$R_s = \frac{Q}{T_h - T_o} = \frac{R_d T_h}{T_h - T_o} < R_c. \tag{3-2a}$$

Solving for R_h gives the inequality

$$R_h < \frac{R_c - R_d}{R_c T_o} \tag{3-2b}$$

where $R_c T_o$ is the number of symbols which could have been transmitted during the overhead time at the maximum hop channel rate.

For example, if $R_c = 20\,$kbps, $R_d = 16\,$kbps, and $T_o = 0.2\,$ms, the maximum hopping rate would be $1000\,$hops/sec; if $T_o = 2.0\,$ms, the maximum hopping rate would be 100 hops/sec. Typically, the "off the air" times of tactical VHF hopping radios is on the order to 10-20% of T_h [26, 29].

If the data rate R_d is low compared to the channel rate R_c, the upper limit to R_h approaches T_o^{-1}, and it is possible to have the situation where the hopping rate is greater than the data rate, commonly referred to as fast hopping.[1] A fundamental limitation which is not expressed by the inequality in (3-2b) is that the hopping rate must be less than R_c, since for fast hopping the hopping rate is dominant in determining the hop bandwidth.

It has been said [28] that the SINCGARS hop rate of about 100 hops per second "was determined by factors such as signal density, assurance of communications in a mutual interference environment, ability to enter the net when out of synchronization, technology and cost limitations of developing a suitable synthesizer, and reduced mean time between failures."

On the other hand, and Italian manufacturer claims [27] that the use of a direct sequence spread spectrum modulation on the hops, rather than the commonly used digital FM or CPFSK, would permit higher hop burst rates (R_s) without incurring mutual interference, and also would enhance the synchronization performance, with the result that a hopping rate four times higher than that of SINCGARS is practical. In fact, the burst rate during the hop dwell times in the JTIDS and EPLRS systems is $5\,$MHz, greater than the hop channel spacing of $3\,$MHz, and both systems employ error control coding[2] and a form of direct sequence spreading—in that they utilize MSK (digital FM with a modulation index of $h = 0.5$, which is very similar to the bi-phase modulation most often associated with direct sequence systems.

---

[1]Some analysts categorize hopping speed on an absolute basis, calling hopping faster than 500 hops/sec fast hopping.

[2]For Army use, neither JTIDS or EPLRS will be used for voice communications. This allows the system designer much more freedom in selecting modulation parameters.

3.1.2   Emissions Control and Hop Transient Effects

As alluded to previously, at the points in time when the hopping signal switches from one carrier frequency to another, there is the possibility of spectral splatter if the amplitude of the waveform is not shaped properly. It is well known that "sharp edges" on signal pulses give them higher spectral sidelobes—and therefore higher potential for adjacent channel interference—than do "smooth edges." For this reason, both EPLRS [32, p. 7-4] and JTIDS [33, p. 23] implementations, for example, control the rise and fall times of the hops. In addition, the JTIDS transmissions are subject to strict controls on the amount of power emitted during the hop dwell time as well as the duty cycle of transmissions. In [29], it is stated that, in order to reduce the amount of splatter into nearby nets, it is necessary that neither the rise time or the fall time of the hop pulse be much less than a bursted symbol time, $T_c = R_c^{-1}$, thus requiring that

$$\min(\text{rise time, fall time}) > \alpha T_c, \tag{3-3}$$

where the factor α is said to be typically between the values 1 and 4.

A separate concern related to emission control is the emission of RF energy in adjacent and other hop channels due to the characteristics of the hopping waveform during the transient period between hops. In effect, the waveform is the result of a frequency modulation of a carrier at the center of the hopping band by a multi-level pulse, one level per possible hop center frequency, and the spectrum of such a modulation can be very wide, containing many spurious harmonics related to the frequency switching. For this reason, VHF hopping radios using an indirect synthesizer, such as the British JAGUAR [34, pp. 6-10, 7-7], employ a "hop mute" or power-down control function during the time that the synthesizer circuitry indicates an "out of tune" condition. If a direct frequency synthesizer is used, it is possible to adequately suppress the spurious harmonics while maintaining a very small switching time [29], in which case the controlling concept in waveshaping is the prevention of splatter.

Even with the use of waveshaping to reduce splatter, there may be undesirable effects at the desired receiver, such as [29] ringing in the IF filter as it is started up with the new hop input, as well as phase discontinuities arising from Doppler shifts, frequency-selective fading, indeterminacy of the IF phase prior to reception of the pulse (assuming the signal power is reduced between pulses), and imperfect synchronization in the receiver.

An analysis of phase transients due to hopping was presented in [30] for the case of

33

a MFSK system that hops once per symbol. The transients were shown to give rise to a spreading of signal energy so that there is a loss of energy in the transmitted symbol's sub-band and undesired energy in the other sub-bands. For hopping systems such as VHF tactical radios which have many symbols per hop, there is a concern that the phase transient will degrade the first symbols on the hop—or, conversely, that if there is a delay in transmitting symbols until the transient settles out, then an effective loss of usable signal energy is incurred, lowering the performance of the system for a given limit to transmitter power [1, 29].

3.1.3 Synchronization Considerations

Generally, hopping radio systems use preambles, special sequences of frequencies and/or data, in order to establish synchronization between hopping radios. This technique assumes that a coarse synchronization has already been achieved, so that the receiver knows what hop frequencies are upcoming but not the exact time of arrival, due to the dependence of the time of arrival upon the relative positions of transmitter and receiver, which may change from message to message.

The timing references in hopping radios are designed to have an accuracy which at least guarantees that hopping by the transmitter and receiver, once synchronized, can maintain synchronism over the duration of a typical multi-hop message. Nevertheless, there is always some residual difference between the timing of the incoming signal and that of the receiver, usually neglected in analyses, but sometimes modelled for the purpose of particular studies (e.g., [31]). As mentioned above, a difference in switching times between the incoming signal and the receiver's synthesizer can produce significant phase discontinuities.

In the following subsections, some of the hopping transient considerations we have discussed are given further attention in the form of detailed analysis.

3.2 ANALYSIS OF HOP TRANSIENT EFFECTS

In [30] it has been shown that the phase transient at the output of an indirect, phase-lock-loop based synthesizer can be modelled by the waveform

$$\theta_t(t) = \frac{\Delta f}{f_n} e^{-\zeta \omega_n t} \frac{1}{\sqrt{1-\zeta^2}} \sin\left(\omega_n \sqrt{1-\zeta^2}\, t\right), \quad \zeta < 1, \tag{3-4}$$

where $\omega_n = 2\pi f_n$ is a loop resonant radial frequency, ζ is a damping factor, and Δf is the desired step change in frequency. Thus, for example, we observe that in general there is

34

some ringing and some overshoot in the phase output. In this section, we utilize a simplified model for the phase transient in order to analyze the spectrum of the hopping transmissions and the effects of phase discontinuities at the receiver IF when transmitter and receiver are not in perfect synchronization.

3.2.1 Model for Synthesizer Transient Waveforms

For the purpose of studying the effects of the transients occurring between hops, we neglect the data modulation and any hop amplitude control, and look very closely at the interval between two hops, taking $t = 0$ to be the moment at which the frequency switching begins. Thus we write for the received signal waveform

$$s_0(t) = A_r \cos[\theta_r(t)] = A_r \cos\left[\int dt\, \dot{\theta}_r(t)\right] \tag{3-5a}$$

where the instantaneous frequency or phase derivative is given by

$$\dot{\theta}_r(t)/2\pi = f_1, \qquad\qquad t < 0 \tag{3-5b}$$

$$= f_1 + \delta t\, \text{sign}(f_2 - f_1), \qquad 0 < t \leq t_s \tag{3-5c}$$

$$= f_2, \qquad\qquad t > t_s. \tag{3-5d}$$

This formulation expresses the concept that, prior to the end of the hop, the carrier has been settled at f_1 and that beginning at $t = 0$ this carrier is linearly frequency-modulated for an interval equal to t_s, the switching time, after which the carrier is f_2. It is assumed in (3-5) that either the frequency rate of change δ is given, in which case it turns out that the switching time is the frequency-dependent quantity

$$t_s = |f_2 - f_1|/\delta, \quad \delta \text{ given}, \tag{3-6a}$$

or the switching time t_s is given, in which case the frequency rate of change must be frequency-dependent:

$$\delta = |f_2 - f_1|/t_s, \quad t_s \text{ given}. \tag{3-6b}$$

3.2.1.1 Received and local oscillator transient phase functions

Whether δ is specified or t_s is specified, using $F \triangleq f_2 - f_1$ the transient phase function is given by (assuming $\theta_r(0) = 0$ for convenience)

$$\theta_r(t) = \int_0^t du\, \dot{\theta}_r(u)$$

$$= 2\pi f_1 t, \qquad\qquad t \leq 0, \tag{3-7a}$$

$$= 2\pi f_1 t + \pi F t^2/t_s, \qquad 0 < t \leq t_s, \tag{3-7b}$$

$$= 2\pi f_1 t + 2\pi F(t - t_s) + \pi F t_s, \qquad t > t_s. \tag{3-7c}$$

35

Assuming that downconversion is employed by the receiver, if the transmitter and the receiver are in perfect synchronism the receiver synthesizer produces the local oscillator frequency $f_{LO} = f_{RF} + f_{IF}$, where f_{RF} and f_{IF} are the selected (hopping) channel carrier frequency and the fixed IF center frequency, respectively.[3] However, allowing the receiver to be late by the time interval τ, the receiver synthesizer waveform is assumed to have the instantaneous frequency or phase derivative

$$\dot{\theta}_{LO}(t)/2\pi = \dot{\theta}_r(t-\tau)/2\pi + f_{IF}. \qquad (3\text{-}8)$$

This assumption leads to the local oscillator transient phase function (neglecting any constant of integration which may differ from that for the received phase function)

$$\begin{aligned}
\theta_{LO}(t) &= \int_0^t du[2\pi f_{IF} + \dot{\theta}_r(u-\tau)] \\
&= 2\pi f_{IF} t + \theta_r(t-\tau) + 2\pi f_1 \tau, \qquad (3\text{-}9)
\end{aligned}$$

since $\theta_r(-\tau) = -2\pi f_1 \tau$.

3.2.1.2 Mixer output transient phase difference

The mixer output then is, prior to the IF bandpass filter,

$$const. \times \cos[\theta_{LO}(t) - \theta_r(t)] = A\cos[2\pi f_{IF} t + \Delta\theta(t)] \qquad (3\text{-}10a)$$

where the transient phase difference $\Delta\theta$ is

$$\Delta\theta(t) = \theta_r(t-\tau) - \theta_r(t) + 2\pi f_1 \tau. \qquad (3\text{-}10b)$$

The form that this function takes depends on the relation between t_s, the synthesizer switching time, and τ, the receiver synchronization offset. For indirect synthesizers —and indeed most synthesizers— it can be assumed that $|\tau| < t_s$. In that case and in the case of $\tau > 0$, the transient phase difference is found to be

$$\begin{aligned}
\Delta\theta(t) &= 0, & t &\leq 0 & (3\text{-}11a) \\
&= -\pi F t^2 / t_s, & 0 &< t \leq \tau & (3\text{-}11b) \\
&= -\pi F(2\tau t - \tau^2)/t_s, & \tau &< t \leq t_s & (3\text{-}11c) \\
&= -2\pi F\tau + \pi F(t-\tau-t_s)^2/t_s, & t_s &< t \leq t_s + \tau & (3\text{-}11d) \\
&= -2\pi F\tau, & t &> t_s + \tau. & (3\text{-}11e)
\end{aligned}$$

Note that if $\tau = 0$, that is, there is no synchronization error, then there is no transient phase difference and the combination of hopping and de-hopping is indeed "transparent"

---

[3]Using this method it is necessary to use additional pre-filtering at RF. such as done by the Jaguar radio [34], to prevent images of non-selected channels from appearing at the mixer output.

as assumed by most simple analyses of hopping systems. Also, we observe that (3-11) describes $\Delta\theta$ as a piecewise continuous function with a succession of linear, quadratic, linear, quadratic, and linear line segments, as illustrated in Figure 3-1.

For the case that $\tau > t_s > 0$, the transient phase difference takes the functional form

$$\Delta\theta(t) = 0, \qquad\qquad\qquad t \leq 0 \qquad\qquad (3\text{-}12\text{a})$$

$$= -\pi F t^2/t_s, \qquad\qquad 0 < t \leq t_s \qquad\qquad (3\text{-}12\text{b})$$

$$= -2\pi F(t-t_s) - \pi F t_s, \qquad t_s < t \leq \tau \qquad\qquad (3\text{-}12\text{c})$$

$$= -2\pi F\tau + \pi F(t-\tau-t_s)^2/t_s, \qquad \tau < t \leq \tau+t_s \qquad (3\text{-}12\text{d})$$

$$= -2\pi F\tau, \qquad\qquad\qquad t > t_s + \tau. \qquad\qquad (3\text{-}12\text{e})$$

As illustrated in Figure 3-1, this functional form has the same structure as the one for the case of $\tau < t_s$.

A more convenient model of the transient phase difference for analytical purposes is easily found to be

$$\Delta\theta(t) = 0, \qquad\qquad\qquad\qquad t \leq 0 \qquad\qquad (3\text{-}13\text{a})$$

$$= -\pi F\tau + \pi F\tau \cos\left(\frac{\pi t}{\tau+t_s}\right), \qquad 0 < t \leq t_s + \tau \qquad (3\text{-}13\text{b})$$

$$= -2\pi F\tau, \qquad\qquad\qquad\qquad t > t_s + \tau. \qquad\qquad (3\text{-}13\text{c})$$

Note that this shifted cosine function, like (3-11) and (3-12), also has quadratic segments at endpoints and a linear segment in the middle, to an excellent approximation, but is continuous on the interval $(0, t_s+\tau)$ rather than piecewise continuous.

3.2.2 Effect of Receiver Filtering on Transients

The harmonic content of the transient phase difference can be discovered by considering expansions of the mixer output signal waveform prior to the IF bandpass filter:

$$s(t) = A\cos\left[2\pi f_{IF} t + \Delta\theta(t)\right]. \qquad\qquad (3\text{-}14)$$

If the functional form for $\Delta\theta(t)$ given by (3-11) or (3-12) is used, then the analysis involves expansion of terms such as

$$\cos\left(at^2\right) = \frac{\partial}{\partial t}\int_0^t dx \cos\left(ax^2\right)$$

$$= \frac{\partial}{\partial t}\sqrt{\frac{2a}{\pi}}\int_0^{t\sqrt{\pi/2a}} dx \cos\left(\frac{\pi}{2}x^2\right)$$

$$= \frac{\partial}{\partial t}\sqrt{\frac{2a}{\pi}}\,C\left(\sqrt{\frac{\pi}{2a}}\,t\right). \qquad\qquad (3\text{-}15)$$
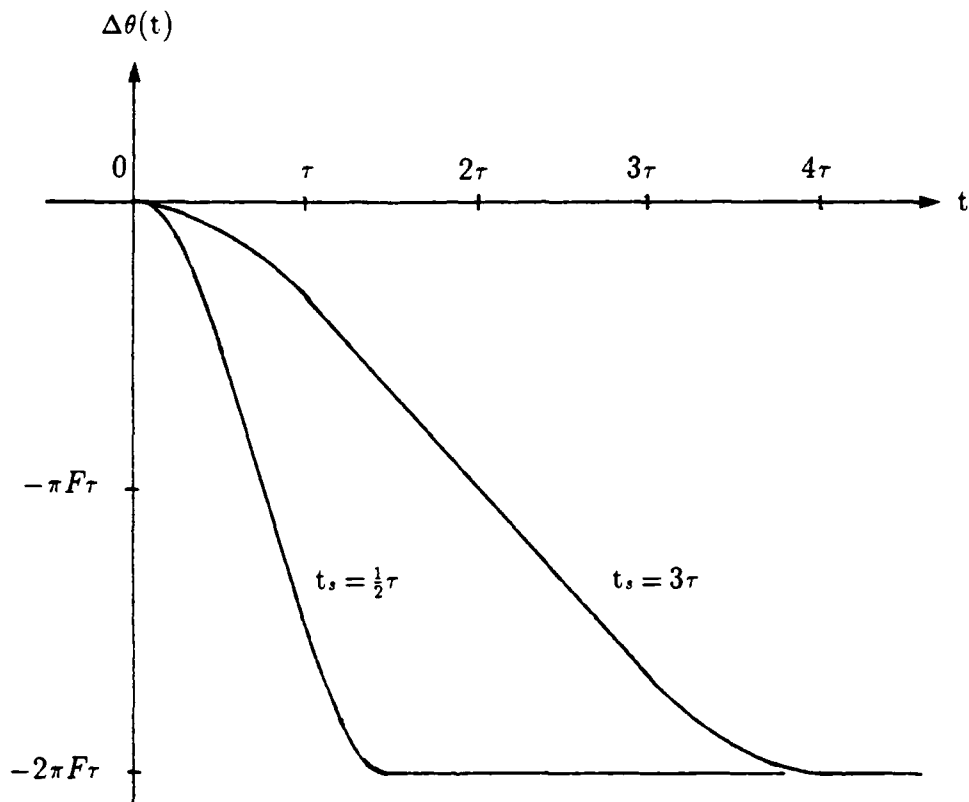
FIGURE 3-1   TRANSIENT PHASE DIFFERENCE MODELS

where $C(x)$ is the Fresnel cosine integral [17, eq. 7.3.1]. The mathematics involved is similar to that for analysis of "chirp radar" systems [35]. Note that the harmonic structure is not yet apparent in (3-15), but requires further development. However, if instead of the models for the transient phase difference given by (3-11) and (3-12) we use the shifted-cosine one given by (3-13), we have terms to evaluate such as

$$\cos(a\cos bt) = J_0(a) + 2\sum_{n=1}^{\infty}(-1)^n J_{2n}(a)\cos(2nbt) \tag{3-16a}$$

$$= \sum_{n=0}^{\infty}(-1)^n \epsilon_n J_{2n}(a)\cos(2nbt) \tag{3-16b}$$

and

$$\sin(a\cos bt) = 2\sum_{n=0}^{\infty}(-1)^n J_{2n+1}(a)\cos[(2n+1)bt], \tag{3-16b}$$

in which the $J_n(x)$ are the Bessel functions of integer order [17, ch. 9] and ϵ_n is Euler's constant, which takes the values $\epsilon_0 = 1$ and $\epsilon_n = 2$ for $n > 0$. Note that using (3-13) for the transient phase difference will therefore give the harmonics directly.

Applying (3-16) to the expression for the mixer output gives the expression

$$s(t) = A\cos(2\pi f_{IF}t), \qquad\qquad t \le 0 \tag{3-17a}$$

$$= A\cos(2\pi f_{IF}t - \pi F\tau)\sum_{n=0}^{\infty}(-1)^n \epsilon_n J_{2n}(\pi F\tau)\cos\left(\frac{2n\pi t}{\tau + t_s}\right)$$
$$+ 2A\sin(2\pi f_{IF}t - \pi F\tau)\sum_{n=0}^{\infty}(-1)^n J_{2n+1}(\pi F\tau)\cos\left(\frac{(2n+1)\pi t}{\tau + t_s}\right),$$
$$0 < t \le t_s + \tau \tag{3-17b}$$

$$= A\cos(2\pi f_{IF}t - 2\pi F\tau), \qquad\qquad t > t_s + \tau. \tag{3-17c}$$

Since it is true that $J_0(0) = 1$ and $J_n(0) = 0$ for $n > 0$, we see that this somewhat complex expression reduces to simply $s(t) = A\cos(2\pi f_{IF}t)$, that is, no transient phase difference at all, for the case of perfect synchronism ($\tau = 0$).

From (3-17) we see immediately that during the interval $(0, t_s + \tau)$ the mixer output's energy is spread about the IF center frequency to the harmonics of

$$f_{\Delta\theta} \triangleq \tfrac{1}{2}(t_s + \tau)^{-1}. \tag{3-18a}$$

The distribution of energy among these harmonics is dependent on $\pi F\tau$, the argument of the Bessel functions. Assuming a synch timing offset of about 1% of the symbol period, T_c, gives a value for τ of about $0.5\,\mu\text{sec}$. For a typical VHF hopping radio, the size of F can be from $25\,\text{kHz}$ to over $50\,\text{MHz}$, but more likely would be from $25\,\text{kHz}$ to around $256 \times 25\,\text{kHz} = 6.4\,\text{MHz}$ because the radios often are set up to hop in a sub-band, rather than over the entire $30\text{-}88\,\text{MHz}$ VHF band. Thus the value of $\pi F\tau$ ranges from around $\frac{1}{80}\pi$ to more than 3.2π. For small values of the argument, the Bessel functions are well approximated by

39

$$J_n(\pi F\tau) \approx \frac{(\frac{1}{2}\pi F\tau)^n}{n!}, \quad \pi F\tau \ll 1. \tag{3-18b}$$

For large values of the argument, we have [17, eq. 9.2.1]

$$J_{2n}(\pi F\tau) \approx \frac{(-1)^n}{\pi}\sqrt{\frac{2}{F\tau}}\cos\left(\pi F\tau - \frac{\pi}{4}\right) \tag{3-18c}$$

and

$$J_{2n+1}(\pi F\tau) \approx \frac{(-1)^n}{\pi}\sqrt{\frac{2}{F\tau}}\sin\left(\pi F\tau - \frac{\pi}{4}\right). \tag{3-18d}$$

From (3-18c) and (3-18d), we observe that the harmonics for large values of $\pi F\tau$ are of approximately equal magnitude, which agrees with the flat spectra for chirp waveforms shown in [35].

It is clear that the transient phase which will appear at the input to the demodulator will be considerably different from that at the mixer output, since the IF bandpass filter will attenuate these harmonics to different degrees. For deriving the effect of the IF bandpass filter on the transient phase difference when it is assumed that a Gaussian-shaped filter is used, a detailed transient analysis is presented in Appendix C. The implications of that analysis are that the IF filter will indeed reject the harmonics of $f_{\Delta\theta}$. Therefore in anticipation of the rejection of the harmonics, we make use the unit step function $U(t)$ to reformulate (3-17) as follows:

$$s(t) = A\cos(2\pi f_{IF}t)\cdot U(-t) + A J_0(\pi F\tau)\cos(2\pi f_{IF}t - \pi F\tau)\cdot[U(t) - U(t - t_s - \tau)]$$

$$+ A\cos(2\pi f_{IF}t - 2\pi F\tau)\cdot U(t - t_s - \tau). \tag{3-19}$$

The corresponding in-phase and quadrature components are

$$I(t) = A\cdot U(-t) + A J_0(\pi F\tau)\cos(\pi F\tau)\cdot[U(t) - U(t - t_s - \tau)]$$

$$+ A\cos(2\pi F\tau)\cdot U(t - t_s - \tau) \tag{3-20a}$$

and

$$Q(t) = A J_0(\pi F\tau)\sin(\pi F\tau)\cdot[U(t) - U(t - t_s - \tau)]$$

$$+ A\sin(2\pi F\tau)\cdot U(t - t_s - \tau). \tag{3-20b}$$

To characterize the IF filter's response to these inputs, we use the notation $S(t)$ to denote the equivalent lowpass filter's response to the unit step function, that is,

$$S(t) \triangleq \int_0^t dx\, h_0(t - x) \tag{3-21a}$$

$$= \int_0^t dx\, h_0(x) = P_G[2\sqrt{\pi}W_{IF}(t - t_d)], \tag{3-21b}$$

where $P_G(\cdot)$ denotes the Gaussian cumulative probability distribution function and t_d is the filter delay. The quadrature components at the output of the IF filter then are

40

$$v(t) = A \cdot S(-t) + A J_0(\pi F\tau) \cos(\pi F\tau) \cdot [S(t) - S(t - t_s - \tau)]$$

$$+ A \cos(2\pi F\tau) \cdot S(t - t_s - \tau) \qquad (3\text{-}22a)$$

and

$$u(t) = A J_0(\pi F\tau) \sin(\pi F\tau) \cdot [S(t) - S(t - t_s - \tau)]$$

$$+ A \sin(2\pi F\tau) \cdot S(t - t_s - \tau). \qquad (3\text{-}22b)$$

Assuming that the filter delay is approximately one symbol duration, that is, about $50\,\mu\text{sec}$, and that the combined switching time and synch offset $t_s + \tau$ are much less than this delay, say about $10\,\mu\text{sec}$, the filtered transient amplitude and phase functions $a_t(t)$ and $\phi_t(t)$ at the output of the IF filter, given by

$$a_t(t) = [u^2(t) + v^2(t)]^{1/2} \qquad (3\text{-}23a)$$

and

$$\phi_t(t) = \tan^{-1}[u(t)/v(t)], \qquad (3\text{-}23b)$$

are as sketched in Figure 3-2 for the assumption of a large value of $\pi F\tau$. The cases considered in that figure are

$$\pi F\tau = m, \ m \pm \tfrac{1}{4}, \ m \pm \tfrac{1}{2}, \qquad (3\text{-}24)$$

where m is an integer. It is evident that the transition event takes place over the time interval defined by

$$|t - t_d - \tfrac{1}{2}(t_s + \tau)| < 3\sigma_h = \frac{3 T_c}{2\sqrt{\pi}} \approx T_c, \qquad (3\text{-}25)$$

assuming that $W_{IF} T_c = 1$, and that in general the signal is subject to an attenuation or energy loss during this interval when the phase is switching. For this reason, it is to be expected that the system noise at the IF filter output will largely determine the value of phase during this transient interval. The critical case is seen to be $\pi F\tau$ equal to an integer plus $\tfrac{1}{2}$, since for this case the signal amplitude decreases momentarily to zero and the (modulo-2π) phase changes rapidly by $\pm \pi$, even in the absence of noise. It is highly likely that an FM noise click or rapid 2π phase shift will occur in this case also.

The conclusion to be drawn from this analysis is that the effects of the transient phase difference between the incoming hopping waveform and the receiver's synthesizer are primarily confined to the interval $(0, T_c + t_s + \tau)$, referenced to the input of the receiver with $t = 0$ at the instant that the incoming signal begins to switch frequencies. Therefore, a one-symbol guard time is advisable before resuming the transmission of data. Typically, as has been mentioned, the amplitude shaping and other procedures designed to control emissions dictate a larger off time, and so are the controlling factor in the determination of what fraction of the dwell time may be used to transmit data.

41
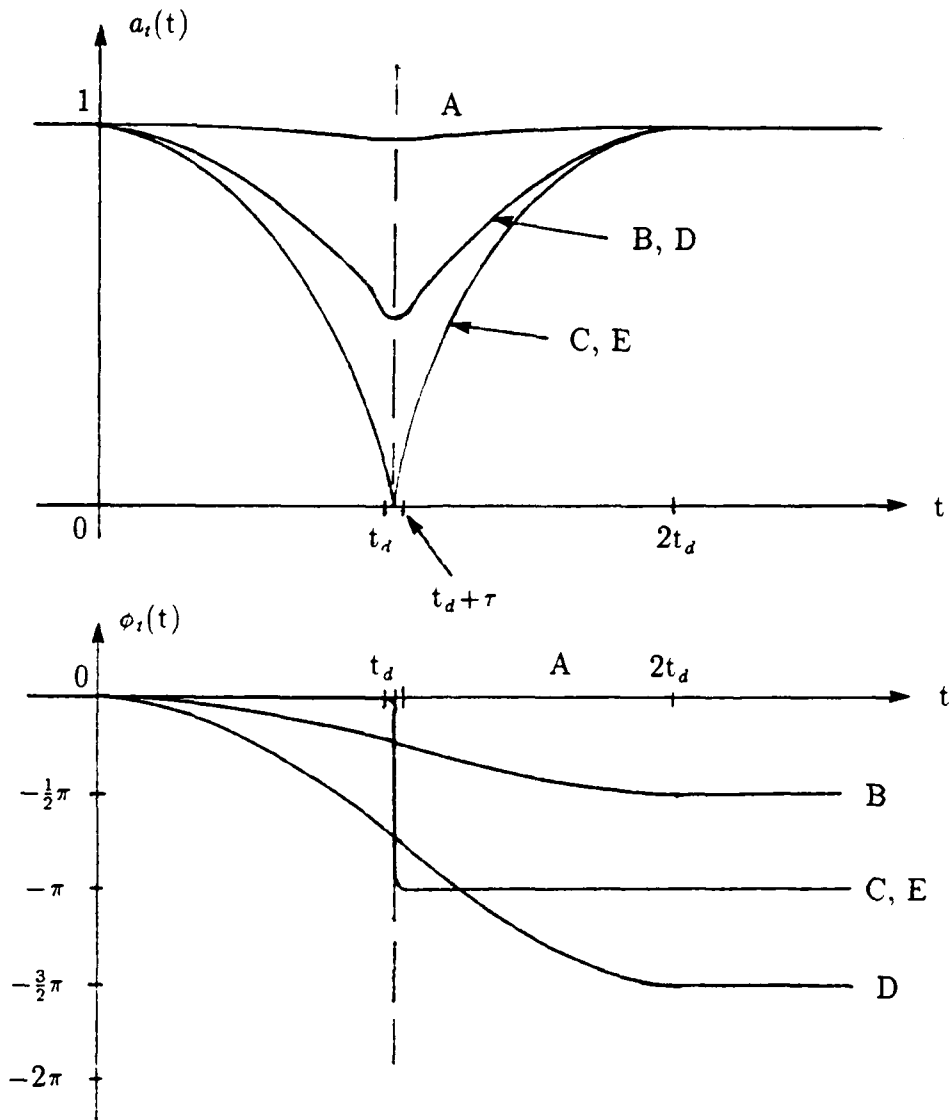
FIGURE 3-2 IF SIGNAL AMPLITUDE AND PHASE TRANSIENT WAVEFORMS

4.0 INVESTIGATION OF ECCM COMBINING TECHNIQUES

In this section we summarize investigations of the effectiveness of various *ad hoc* diversity combining techniques for improving the uncoded performance of FH/CPFSK in worst-case partial-band noise jamming. Techniques used in conjunction with the limiter-discriminator receiver are discussed in Section 4.2, and those pertaining to the differential detector are treated in Section 4.3.

4.1 BACKGROUND: NONCOHERENT COMBINING LOSS

When the FH/CPFSK signal is accompanied by stationary Gaussian noise only (either background noise or continuously present noise jamming), the use of multihop per symbol diversity is not called for, except perhaps to reduce the interceptability of the signal by spreading the signal energy in frequency. As illustrated in Figure 4-1, for noise-only conditions the unjammed probability of bit error increases with L, the number of times the bit is split into chips which are transmitted on different hops, with the bit recovered by examining the sign of the sum of the demodulated differential phase samples. This loss in performance as L increases is commonly termed "noncoherent combining loss" (NCL).

4.1.1 Diversity Sum Error without FM Noise Clicks

An understanding of the mechanisms which give rise to NCL for FH/CPFSK systems can be gained by considering a simplified analysis of differential phase combining. If FM noise clicks are ignored, the differential phase samples for L hops/symbol

$$z_{kq} = \Delta\Phi(t_{kq}), \quad q = 1, 2, ..., L \qquad (4\text{-}1)$$

for the kth symbol are approximately Gaussian random variables, with identical means $\mu_z = \Delta\phi$ and variances $\sigma_z^2 = L/\rho$. That is, such is the case when the symbol energy is kept constant as L changes, so that the effective SNR when the samples are taken is ρ/L. The mean value $\Delta\phi$ is the (distorted) differential phase in the absence of noise.

Using then the approximation that the samples are Gaussian random variables, the sum of the L differential phases is approximately Gaussian with mean $L\mu_z = L\Delta\phi$ and variance $L\sigma_z^2 = L^2/\rho$, denoted by

$$z_k = \sum_{q=1}^{L} z_{kq}$$

$$\approx G(L\Delta\phi, L^2/\rho) = L \cdot G(\Delta\phi, 1/\rho). \qquad (4\text{-}2)$$
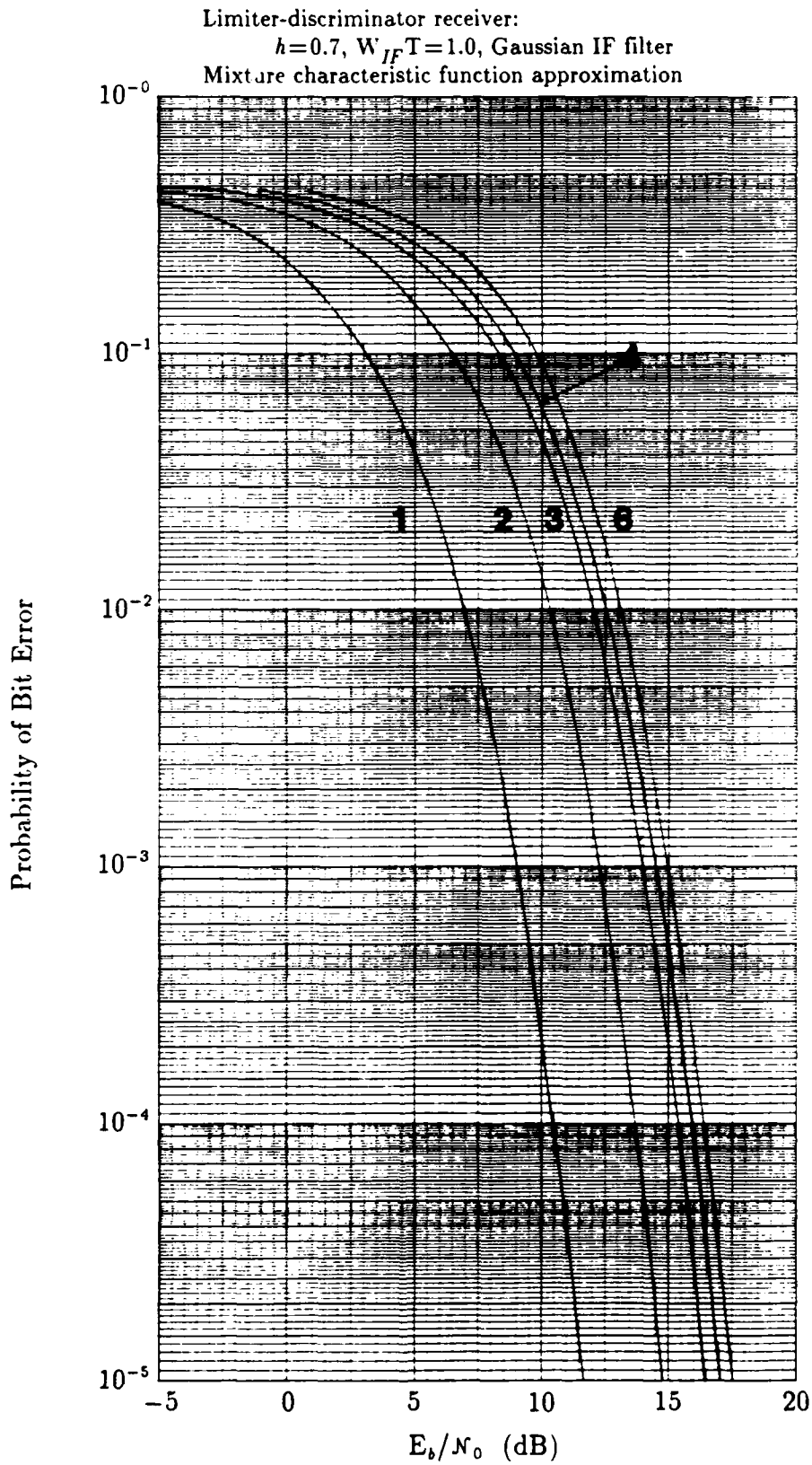
43

FIGURE 4-1 UNJAMMED P_e FOR FH/CPFSK FOR $L = 1, 2, 3, 4, 6$

44

In (4-2) we use $G(\mu, \sigma^2)$ to represent a Gaussian random variable with mean μ and variance σ^2, and in the last line of (4-2) we make use of the fact that multiplication of such a random variable by a constant K gives $K \cdot G(\mu, \sigma^2) = G(K\mu, K^2\sigma^2)$.

Now, since the symbol decision is made of the basis of the sign of z_k, (4-2) implies that in the absence of FM clicks, the symbol error probability for any value of L is approximately given by

$$
\begin{aligned}
P_e(L) &= \Pr\{z_k < 0 \mid d_k = 1\} \\
&\approx \Pr\{L \cdot G(\Delta\phi, 1/\rho) < 0\} \\
&= \Pr\{G(\Delta\phi, 1/\rho) < 0\},
\end{aligned}
\tag{4-3}
$$

which does not depend on the value of L. That is, there is no combining loss.

4.1.2 Effects of FM Noise Clicks

However, when the clicks are included in the analysis, by raising the characteristic function for one of the $\Delta\Phi$ samples[1] to the Lth power we can deduce that the sum of the differential phase samples is conditionally Gaussian, given the value of N_c, the number of clicks. The average number of clicks in the sum is L times $\alpha_L = e^{-\rho/L}|\Delta\phi|/2\pi$, the average number of clicks for one hop, and if $N_c = n$, the Gaussian variable's mean and variance are

$$
\mu_n = L\Delta\phi - \text{sgn}(\Delta\phi) \cdot 2\pi n, \quad \sigma_n^2 = L^2/\rho.
\tag{4-4}
$$

Thus with clicks included in the analysis, the error probability is

$$
P_e(L) \approx \sum_{n=0}^{\infty} \frac{(L\alpha_L)^n}{n!} e^{-L\alpha_L} \Pr\{G(\Delta\phi - \tfrac{2\pi n}{L}, 1/\rho) < 0\}
\tag{4-5a}
$$

$$
= \sum_{n=0}^{\infty} \frac{(L\alpha_L)^n}{n!} e^{-L\alpha_L} Q_G[(\Delta\phi - \tfrac{2\pi n}{L})\sqrt{\rho}],
\tag{4-5b}
$$

which clearly does depend on the value of L. In (4-5b), $Q_G(\cdot)$ is the Gaussian complementary cumulative distribution function.

To provide a numerical example, let $\Delta\phi$ be positive. Then we have for $L = 1$ and for $L = 2$ the following results:

$$
\begin{aligned}
P_e(1) &= e^{-\alpha_1}Q_G(\Delta\phi\sqrt{\rho}) + \alpha_1 e^{-\alpha_1}Q_G[(\Delta\phi - 2\pi)\sqrt{\rho}] + \cdots \\
&\approx \alpha_1 e^{-\alpha_1} \to \alpha_1 \text{ for high SNR;}
\end{aligned}
\tag{4-6a}
$$

---

[1] The characteristic function shown in (2-52a) may be used, with $\gamma = 0$ and $\alpha_0 = \alpha_L$.

45

and
$$P_e(2) = e^{-2\alpha_2}Q_G(\Delta\phi\sqrt{\rho}) + 2\alpha_2 e^{-\alpha_2}Q_G[(\Delta\phi-\pi)\sqrt{\rho}] + \cdots$$

$$\approx 2\alpha_2 e^{-2\alpha_2} \rightarrow 2\alpha_2 \text{ for high SNR.} \tag{4-6b}$$

Thus for high SNR the ratio of $P_e(2)$ to $P_e(1)$ is about equal to

$$P_e(2)/P_e(1) \approx 2\alpha_2/\alpha_1 = 2e^{r/2}. \tag{4-6c}$$

Because of the amplitude distortion $a(t)$, the SNR is less than $E_b\backslash N_0$; a typical value is $\rho = 0.7 E_b\backslash N_0$. For $E_b\backslash N_0 = 10\,\mathrm{dB}$, then, (4-6c) gives a ratio of 66.2. In Figure 4-1, the ratio of error probabilities for $L=1$ and $L=2$ when $E_b\backslash N_0 = 10\,\mathrm{dB}$ is 0.0133/0.0002 = 66.5. This agreement confirms that the so-called noncoherent combining loss for limiter-discriminator detection of CPFSK is attributable to the FM noise clicks.

When the FH/CPFSK system is subject to full-band noise jamming, the NCL shows up as different asymptotes (minimum error) for fixed $E_b\backslash N_0$ as jamming power is decreased. For example, in Figure 4-2 we show the effect of full-band jamming on the error probability for an L hop/bit FH/CPFSK system with linear (sum) combining of the differential phase chips when $E_b\backslash N_0$ is selected to give a 10^{-5} P_e for $L=1$.

4.2. HARD-DECISION COMBINING RECEIVER

For the hard-decision (HD) receiver for FH/CPFSK, a polarity (± 1) decision is made as each chip is received,—equivalent to estimating the original chip sequence d_{kq} by $\hat{d}_{kq}$—and the bit or symbol decision after all L chips have been received is according to the rule

$$\hat{d}_k = \text{sign}\left\{\sum_{q=1}^{L} \hat{d}_{kq}\right\}. \tag{4-7}$$

4.2.1 Analysis of the HD Receiver

A correct symbol decision is made if a majority of the chip decisions are correct[2]: in the case of a tie, which is only possible if L is even-valued, a random binary decision is made. Therefore, the probability of error for a hard decision combining receiver is

$$P_e(L; R_N, R_J, \gamma) = \sum_{k=0}^{(L-1)/2} \binom{L}{k} (1-p_1)^k p_1^{L-k}, \quad L \text{ odd} \tag{4-8a}$$

$$= \sum_{k=0}^{(L-2)/2} \binom{L}{k} (1-p_1)^k p_1^{L-k} + \tfrac{1}{2}\binom{L}{L/2}[(1-p_1)p_1]^{L/2}, \quad L \text{ even} \tag{4-8b}$$

where

$$p_1 \triangleq P_e(1; \tfrac{1}{L}R_N, \tfrac{1}{L}R_J, \gamma) \tag{4-8c}$$

and where we have used the notation $R_N = E_b/N_0$ and $R_J = E_b/N_J$.

---

[2]Note that this rule is equivalent to using the sign of the median of the L chips, for L odd.
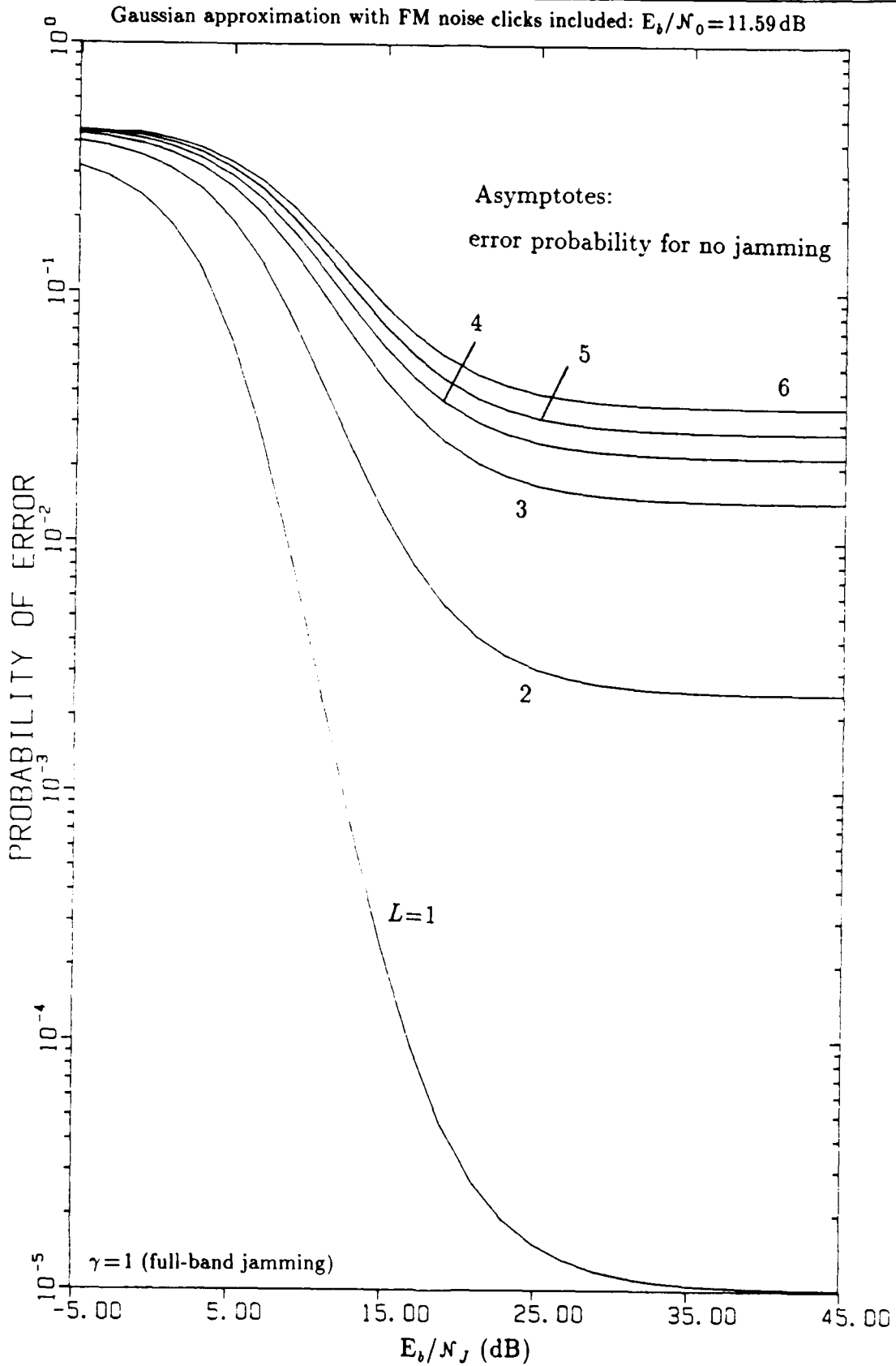
FIGURE 4-2 EFFECT OF FULLBAND JAMMING ON L HOPS/BIT FH/CPFSK

By reversing the order of these sums, the functional form for $P_e(L)$ can also be written

$$P_e(L) = \sum_{k=m+1}^{2m+1} \binom{2m+1}{k} p_1^k (1-p_1)^{2m+1-k} \qquad \text{for } L=2m+1 \text{ (odd)} \qquad (4\text{-}9a)$$

$$= \sum_{k=m+1}^{2m+2} \binom{2m+2}{k} p_1^k (1-p_1)^{2m+2-k} - \tfrac{1}{2}\binom{2m+2}{m+1}[(1-p_1)p_1]^{m+1}$$

$$\text{for } L=2m+2 \text{ (even)}. \qquad (4\text{-}9b)$$

By substituting

$$\binom{2m+2}{k} = \binom{2m+1}{k} + \binom{2m+1}{k-1} \qquad (4\text{-}10a)$$

into the the equation for L even, and noting that

$$\binom{2m+1}{k} = 0 \quad \text{for } k > 2m+1, \qquad (4\text{-}10b)$$

it is straightforward to establish that the functional form of P_e as a function of p_1 for L even is the same as for the next lower odd value of L. For example, functionally,

$$P_e(2; p_1) = P_e(1; p_1) = p_1. \qquad (4\text{-}11a)$$

$$P_e(4; p_1) = P_e(3; p_1) = 3p_1^2 - 2p_1^3, \text{ etc.} \qquad (4\text{-}11b)$$

A general expression can be found by noting that [17, §6.6]

$$P_e(2m+1; p_1) = \frac{(2m+1)!}{m!\,m!} \int_0^{p_1} dx \, (1-x)^m x^m$$

$$= \frac{(2m+1)!}{m!\,m!} \sum_{n=0}^{m} \binom{m}{n} \frac{(-1)^n}{m+n+1} p_1^{m+n+1}. \qquad (4\text{-}12)$$

However, it should be noted that p_1 itself is a function of L, as stated in its definition above. The practical application of this observation about the functional form of P_e for the HD receiver is that in programming any calculations of $P_e(L)$, we may consider only odd values of L. The error probability for even values of L can be obtained after computing $P_e(L-1)$ simply by replacing the ratios R_N and R_J with $R_N \times (L-1)/L$ and $R_J \times (L-1)/L$ and then reusing the subroutine for $P_e(L-1)$ to compute $P_e(L)$.

In [8] it was shown that a precise expression for p_1 is

$$p_1 = \langle (1-\gamma) F(R_N/L) + \gamma F(R_T/L) \rangle_{\text{ISI patterns}} \qquad (4\text{-}13a)$$

where for a particular ISI pattern (indexed by the parameters $\Delta\phi$, U, V, and W) and

using a limiter-discriminator receiver,

$$F(R) = 1 - e^{-\alpha} + e^{-\alpha}\,\frac{r\sin\Delta\phi}{4\pi}\int_{-\pi/2}^{\pi/2} dx \,\frac{\exp\left\{\frac{U-V\sin x+W\cos x}{1+r\cos\Delta\phi\cos x}\right\}}{1+r\cos\Delta\phi\cos x}$$

$$+ e^{-\alpha}\,\frac{W\sin\Delta\phi}{4\pi}\int_{-\pi/2}^{\pi/2} dx \,\frac{\exp\left\{\frac{U-V\sin x-W\cos\Delta\phi\cos x}{1-r\cos x}\right\}}{1-r\cos x}. \quad (4\text{-}13\text{b})$$

An accurate approximation for modulation and receiver parameters $h=0.7$, $W_{IF}T=1.0$, and a Gaussian IF filter, is the following:

$$\langle F(R)\rangle \approx \begin{cases} \frac{1}{2}\exp\{-.974717\,R\}, & R < 0.5 \\ .346664\exp\{-.705883\,R+.115918\,R^{-1}\} & R \geq 0.5. \end{cases} \quad (4\text{-}14)$$

Figure 4-3 shows a comparison of this approximation with the exact unjammed error probability. Note that a linear scale is used for the SNR.

4.2.2 Results Using the HD Receiver with Diversity

Using the approximation given above for the chip error probability as a function of SNR, we calculated the uncoded performance of hard-decision combining of L-hop/bit FH/CPFSK in worst-case partial-band noise jamming. The worst-case result was found by maximizing $P_e(L; \gamma)$ with respect to γ, the partial-band jamming fraction, for given values of R_N and R_J.

In Figures 4-4 and 4-5. for $E_b/N_0 = 20\,\text{dB}$, we show the worst-case P_e for $L=1$ to 7 and for $L=7$ to 12, respectively. As noted above, characteristically for the hard-decision receiver, $P_e(L=2m) > P_e(L=2m-1)$, that is, the error is higher for $L=2$ than for $L=1$. higher for $L=4$ than for $L=3$, etc. This behavior is attributable to the necessity of making a random decision in the case of a tie when L is even-valued. Except for this predictable variation. the trend is that the value of R_J required for a 10^{-5} uncoded bit error probability decreases as L increases, indicating a diversity gain.

For clarity, the error curves for only the odd values of L are plotted in Figure 4-6. Here the facts that there is a diversity gain and an optimum value of diversity are more clearly observable. Not that the error curves are "inverse linear" for the given scale, with slopes equal to $-\frac{1}{2}(L+1)$, revealing that the worst-case error is inversely proportional to the $\frac{1}{2}(L+1)$th power of the signal enery-to-jamming noise density, R_J.
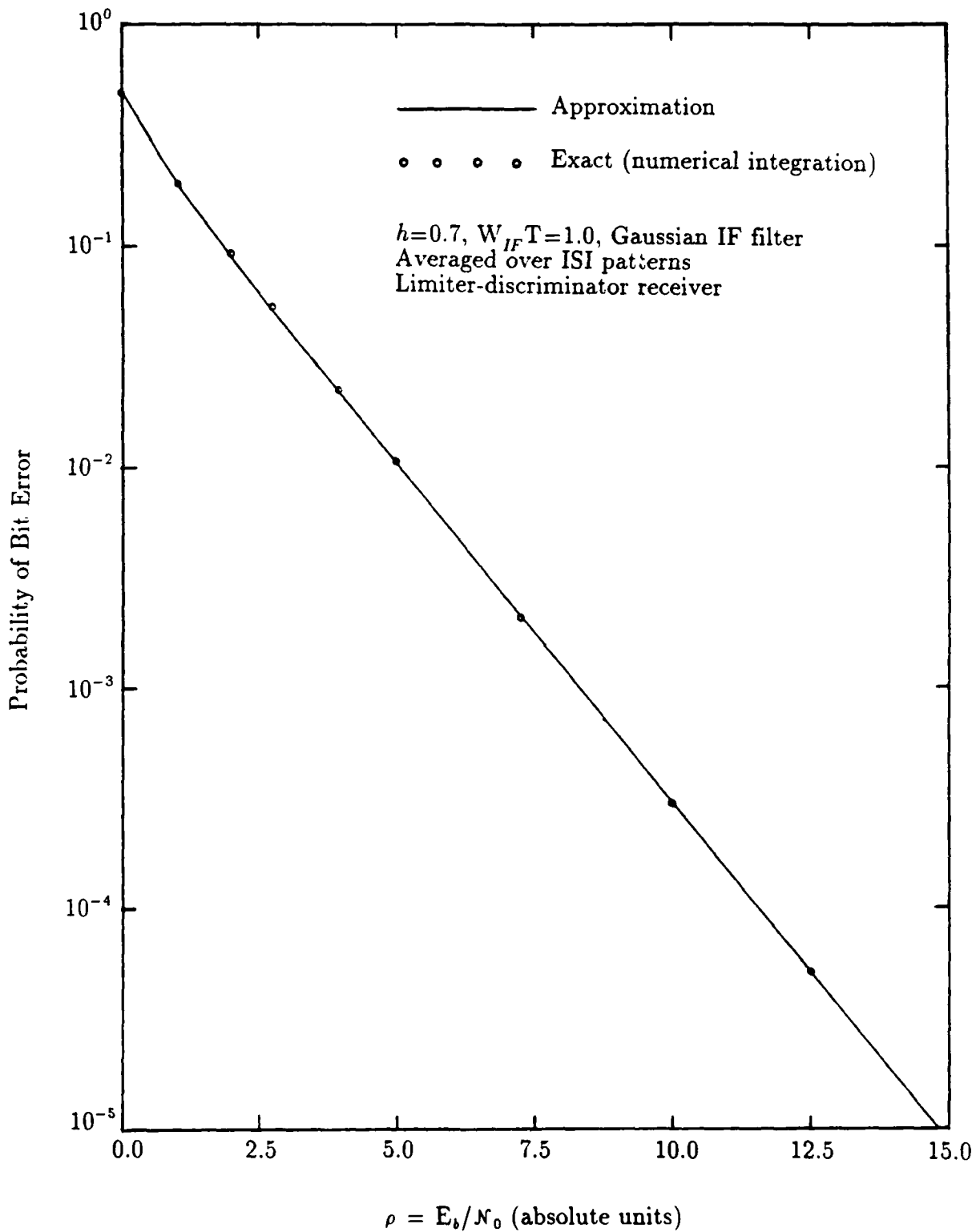
FIGURE 4-3   EXACT AND APPROXIMATE CPFSK ERROR PROBABILITY
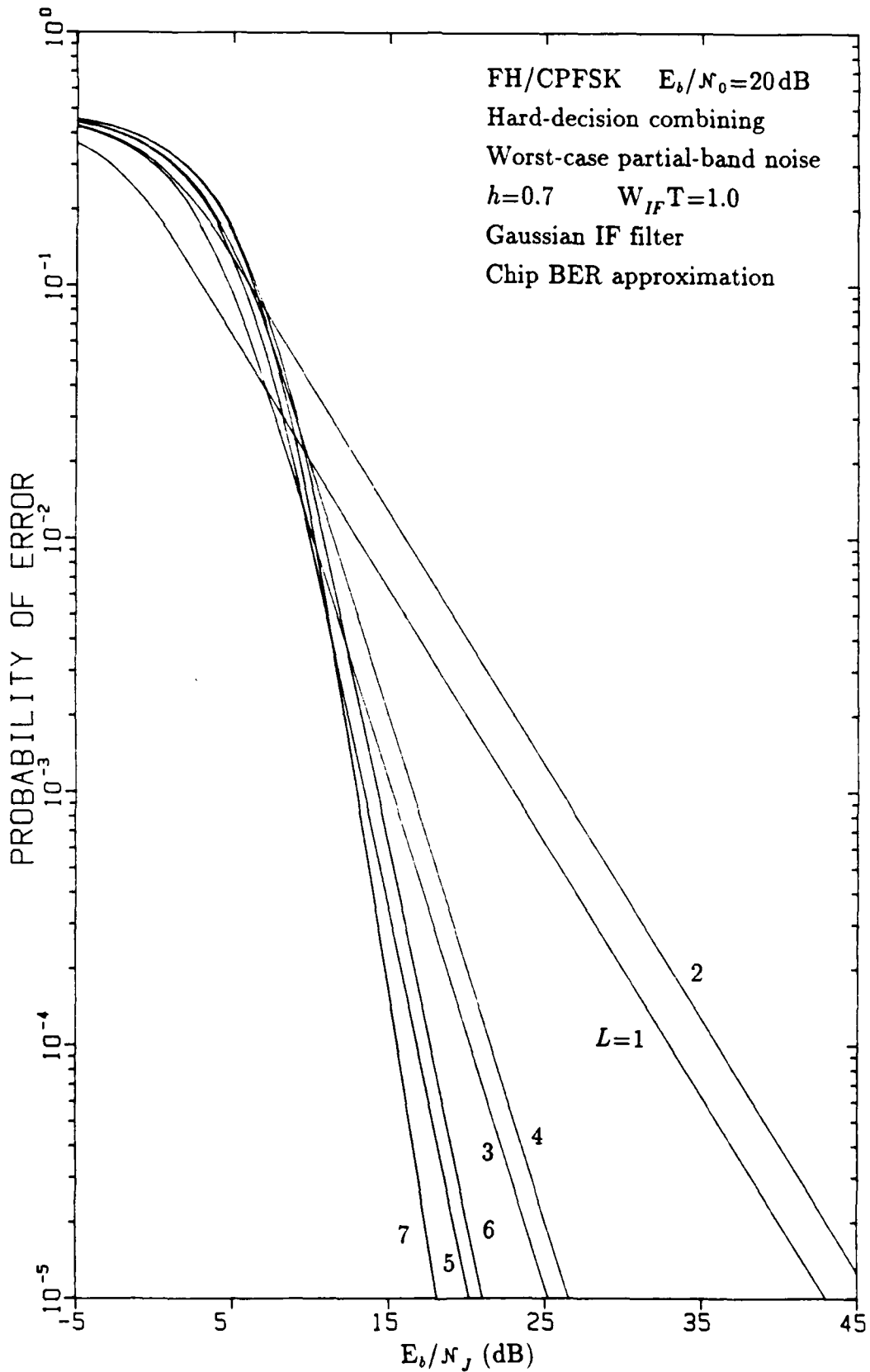COMPARISON FOR LIMITER-DISCRIMINATOR DETECTION

FIGURE 4-4   HARD-DECISION DIVERSITY PERFORMANCE FOR $L=1$ TO 7
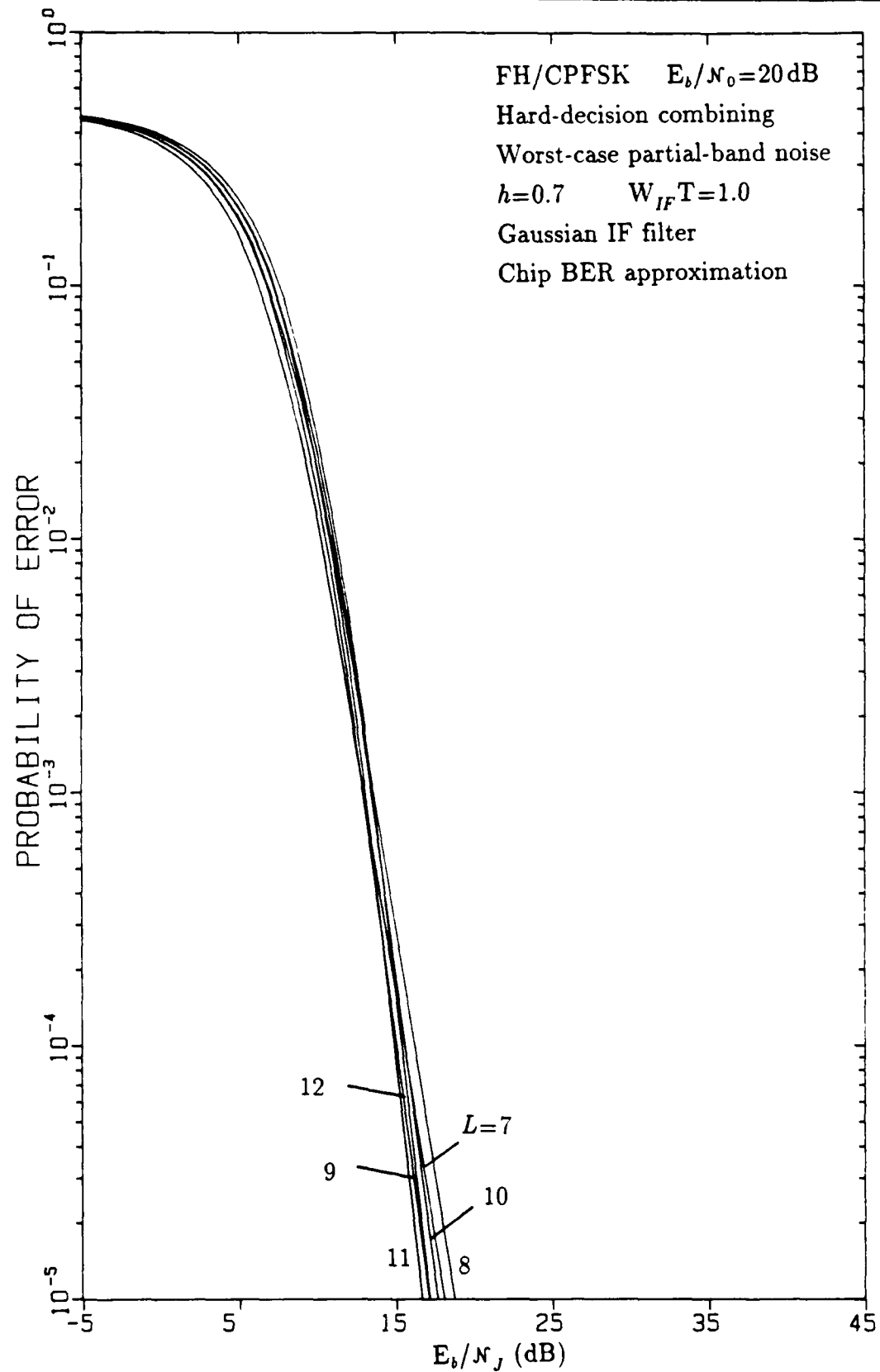
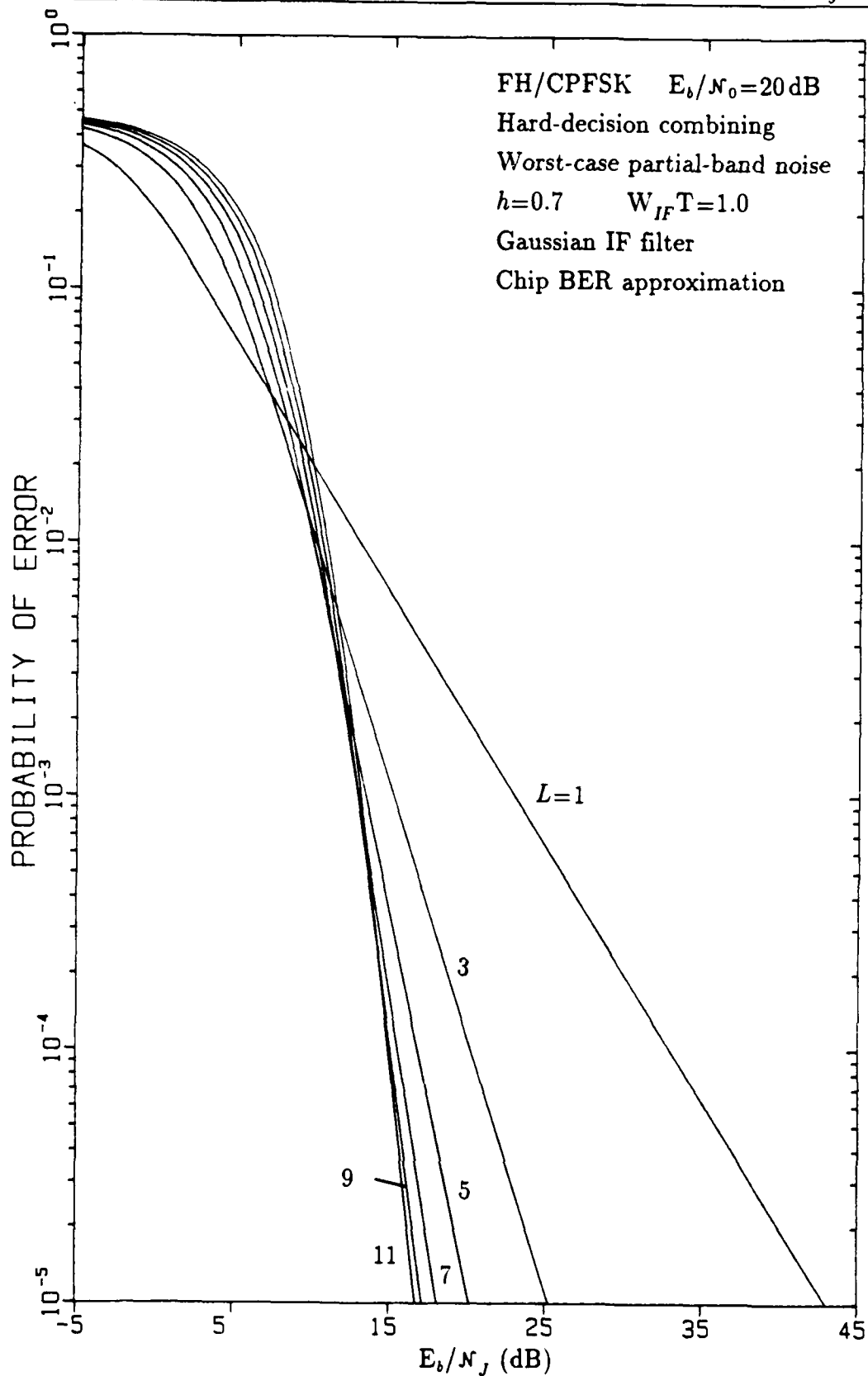FIGURE 4-5   HARD-DECISION DIVERSITY PERFORMANCE FOR $L=7$ TO 12

FIGURE 4-6   HARD-DECISION DIVERSITY PERFORMANCE FOR ODD L

If E_b/N_0 is reduced (the thermal and system noise is increased relative to the signal energy), the noncoherent combining losses (NCL) will affect the diversity gains against the jamming. In Figure 4-7, for $E_b/N_0 = 15\,dB$, we observe that the maximum value of optimum diversity is $L=7$, for a narrow range of R_J around the value $R_J \approx 20\,dB$, and in Figure 4-8, for $E_b/N_0 = 13\,dB$, the highest value of diversity for which improvement is noted is $L=3$. It is apparent also from Figure 4-8 that, as the thermal noise increases, the NCL for hard-decision combining is significantly greater for even values of L than it is for odd values.

4.3 LIMITER-DISCRIMINATOR TECHNIQUES

In this subsection we summarize our analysis and present numerical results connected with studies of possible ECCM weighting schemes to enhance the performance of a limiter-discriminator-based FH/CPFSK receiver against partial-band noise jamming.

4.3.1 Approximations to the Differential Phase PDF and CDF

Analytically it is quite convenient to utilize the probability of error expression involving the characteristic function (CHF) of the diversity sum decision variable, z:

$$P_e = \tfrac{1}{2} - \tfrac{1}{\pi}\int_0^\infty \frac{d\nu}{\nu}\,\mathrm{Im}\{\,C_z(\nu)\,\}. \tag{4-15}$$

The convenience associated with using this form arises from the fact that the CHF for the sum of L independent, identically distributed random variables is simply that for one variable, raised to the Lth power:

$$C_z(\nu) = [\,C_{z_q}(\nu)\,]^L \tag{4-16a}$$

when
$$z = \sum_{q=1}^{L} z_q. \tag{4-16b}$$

A general expression for $C_{z_q}(\nu)$ was given in Section 2.3, including FM noise clicks and partial-band noise jamming. To use that expression, it is necessary to formulate the CHF corresponding to $p_\psi(x)$, the probability density function (PDF) for a single 2π interval of possible $\Delta\Phi$ sample values. Thus we require an expression for

$$C_\psi(\nu) = \int_{-\infty}^{\infty} dx\, e^{j\nu x}\, p_\psi(x). \tag{4-17}$$

Unfortunately, an exact analytical expression for this CHF cannot be found in closed form, since $p_\psi(x)$ itself, given previously in (2-29), is in integral form. Therefore we have investigated several approximate expressions.
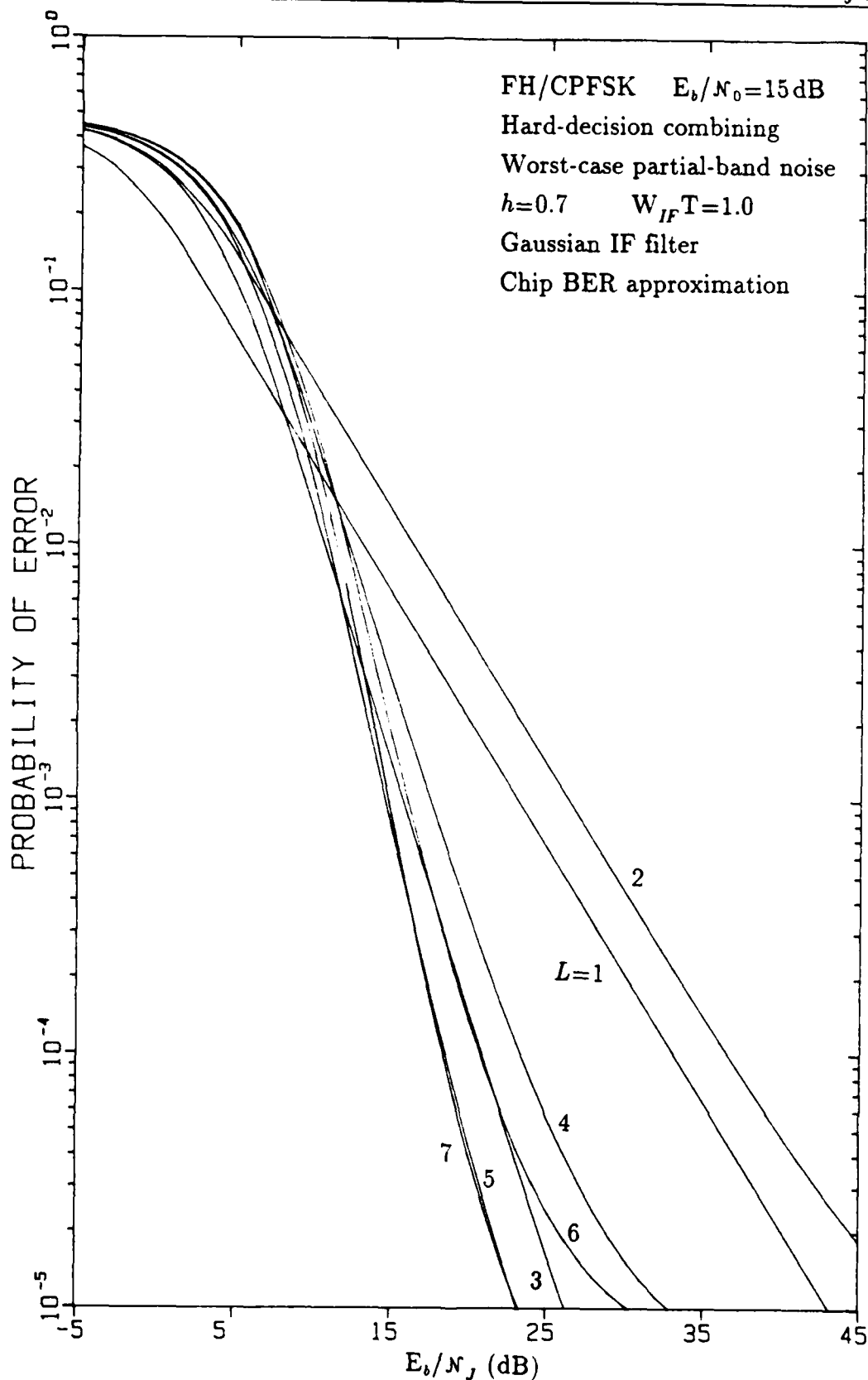
FIGURE 4-7   HARD-DECISION DIVERSITY PERFORMANCE FOR $E_b/\mathcal{N}_0=15\,\text{dB}$

FH/CPFSK $E_b/\mathcal{N}_0 = 13\,$dB
Hard-decision combining
Worst-case partial-band noise
$h = 0.7$ $W_{IF}T = 1.0$
Gaussian IF filter
Chip BER approximation
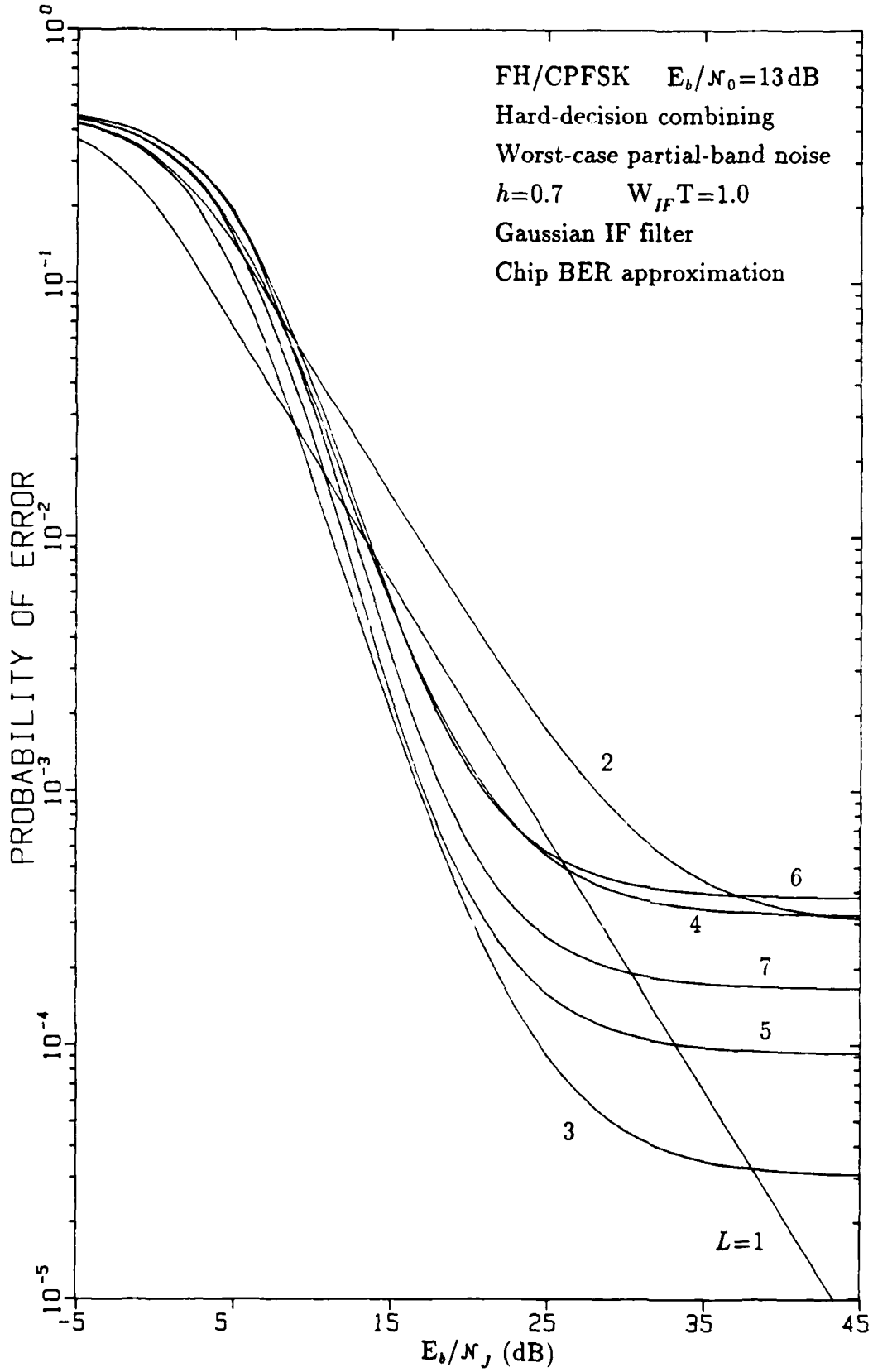
FIGURE 4-8   HARD-DECISION DIVERSITY PERFORMANCE FOR $E_b/\mathcal{N}_0 = 13\,$dB

4.3.1.1 Expansion of the CHF in terms of cumulants

The CHF for a random variable x can be expressed in terms of its moments or in terms of its distribution's semi-invariants or cumulants. The general expression is

$$C_x(\nu) = \sum_{r=0}^{\infty} \frac{(j\nu)^r}{r!}\, m_r \tag{4-18}$$

$$= \exp\left\{ \sum_{n=1}^{\infty} \frac{(j\nu)^n}{n!}\, \kappa_n \right\}, \tag{4-19}$$

in which the quantities $\{m_r\}$ are the (noncentral) moments and the $\{\kappa_n\}$ are the semi-invariants or cumulants [17]. For example, in terms of the moments, some of the cumulants can be shown to be

$$\kappa_1 = m_1 \tag{4-20a}$$
$$\kappa_2 = \sigma^2 = m_2 - m_1^2 \tag{4-20b}$$
$$\kappa_3 = m_3 - 3\,m_1 m_2 - m_1^3 \tag{4-20c}$$
$$\kappa_4 = m_4 - 4\,\kappa_1\kappa_3 - 3\,\kappa_2^2 - 6\,\kappa_1^2\kappa_2 - \kappa_1^4. \tag{4-20d}$$

For the Gaussian distribution, all the cumulants higher than κ_1 and κ_2 (the mean and variance) are zero.

Since for high SNR the PDF for the modulo-2π differential phase is approximately Gaussian [13, 18], we reasoned that the CHF $C_\psi(\nu)$ could be well-approximated by a truncated version of (4-19),

$$C_\psi(\nu) \approx e^{j\nu\,\Delta\phi}\exp\left\{ \sum_{n=1}^{6} \frac{(j\nu)^n}{n!}\, \kappa_n \right\}, \tag{4-21a}$$

using exact cumulant values obtained from calculations of the moments about $\Delta\phi$:

$$m_r = E\{(\psi - \Delta\phi)^r\} = \int_{-\pi}^{\pi} dx\; x^r p_\psi(x + \Delta\phi), \tag{4-21b}$$

using the expression given in (2-29) for the PDF of ψ.

For zero SNR (noise only), $p_\psi(x)$ is the uniform PDF, with zero-valued odd moments and even moments given by

$$m_{2r} = \frac{\pi^{2r}}{2\,r+1} \tag{4-22a}$$

which give rise to zero-valued odd cumulants ($\kappa_1 = \kappa_3 = \kappa_5 = 0$) and

$$\kappa_2 = \tfrac{1}{3}\pi^2 = 3.29 \tag{4-22b}$$
$$\kappa_4 = -\tfrac{2}{15}\pi^4 = -13.0 \tag{4-22c}$$
$$\kappa_6 = -\tfrac{53}{21}\pi^6 = -1358. \tag{4-22d}$$

It is evident from (4-22) that for sufficiently low SNR, the higher cumulants of the

differential phase PDF do not diminish quickly enough to permit representation of the CHF with a reasonably small number of cumulants. Therefore, this approach to approximating the CHF was abandoned.

4.3.1.2 CHF based on approximation of the PDF

For high SNR, it is well known [18] that the PDF of the modulo-2π differential phase ψ is well approximated by a Gaussian PDF. In Figure 4-9, we show a direct comparison of the exact PDF $p_\psi(x)$ with the PDF for a Gaussian random variable with the same mean and variance. As seen in the figure, the approximation is excellent for high SNR but for low SNR begins to depart significantly from the exact PDF, especially for ψ values near to $\Delta\phi \pm \pi$. Moreover, the region over which the Gaussian PDF has significant value increases with the value of the variance, whereas the exact PDF has the finite domain $|\psi - \Delta\phi| \leq \pi$; therefore, use of the Gaussian characteristic function

$$C_G(\nu) = e^{j\mu\nu - \sigma^2\nu^2/2} \tag{4-23}$$

in the error probability calculation is not expected to approximate the the system performance faithfully for low SNR.

For this reason, we have developed an approximation to the differential phase characteristic function starting with a "truncated Gaussian" PDF that we define by

$$p_{TG}(x) \triangleq \begin{cases} K e^{-x^2/2\sigma_0^2} & \text{for } |x| \leq \pi \\ 0 & \text{elsewhere.} \end{cases} \tag{4-24a}$$

The properties of this distribution are discussed in Appendix B. For example, the normalization factor K in (4-24a) is given by

$$K^{-1} = \sigma_0 \sqrt{2\pi} \ \text{erf}\left(\pi/\sigma_0\sqrt{2}\right), \tag{4-24b}$$

and it can be shown that, as the parameter $\sigma_0 \to \infty$, the PDF $p_{TG}(x)$ becomes a uniform PDF on the interval $(-\pi, \pi)$. Also, the variance of the distribution σ_{TG}^2 is related to σ_0^2 by the expression

$$\sigma_{TG}^2 = \sigma_0^2 \left[1 - \sqrt{2\pi} \ e^{-\pi^2/2\sigma_0^2} \Big/ \sigma_0 \text{erf}\left(\pi/\sigma_0\sqrt{2}\right) \right]. \tag{4-24c}$$

The characteristic function for the truncated Gaussian distribution may be approximated by the "mixture" characteristic function

$$C_M(\nu) \triangleq \epsilon \ \text{sinc}(\nu) + (1-\epsilon)e^{-\sigma_0^2\nu^2/2}, \tag{4-25a}$$
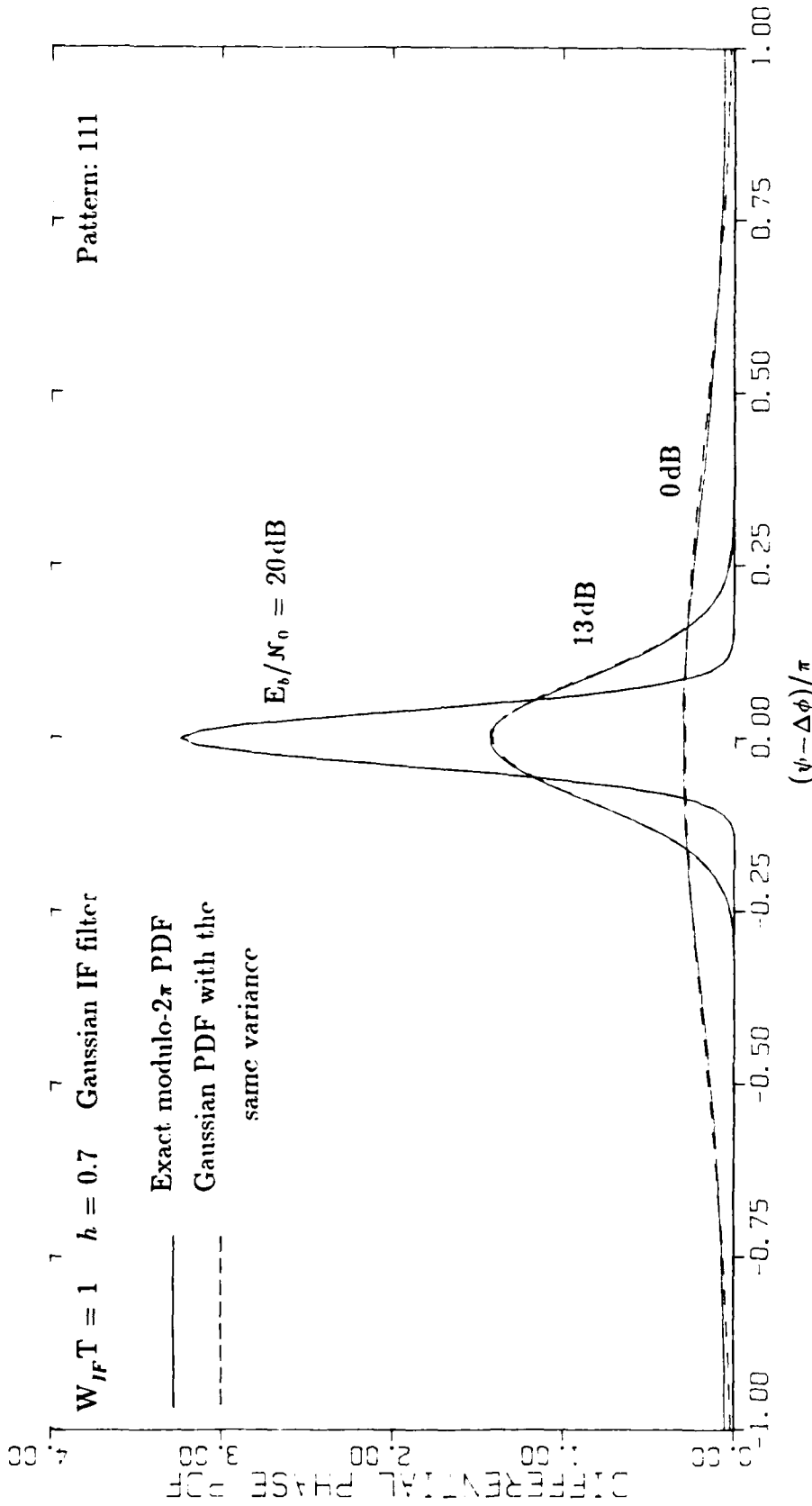
FIGURE 4-9 COMPARISON OF EXACT AND GAUSSIAN APPROXIMATION PDF'S

where the mixture parameter ϵ is SNR-dependent and is given by

$$\epsilon = \sqrt{\pi}\, e^{-\pi^2/2\sigma_0^2}\Big[\sigma_0\sqrt{2}\,\mathrm{erf}\left(\pi/\sigma_0\sqrt{2}\right)\Big]^{-1}; \qquad (4\text{-}25b)$$

also, $\mathrm{sinc}(\nu) \equiv \sin(\pi\nu)/\pi\nu$ is the CHF for the uniform distribution over the interval $(-\pi, \pi)$. The first and second terms of $C_M(\nu)$ correspond to low-SNR (uniform) and high-SNR (Gaussian) versions of the differential phase CHF, that is, $C_M(\nu)$ may be interpreted as

$$C_M(\nu) = \epsilon(\rho)\cdot C_U(\nu) + [1-\epsilon(\rho)]\cdot C_G(\nu), \qquad (4\text{-}25c)$$

with ϵ decreasing as the SNR, ρ, increases.

In effect, the use of (4-25) approximates the differential phase PDF $p_\psi(x)$ by a mixture of of PDF's. Figure 4-10 illustrates the accuracy of this PDF approximation when σ_0^2 is taken to be the inverse function of the truncated Gaussian variance σ^2 given by (4-24c). Evidently, for low SNR this value of σ_0^2 is too high, judging from the curves in Figure 4-10 when $E_b/N_0 = 0\,\mathrm{dB}$.

Taking the mixture approximation concept a step further, we found by trial and error that the differential phase PDF is well approximated by the simple, heuristic approximation based on (4-25a) with ϵ and σ_0^2 given by

$$\epsilon = e^{-2\,\mathrm{SNR}} \qquad (4\text{-}26a)$$

and

$$\sigma_0^2 = \frac{\sigma^2 - \pi^2\epsilon/3}{1-\epsilon}. \qquad (4\text{-}26b)$$

The formula for σ_0^2 is based on matching the actual variance, σ^2, with that of the approximation, $(1-\epsilon)\sigma_0^2 + \pi^2\epsilon/3$. In Figure 4-11, we observe that this simplified mixture approximation gives a better fit to the actual PDF.

In Figure 4-12 we compare the unjammed CPFSK probability of error for $L=1$, as obtained using exact and approximate PDF's, averaged over the intersymbol interference (ISI) patterns. The click average used by the approximations was estimated by

$$\hat{a}_i = \frac{\Delta\phi_i}{2\pi}e^{-U_i} \quad \text{for pattern } i. \qquad (4\text{-}27)$$

For high E_b/N_0, when $\epsilon \ll 1$ and also $\alpha \ll 1$, the approximations all converge to Gaussian approximations and give the same result, as shown, which underestimates the error as if $0.15\,\mathrm{dB}$ were added to E_b/N_0. For $E_b/N_0 < 5.5\,\mathrm{dB}$, all of the approximations overestimate the error probability; it is somewhat surprising that the use of a purely Gaussian approximation. taking care to match only the first two cumulants of the exact differential phase distribution. actually results in the best fit to the exact P_e curve.
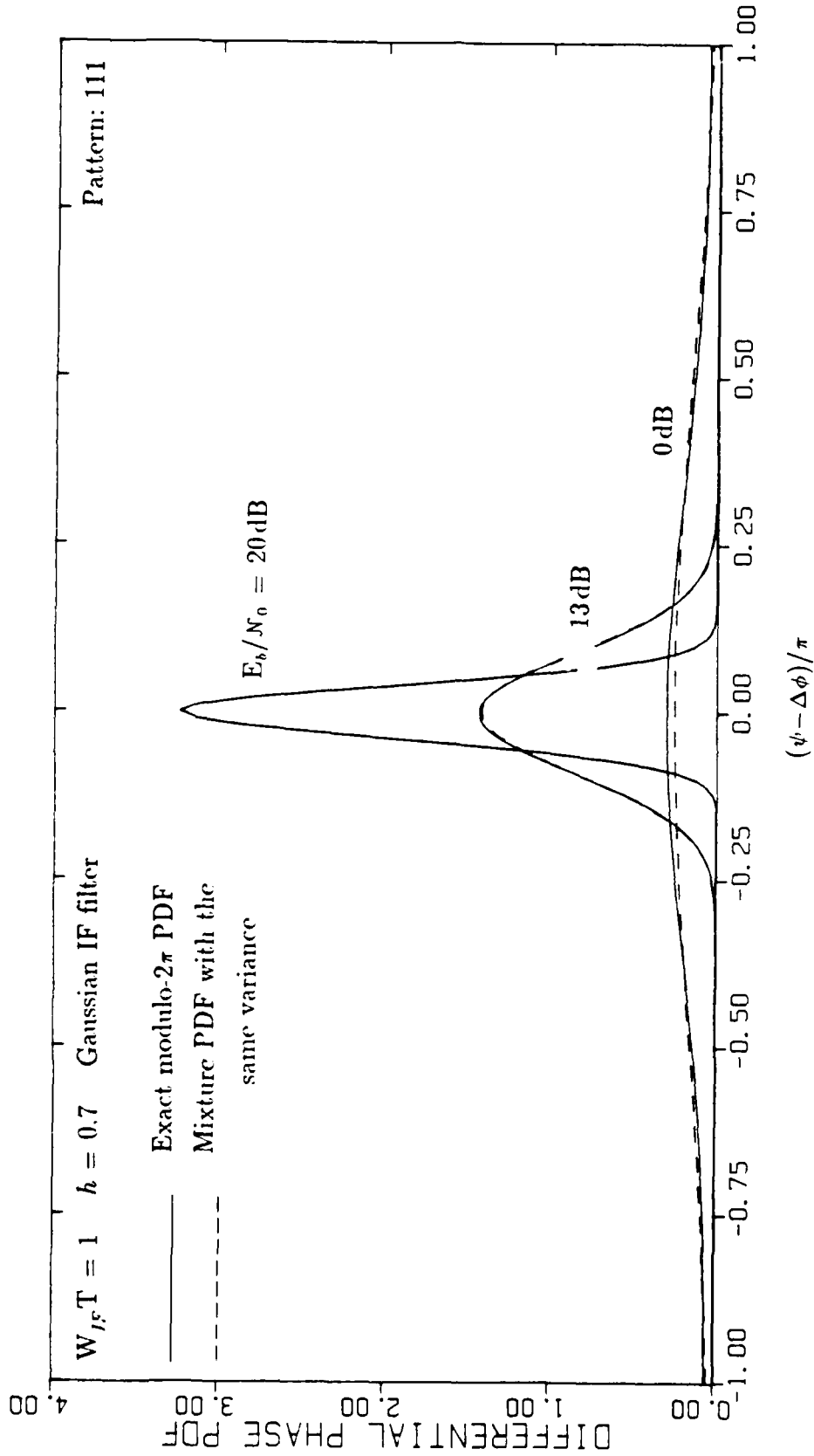
FIGURE 4 10 COMPARISON OF EXACT AND ANALYTICAL MIXTURE APPROXIMATION PDF'S
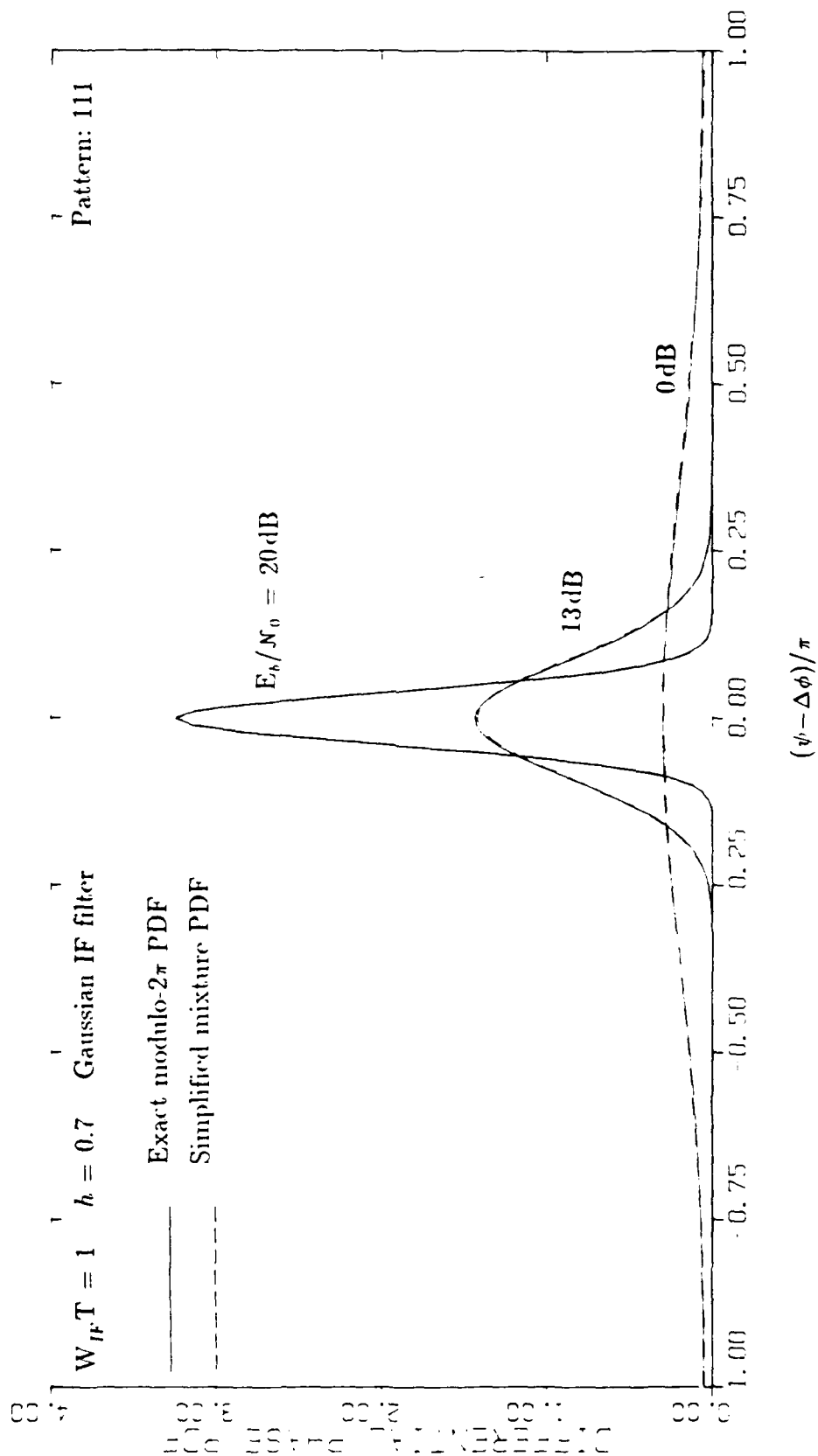
FIGURE 4 11 COMPARISON OF EXACT AND SIMPLIFIED MIXTURE APPROXIMATION PDF'S

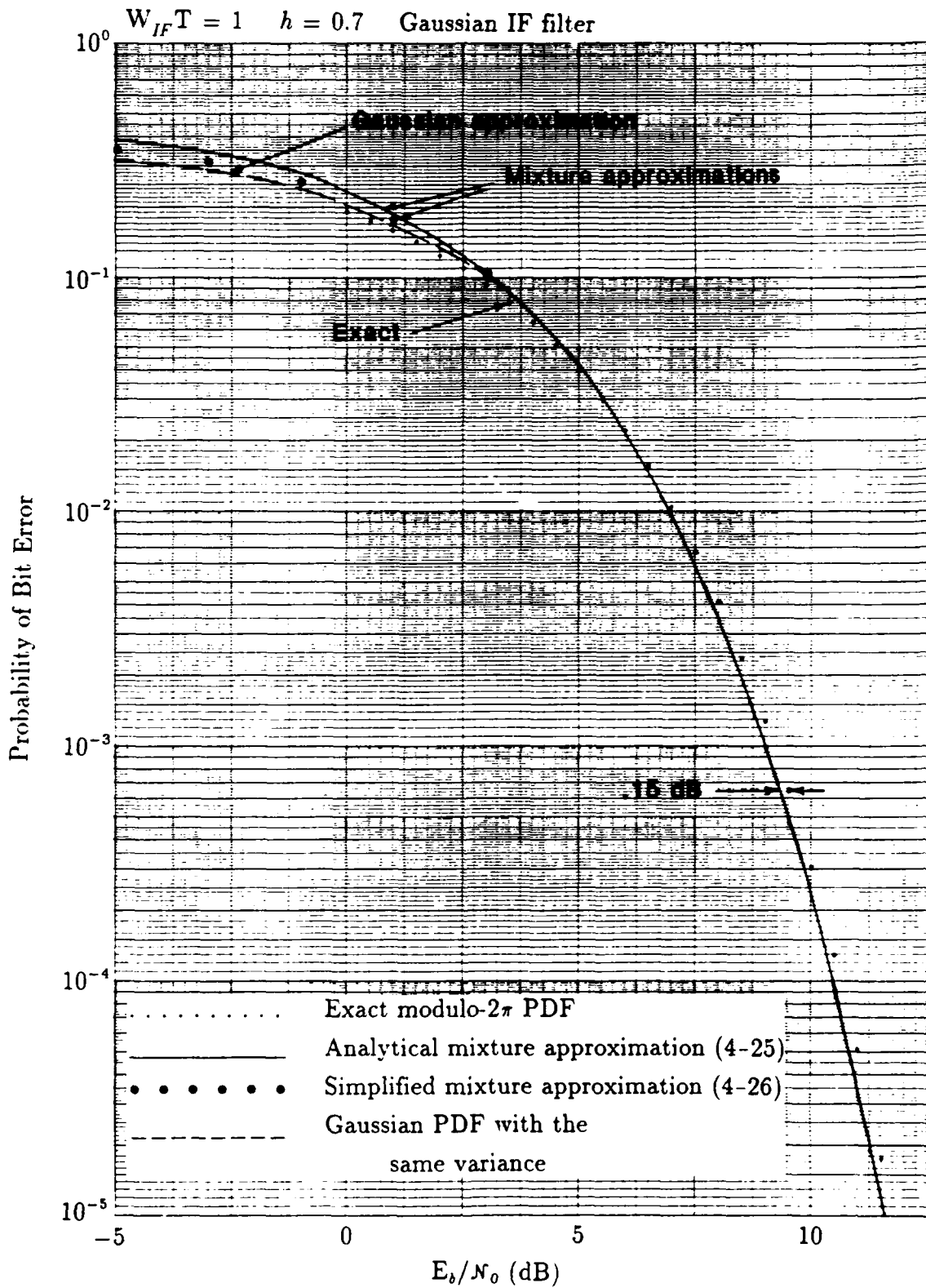$W_{IF}T = 1 \quad h = 0.7 \quad$ Gaussian IF filter

FIGURE 4-12 COMPARISON OF EXACT AND APPROXIMATE CPFSK
BIT ERROR PROBABILITY CALCULATIONS

4.3.2   Adaptive Gain Control (AGC) Scheme

For the case of frequency-hopped noncoherent BFSK in partial-band noise jamming, it has been shown that an "AGC" or adaptive gain control ECCM scheme is successful in mitigating the effects of the jamming [21, 22]. Under this scheme, the different chips constituting a transmitted symbol are weighted in inverse proportion to the noise power on the hops on which they are individually received. Therefore, analysis and computations were performed to evaluate the jammed performance of FH/CPFSK when, as discussed in Section 2.1.4, the differential phase samples $\{z_{k_q}\}$ from different hops are weighted by the factors $\{w_q\}$:

$$z_k = \sum_q^L w_q z_{k_q}. \tag{4-28a}$$

Instead of the weights being the inverses of noise *power* (σ^2) as previously discussed, in this study they are taken to be the inverses of noise standard deviation (σ) according to the relation

$$w_q = 1/\sigma_q \tag{4-28b}$$

$$= 1/\sigma_N. \qquad \text{hop not jammed} \tag{4-28c}$$

$$= 1/\sigma_T. \qquad \text{hop jammed.} \tag{4-28d}$$

The use of σ instead of σ^2 is reasonable in view of the fact that the variance of the phase noise is proportional to that of the IF noise; that is, when corrupted by noise, the differential phase samples are random variables with scale factors $\{\sigma_q\}$. Normalization by σ_q then has the effect of equalizing the noise power received on each hop, thereby reducing the tendency of the stronger noise on the jammed hops from dominating in the sum of weighted differential phase samples.

4.3.2.1   Analysis

Without loss of generality, we can formulate the error probability for the L hops/symbol FH/CPFSK system when an AGC scheme is used by assigning the weights $w_0 = 1$ to unjammed hops and w_1 to jammed hops, where

$$w_1 = \sigma_N/\sigma_T = \sqrt{\rho_T/\rho_N} = 1/\sqrt{\kappa}. \tag{4-29}$$

In Section 2.2.1, an analysis of possible jamming events made use of a conditional characteristic function (CHF) for the sum of the samples, conditioned upon the number of hops which have been jammed. An unconditional CHF for a weighted differential phase sample $\zeta_{k_q} = w_q z_{k_q}$ can be written

$$C_\zeta(\nu; \gamma) = (1-\gamma)\, C_\zeta(\nu; \sigma_N^2) + \gamma\, C_\zeta(w_1\nu; \kappa\sigma_N^2). \tag{4-30}$$

64

The advantage of the unconditional form is that the CHF for the weighted sum is simply the Lth power of the single-sample CHF (4-30), giving for the ith ISI data pattern the error probability expression [a special case of (2-56)]

$$\mathbf{P}_{ei}(L; \gamma) = \tfrac{1}{2} - \tfrac{1}{\pi} \int_0^\infty \frac{d\nu}{\nu} \mid C_{\zeta i}(\nu; \gamma) \mid^L \sin\Big(L \arg[\, C_{\zeta i}(\nu; \gamma)]\Big), \qquad (4\text{-}31)$$

which must be averaged over the variation in parameters due to the ISI patterns, as discussed in Appendix A.

Now, making use of the FM click noise analysis of Section 2.3, we use (2-59) to write (suppressing the ISI-pattern-dependent notation)

$$C_\zeta(\nu; \gamma) = (1-\gamma)\, e^{-\alpha_0(1-\cos 2\pi\nu) - j\alpha_0 \sin 2\pi\nu}\, C_\psi(\nu; \rho_N)$$

$$+ \gamma\, e^{-\alpha_1(1-\cos 2\pi w_1\nu) - j\alpha_1 \sin 2\pi w_1\nu}\, C_\psi(w_1\nu; \rho_T) \qquad (4\text{-}32)$$

in which the pattern-dependent CHF for the modulo-2π differential phase without clicks is denoted by $C_\psi(\nu; \rho)$ when the SNR is ρ, and the click averages α_1 and α_0 are given by (2-28) under jammed and unjammed conditions, respectively. For convenience, we separate the signal and noise components of the differential phase:

$$\nu = \Delta\phi + \Delta\eta. \qquad (4\text{-}33a)$$

Then, $C_\nu(\nu; \rho)$ can be written

$$C_\nu(\nu; \rho) = e^{j\nu\Delta\phi} C_{\Delta\eta}(\nu; \rho), \qquad (4\text{-}33b)$$

and we use the mixture approximation (4-25), calibrated by taking σ_0^2 to be the inverse of the variance $\sigma_\nu^2 = \sigma_{\Delta\eta}^2$ and explicitly accounting for the possibility of a nonzero phase noise mean value $\mu_{\Delta\eta}$ by writing

$$C_{\Delta\eta}(\nu; \rho) = e^{j\nu\mu_{\Delta\eta}}\{\epsilon(\rho)\cdot C_U(\nu) + [1-\epsilon(\rho)]\cdot C_G(\sigma_0\nu)\}. \qquad (4\text{-}33c)$$

The required mean and variance may be calculated using the exact modulo-2π differential phase probability density function $p_\psi(x)$ given as (2-29):

$$\mu_{\Delta\eta} = \mu_{\Delta\eta}(\rho) = \int_{-\pi}^{\pi} dx\, x\, p_\psi(x; \Delta\phi=0) \qquad (4\text{-}34a)$$

and

$$\sigma_{\Delta\eta}^2 = \sigma_{\Delta\eta}^2(\rho) = \int_{-\pi}^{\pi} dx\,(x-\mu_{\Delta\eta})^2 p_\psi(x; \Delta\phi=0). \qquad (4\text{-}35a)$$

The analytical forms of the magnitude and phase of the CHF needed to perform the calculation indicated in (4-31) are somewhat tedious but are straightforward to derive. Again suppressing the notation necessary to remind us of the ISI pattern dependence, the real and imaginary parts are given by

$$\text{Re}\{C_\zeta(\nu;\gamma)\} = (1-\gamma)e^{-\alpha_0(1-\cos2\pi\nu)}\cos[\nu(\Delta\phi+\mu_0)-\alpha_0\sin2\pi\nu]$$
$$\times [\epsilon_0 C_U(\nu)+(1-\epsilon_0) C_G(\sigma_{00}\nu)]$$

$$+ \gamma e^{-\alpha_1(1-\cos2\pi w_1\nu)}\cos[w_1\nu(\Delta\phi+\mu_1)-\alpha_1\sin2\pi w_1\nu]$$
$$\times [\epsilon_1 C_U(w_1\nu)+(1-\epsilon_1) C_G(w_1\sigma_{01}\nu)] \qquad (4\text{-}36\text{a})$$

and

$$\text{Im}\{C_\zeta(\nu;\gamma)\} = (1-\gamma)e^{-\alpha_0(1-\cos2\pi\nu)}\sin[\nu(\Delta\phi+\mu_0)-\alpha_0\sin2\pi\nu]$$
$$\times [\epsilon_0 C_{U}(\nu)+(1-\epsilon_0) C_G(\sigma_{00}\nu)]$$

$$+ \gamma e^{-\alpha_1(1-\cos2\pi w_1\nu)}\sin[w_1\nu(\Delta\phi+\mu_1)-\alpha_1\sin2\pi w_1\nu]$$
$$\times [\epsilon_1 C_{U}(w_1\nu)+(1-\epsilon_1) C_G(w_1\sigma_{01}\nu)], \qquad (4\text{-}36\text{b})$$

in which we have used the subscripts 0 and 1 in a consistent way to denote values of the parameters without and with jamming, respectively.

The total error probability then is, after averaging over the three ISI data patterns,

$$P_e(L;\gamma) = \tfrac{1}{4}[P_{e1}(L;\gamma) + P_{e2}(L;\gamma) + 2P_{e3}(L;\gamma)]. \qquad (4\text{-}37)$$

4.3.2.2   Numerical results

In the computations of FH/CPFSK error probability for L hops per symbol and partial-band noise jamming, the mixture approximation (4-25) based on the truncated Gaussian distribution was utilized. Inadvertently instead of the mixture parameter $\epsilon(\rho)$ given by (4-25b), we in effect used

$$\epsilon' = \frac{\epsilon/2}{1-\epsilon} \qquad (4\text{-}38)$$

but this departure from the analytical procedures described previously did not have a great influence on the result, since computations based on the simplified mixture parameters given by (4-26) did not produce different results in the regions of the computed curves which were of interest.[3]   Files of pre-computed first and second cumulants were used as well as pre-computed ISI parameters based on the assumption that $h = 0.7$, $W_{IF}T = 1.0$, and that a Gaussian-shaped IF filter is used in the receiver.

---

[3]Further comments on this point are made below.

In Figure 4-13, the FH/CPFSK uncoded bit error for $L=1$ is plotted vs. $E_b/\mathcal{N}_J$ for the case of $E_b/\mathcal{N}_0=20\,\text{dB}$ and for various values of the partial-band jamming fraction, γ. It is clear from the figure that the worst-case value of γ (in terms of maximizing the error) is a function of $E_b/\mathcal{N}_J$. The upper envelope on the overlapping curves is easily determined to be, approximately,

$$\max_{\gamma} P_e(1; \gamma) = P_e(1; \gamma=1), \qquad E_b/\mathcal{N}_J \leq 1\,\text{dB} \qquad (4\text{-}39a)$$

$$= \frac{0.238}{E_b/\mathcal{N}_J}, \qquad E_b/\mathcal{N}_J > 1\,\text{dB}. \qquad (4\text{-}39b)$$

This dependence is the well known "inverse linear" characteristic of the error performance of communications systems in worst-case partial-band noise jamming. It also can be determined from the figure that the worst-case value of γ is approximately

$$\gamma_{\text{WC}} = \frac{1.26}{E_b/\mathcal{N}_J}, \qquad E_b/\mathcal{N}_J > 1\,\text{dB}. \qquad (4\text{-}39c)$$

Although not shown in Figure 4-13, there is a different asymptotic value for P_e for each parametric curve to the left, that is, as $E_b/\mathcal{N}_J$ decreases (jammer power increases). The value of the asymptote is approximately given by assuming that the error probability is 0.5 when jammed, and negligible (for the $E_b/\mathcal{N}_0=20\,\text{dB}$ case presented) when not jammed, giving the value $\gamma/2$ for the asymptote.

A set of $L=1$ curves similar to those shown in Figure 4-13 was generated for the simplified mixture approximation to the PDF given by (4-26). The appearance of the curves cannot be distinguished from those in Figure 4-13; examination of the computer printout reveals that the error curves computed using the simplified mixture model give a value for the error that is generally lower, but only to the extent that the second significant figure is affected.

Keeping all other parameters the same, in Figure 4-14 we show the effect of increasing the value of the diversity, L, from 1 to 2. The worst-case $P_e(2; \gamma)$ can be seen to have a generally more rapid decrease with $E_b/\mathcal{N}_J$ than was the case for $L=1$. In fact, for values of $E_b/\mathcal{N}_J$ between about 7 and 20 dB, the slope of the upper envelope of the parametric curves in Figure 4-14 is very close to being -2, indicating a dependence upon the inverse of $(E_b/\mathcal{N}_J)^2$. For $E_b/\mathcal{N}_J$ greater than $20\,\text{dB}$, for the range of P_e values shown the slope of the worst-case error is approximately -1, indicating a dependence upon $(E_b/\mathcal{N}_J)^{-1}$.

For the curves corresponding to γ values of 0.02, 0.01, and 0.005 in Figure 4-14, an unusual dependence on $E_b/\mathcal{N}_J$ can be observed. The curves imply that there is a peak

FIGURE 4-13 PERFORMANCE OF FH/CPFSK IN PARTIAL-BAND JAMMING
FOR $L=1$ HOP/BIT, L/D RECEIVER, AND AGC WEIGHTING

FIGURE 4-14 PERFORMANCE OF FH/CPFSK IN PARTIAL-BAND JAMMING
FOR $L=2$ HOPS/BIT, L/D RECEIVER, AND AGC WEIGHTING

value of the error for some finite value of E_b/N_J, whereas we would expect the error to increase uniformly as the value of E_b/N_J is decreased (jammer power increased). This behavior was checked out thoroughly, and was found to be an artifact of the computational method, which uses the trapezoidal rule for numerical integration to calculate the error probability according to (4-31). The spacing between the samples of the integrand was decreased for the purposes of checking the result for fixed γ in Figure (4-14), and it was found that with a small enough spacing the error probability as calculated by this integration rule does indeed behave as expected. However, the value of the result for the portion of the curve which touches the upper envelope (worst-case error) was found to be unaffected to any significant degree by the decrease in spacing, so the whole set of curves was not recomputed in the interest of saving computational time.

Figures 4-15, 4-16, and 4-17 show the effect of raising the value of L to 3, 4, and 6, respectively. In Figure 4-15, for $L=3$ the slope of the worst-case error probability (the upper envelope of the parametric curves for fixed values of γ), is seen to be approximately -3 for E_b/N_J in the range of 10 to 20 dB. Similarly, for $L=4$, in Figure 4-16 the slope is about -4 for the same general range of E_b/N_J values. However, in Figure 4-17, the slope is not -6, as might be expected; it is closer to being -4. This behavior can be explained by the fact that, even though E_b/N_0 is very high (20 dB), as the transmitted symbols (bits if no coding is used) are subdivided increasingly finer by making L higher the system becomes subject to significant noncoherent combining losses.

A composite of the worst-case error performances of FH/CPFSK for different values of L using AGC weighting is presented in Figure 4-18. In that figure we observe that for low values of E_b/N_J (high values of jammer power), the tendency is for the error to increase as L is increased, but for high values of E_b/N_J (low values of jammer power), the tends to be a diversity improvement as L increases. This behavior is reasonable in view of the fact that for strong jamming, the worst-case value of γ, the jamming fraction, tends to be $\gamma=1$, corresponding to fullband jamming, and we know that noncoherent combining losses cause the error to increase with L for a stationary Gaussian noise channel.

For reference, in Figure 4-18 there also is plotted a curve which corresponds to fullband jamming and no system noise. Against this reference, we can observe the effect of choosing the value of L which gives the lowest worst-case error probability—the lower envelope of the curves parametric in L. From this point of view, we see that if it were possible to use of the optimum value of diversity (which depends on E_b/N_J) the

FIGURE 4-15 PERFORMANCE OF FH/CPFSK IN PARTIAL-BAND JAMMING
FOR $L=3$ HOPS/BIT, L/D RECEIVER, AND AGC WEIGHTING
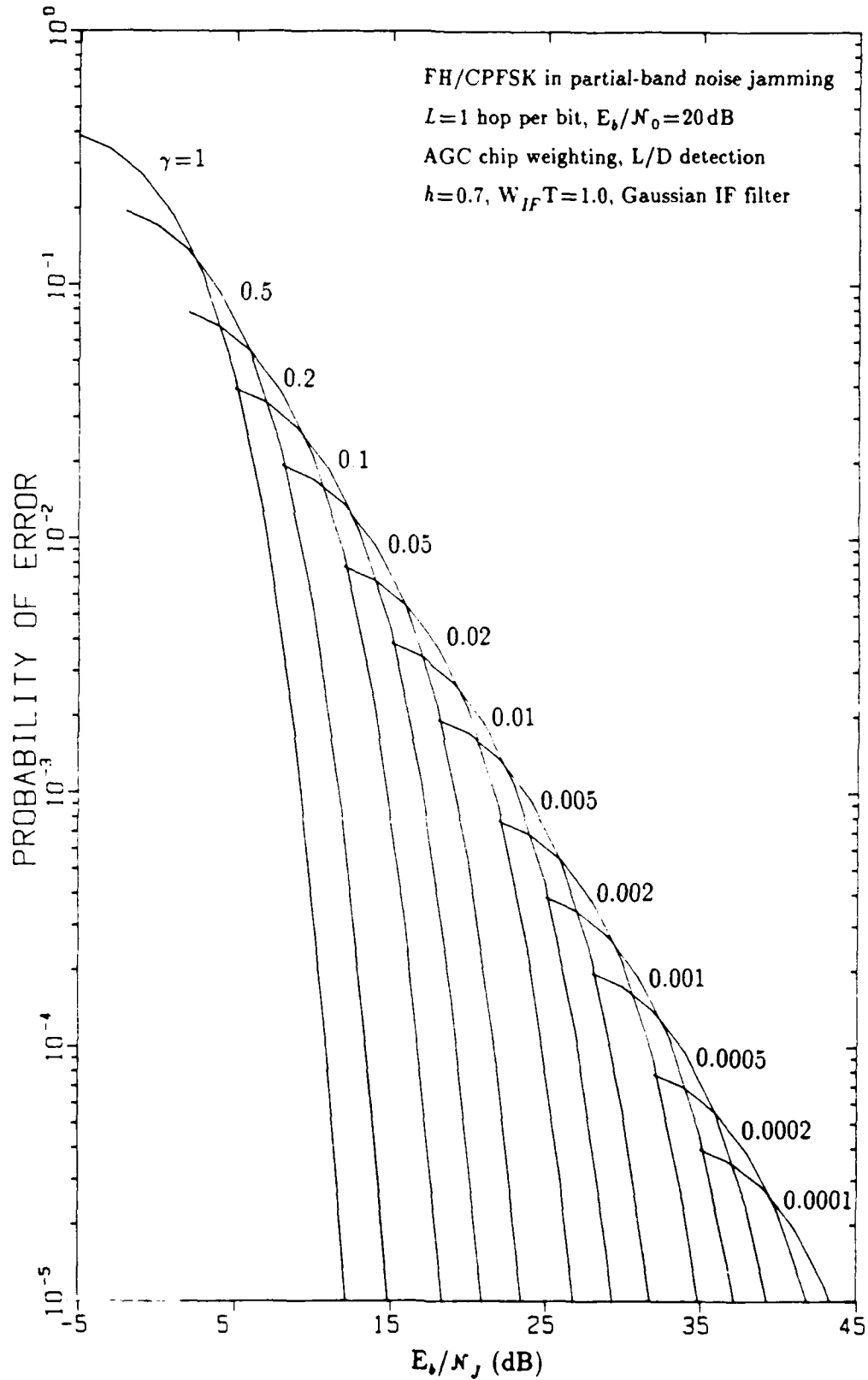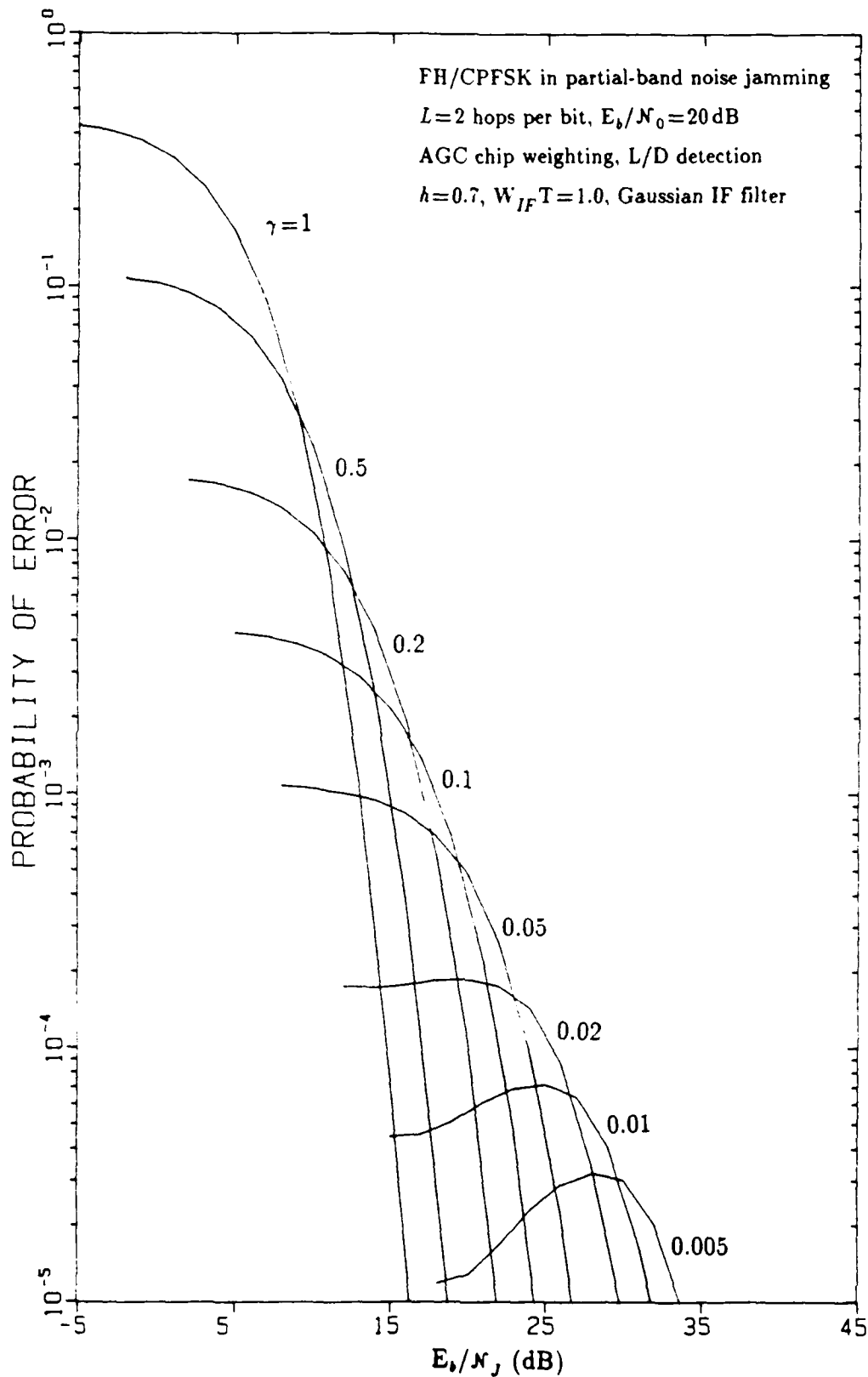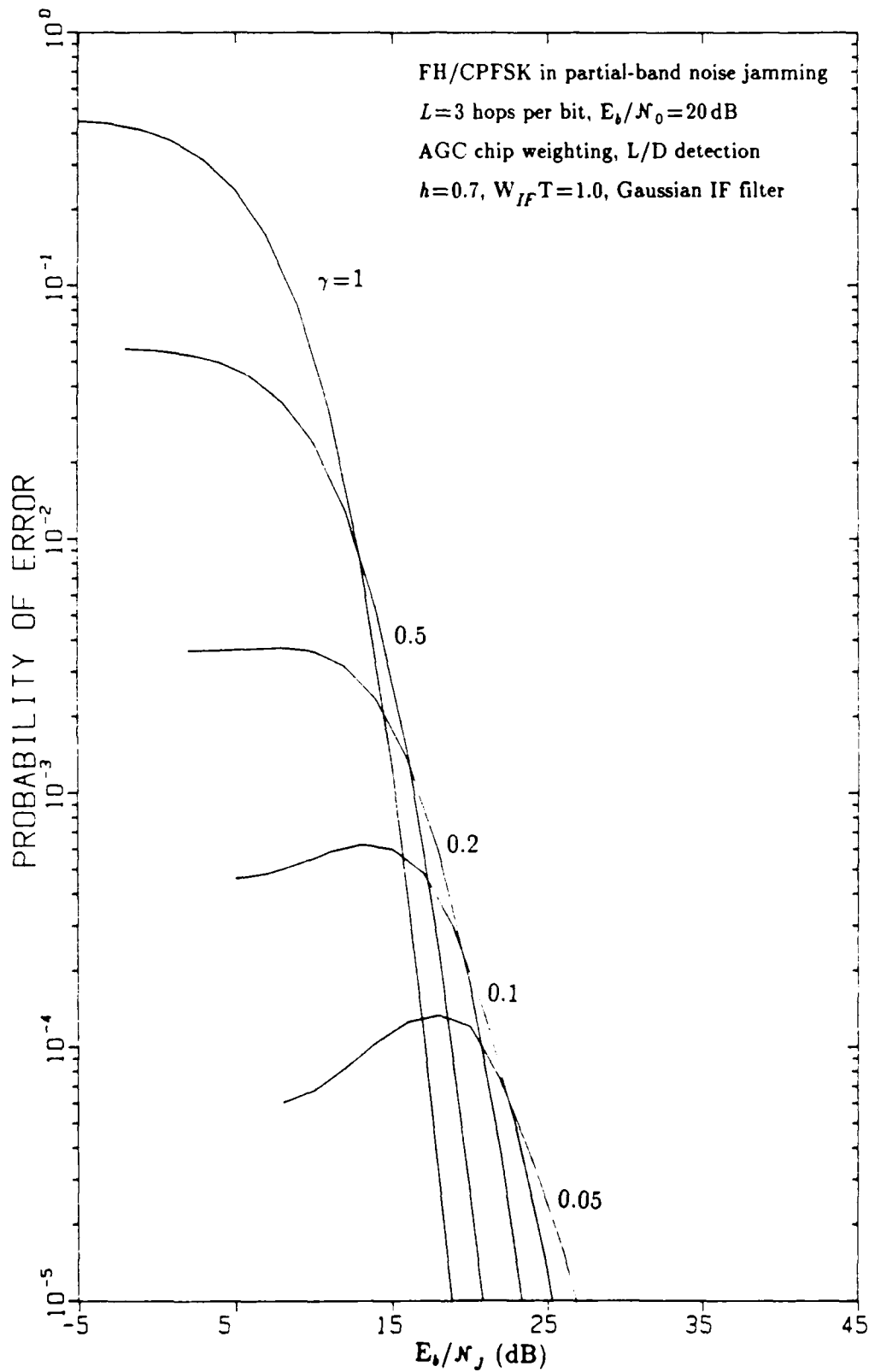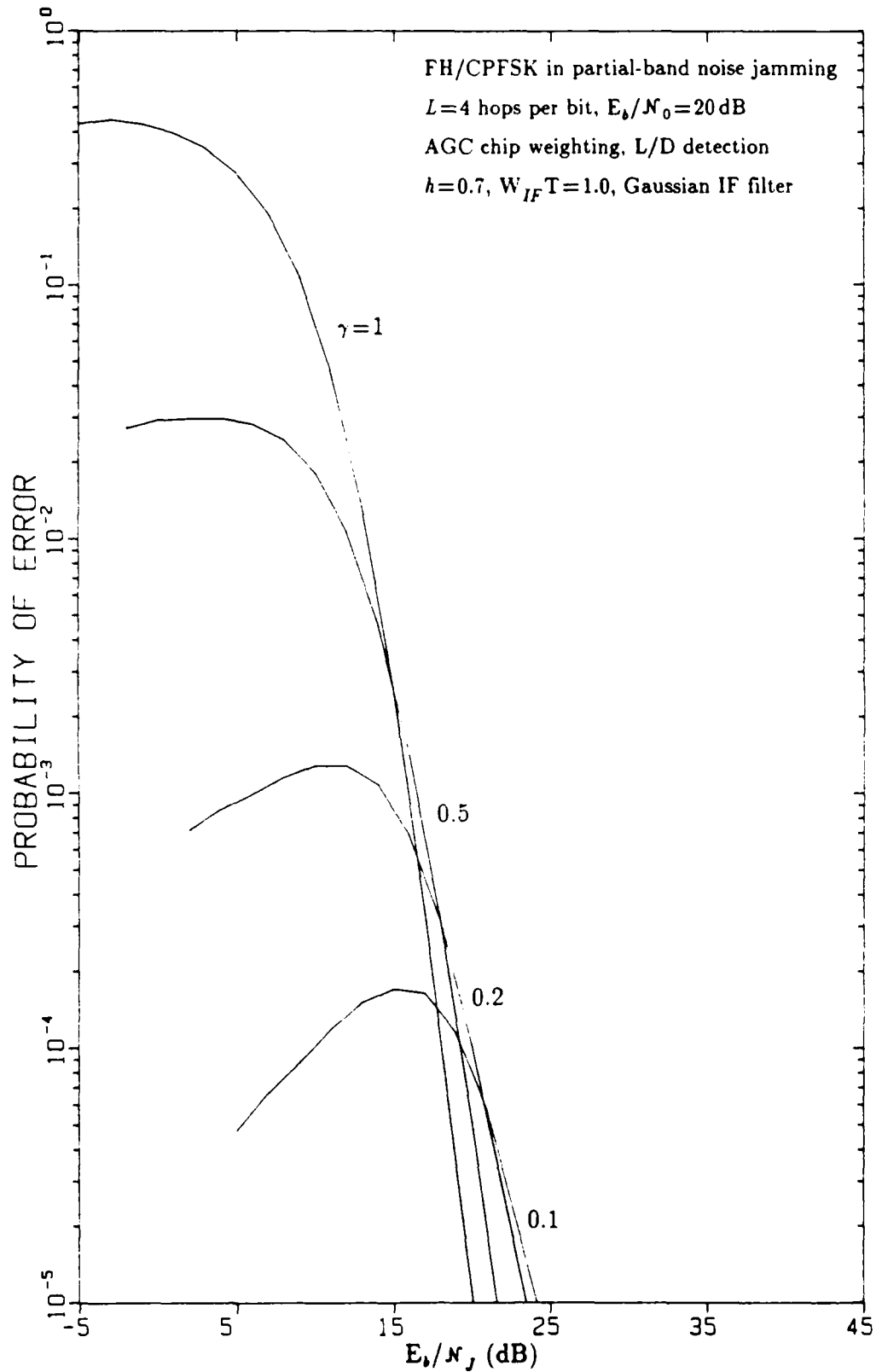
71

FIGURE 4-16 PERFORMANCE OF FH/CPFSK IN PARTIAL-BAND JAMMING
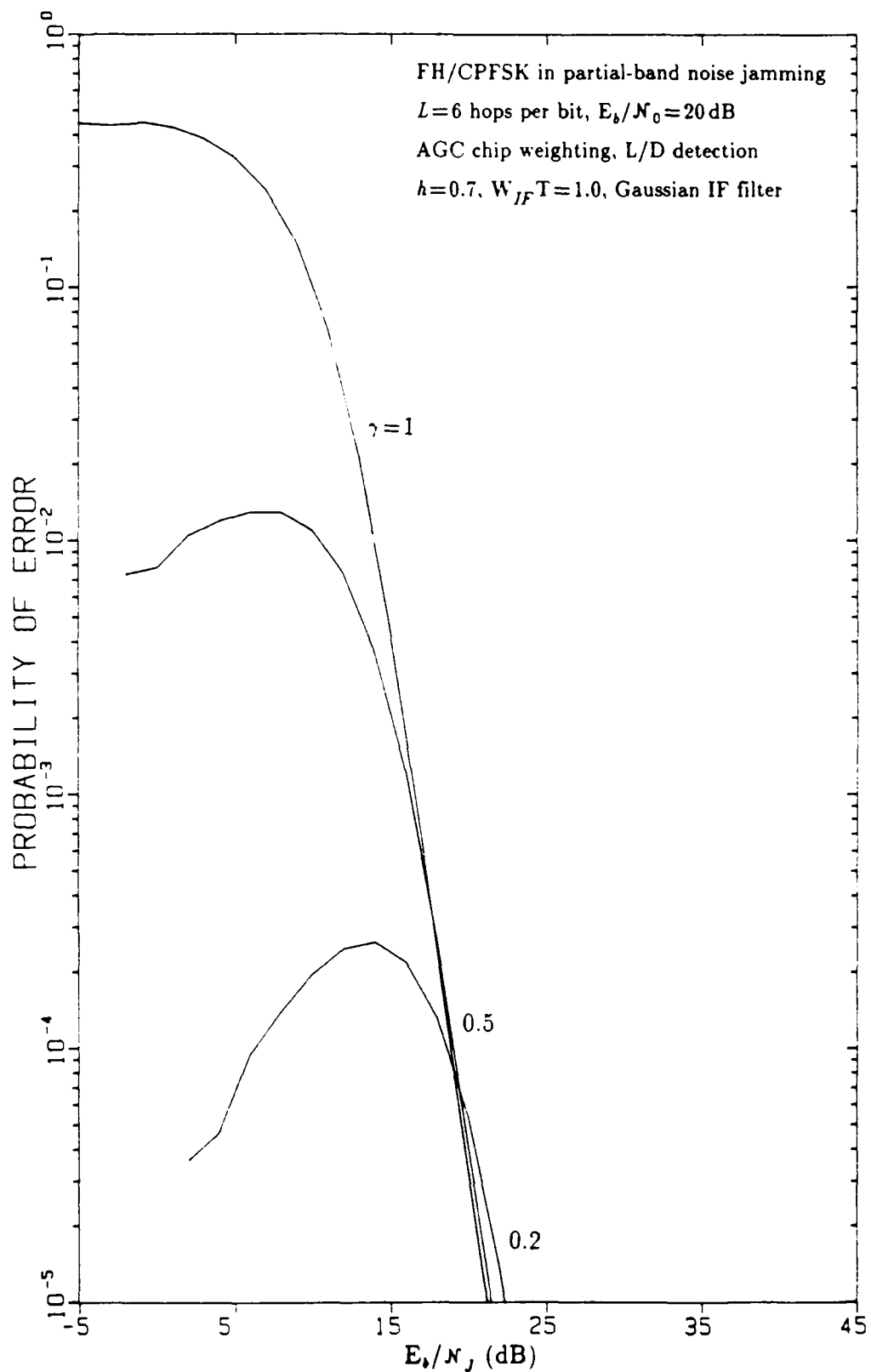FOR $L=4$ HOPS/BIT, L/D RECEIVER, AND AGC WEIGHTING

FIGURE 4-17 PERFORMANCE OF FH/CPFSK IN PARTIAL-BAND JAMMING
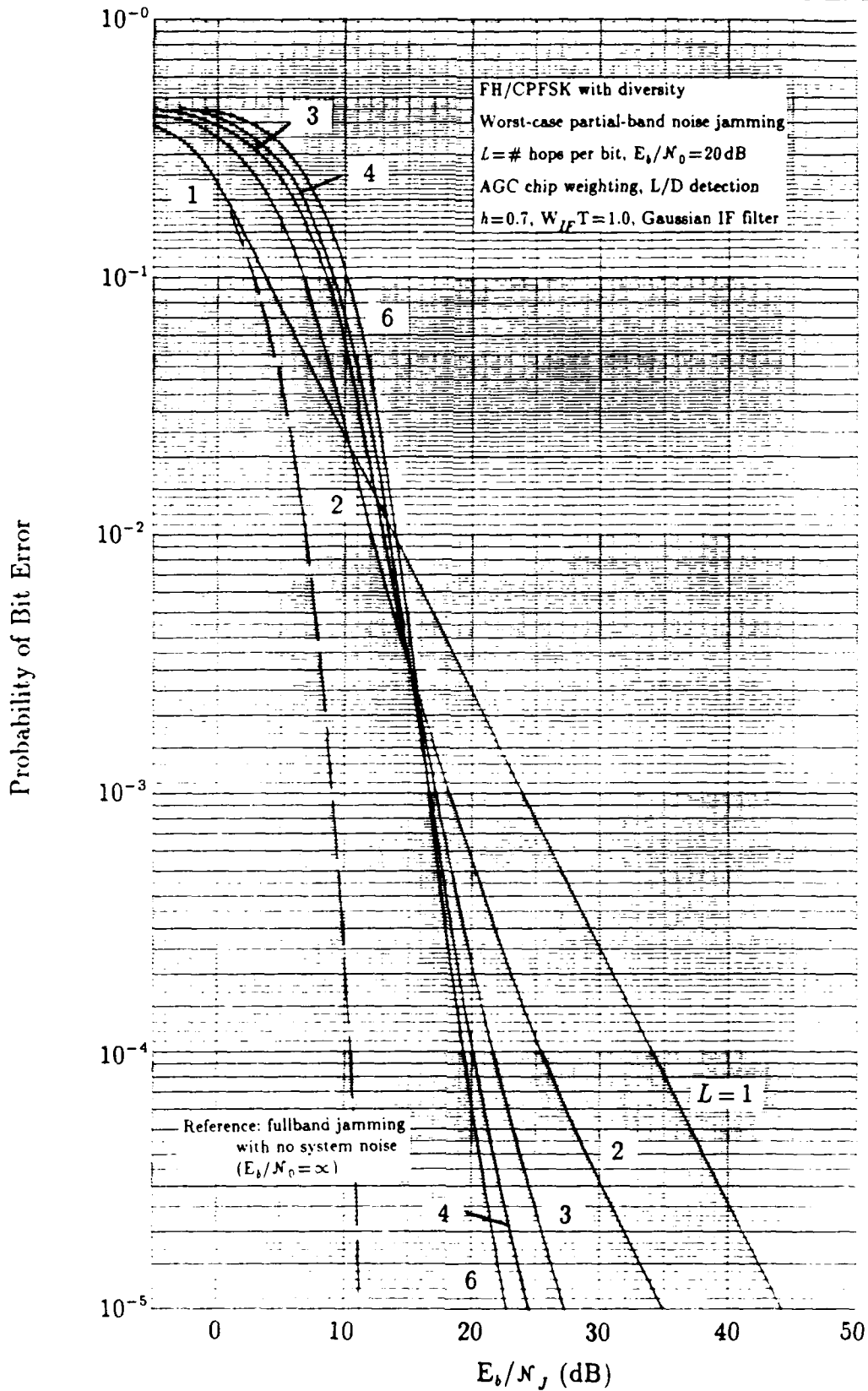FOR $L=6$ HOPS/BIT, L/D RECEIVER, AND AGC WEIGHTING

FIGURE 4-18 DIVERSITY PERFORMANCE OF FH/CPFSK IN
PARTIAL-BAND NOISE JAMMING WITH AGC WEIGHTING

worst-case error performance of the system could be improved greatly from the situation holding for no diversity. Instead of requiring about 44 dB to produce a 10^{-5} error probability,—a loss of 32 dB in performance from the ideal (fullband jamming) case, which requires about 12 dB—with optimum diversity, the loss due to the worst-case jamming can be held to less than 10 dB for some value of L.

4.4 DIFFERENTIAL DETECTION RECEIVER TECHNIQUES

The differential detector implementation of the receiver for FH/CPFSK, shown in Figure 2-3 and discussed in Section 2.1.3, is somewhat easier to analyze than the limiter-discriminator receiver. Even though the probability density function (PDF) for the differential detector's output is not available in closed form, its characteristic function (CHF) is.

4.4.1 Characteristic Function for the Differential Detector in Jamming

It has been shown [8] that the output of the differential detector, conditioned on the CPFSK intersymbol interference parameters, is equivalent to the difference of two scaled, independent noncentral chi-squared random variables. Let z_{q_i} denote the qth chip on a particular hop of an L-hop/bit FH/CPFSK transmission, given the ith intersymbol interference (ISI) pattern, where i may be 1, 2, or 3 (see Appendix A). We may write the CHF for the jammed receiver as

$$C_{z_{q_i}}(\nu) = \tfrac{1}{4}C_{z_{q_1}}(\nu) + \tfrac{1}{4}C_{z_{q_2}}(\nu) + \tfrac{1}{2}C_{z_{q_3}}(\nu). \tag{4-40a}$$

where the pattern-dependent CHF, assuming an unspecified ECCM weighting scheme using weights w_0 and w_1 for unjammed and jammed hops, respectively, is given by

$$C_{z_{q_i}}(\nu) = (1-\gamma)\, C_z(w_0\nu;\ \Delta\phi_i,\ \tfrac{1}{L}U_{i0},\ \tfrac{1}{L}W_{i0},\ \sigma_N^2)$$

$$+ \gamma\, C_z(w_1\nu;\ \Delta\phi_i,\ \tfrac{1}{L}U_{i1},\ \tfrac{1}{L}W_{i1},\ \sigma_T^2) \tag{4-40b}$$

From (2-35), the conditional CHF for an IF filter that is symmetric about the center frequency ($\lambda=0$) is

$$C_z(\nu;\ \Delta\phi,\ U,\ W,\ \sigma^2) = \frac{1}{1+\tfrac{1}{4}\sigma^4\nu^2(1-r^2)}\exp\left\{\frac{j\nu\sigma^2 W\sin\Delta\phi+\tfrac{1}{2}\sigma^4\nu^2(U-rW\cos\Delta\phi)}{1+\tfrac{1}{4}\sigma^4\nu^2(1-r^2)}\right\}. \tag{4-41}$$

Without loss of generality, we may replace z with the normalized variable,

$$z' = \frac{4z}{w_0\sigma^2\sqrt{1-r^2}}. \tag{4-42}$$

which yields (after leaving off the prime)

$$
C_{z_{q_i}}(\nu) = (1-\gamma)\frac{1}{1+4\nu^2}\exp\left\{\frac{4j\nu\alpha-8\nu^2\beta}{1+4\nu^2}\right\}
$$

$$
+ \gamma\,\frac{1}{1+4\kappa\nu^2(w_1/w_0)^2}\exp\left\{\frac{4j\nu\alpha(w_1/w_0)-8\kappa\nu^2\beta(w_1/w_0)^2}{1+4\kappa\nu^2(w_1/w_0)^2}\right\} \tag{4-43a}
$$

with

$$
\alpha \triangleq W_{i0}\sin\Delta\phi_i/L\sqrt{1-r^2} \tag{4-43b}
$$

and

$$
\beta \triangleq (U_{i0}-rW_{i0}\cos\Delta\phi_i)/L\sqrt{1-r^2}, \tag{4-43c}
$$

in which we have used the fact that the jammed and unjammed parameters are related by the parameter κ, defined in (2-42), in the following way:

$$
\kappa \triangleq \sigma_T^2/\sigma_N^2 \tag{4-43d}
$$

and
$$
U_{i1} = U_{i0}/\kappa \quad\text{and}\quad W_{i1} = W_{i0}/\kappa. \tag{4-43e}
$$

4.4.2 AGC Weighting Scheme

4.4.2.1 Analysis

For the AGC weighting scheme, we use the weights $w_0=1$ and $w_1=\sigma_N^2/\sigma_T^2=\kappa^{-1}$ for the differential detector. This choice is logical in view of the fact that the differential detector output is proportional to noise power (σ^2). Substitution of these weights into (4-43) gives the CHF

$$
C_{z_{q_i}}(\nu) = \frac{1}{1+4\nu^2}\left((1-\gamma)\,\exp\left\{\frac{-8\nu^2\beta}{1+4\nu^2}\right\}\exp\left\{\frac{4j\nu\alpha}{1+4\nu^2}\right\}\right.
$$

$$
\left.+ \gamma\exp\left\{\frac{-8\nu^2\beta/\kappa}{1+4\nu^2}\right\}\exp\left\{\frac{4j\nu\alpha/\kappa}{1+4\nu^2}\right\}\right) \tag{4-44}
$$

The imaginary part needed for the error probability calculation using the methodology described in Section 2.3 is

$$
\text{Im}\left\{[C_{z_{q_i}}(\nu)]^L\right\} = |C_{z_{q_i}}(\nu)|^L\,\sin\left\{L\arg[C_{z_{q_i}}(\nu)]\right\} \tag{4-45a}
$$

where

$$
|C_{z_{q_i}}(\nu)|^2 = \{\text{Re}[C_{z_{q_i}}(\nu)]\}^2 + \{\text{Im}[C_{z_{q_i}}(\nu)]\}^2 \tag{4-45b}
$$

and

$$
\arg[C_{z_{q_i}}(\nu)] = \tan^{-1}\left\{\frac{\text{Im}[C_{z_{q_i}}(\nu)]}{\text{Re}[C_{z_{q_i}}(\nu)]}\right\}. \tag{4-45c}
$$

The required real and imaginary parts of the CHF are given by

$$
\mathrm{Re}\left[C_{z q_i}(\nu)\right] = \frac{1}{1+4\nu^2} \left((1-\gamma) \exp\left\{\frac{-8\nu^2\beta}{1+4\nu^2}\right\} \cos\left\{\frac{4\nu\alpha}{1+4\nu^2}\right\} \right.
$$
$$
\left. + \gamma \exp\left\{\frac{-8\nu^2\beta/\kappa}{1+4\nu^2}\right\} \cos\left\{\frac{4\nu\alpha/\kappa}{1+4\nu^2}\right\} \right) \tag{4-46a}
$$

and

$$
\mathrm{Im}\left[C_{z q_i}(\nu)\right] = \frac{1}{1+4\nu^2} \left((1-\gamma) \exp\left\{\frac{-8\nu^2\beta}{1+4\nu^2}\right\} \sin\left\{\frac{4\nu\alpha}{1+4\nu^2}\right\} \right.
$$
$$
\left. + \gamma \exp\left\{\frac{-8\nu^2\beta/\kappa}{1+4\nu^2}\right\} \sin\left\{\frac{4\nu\alpha/\kappa}{1+4\nu^2}\right\} \right). \tag{4-46b}
$$

Using numerical integration the error probability for the ith pattern becomes

$$
\mathrm{P}_{ei}(L; \gamma) = \tfrac{1}{2} - \tfrac{1}{\pi} \int_0^\infty \frac{d\nu}{\nu} \mathrm{Im}\left\{ \left[C_{z q_i}(\nu)\right]^L \right\} \tag{4-47}
$$

and the total error probability is, after averaging over the three ISI patterns,

$$
\mathrm{P}_e(L; \gamma) = \tfrac{1}{4}\left[\mathrm{P}_{e1}(L; \gamma) + \mathrm{P}_{e2}(L; \gamma) + 2\mathrm{P}_{e3}(L; \gamma) \right]. \tag{4-48}
$$

4.4.2.2 Numerical results

Calculations of the differential detector error probability (4-48) were made using numerical integration of (4-47). In Figure 4-19, the case of $L=1$ (no diversity) is presented. In this figure, P_e is plotted as a function of E_b/N_J for fixed values of γ, the partial-band jamming fraction, when $E_b/N_0 = 20$ dB. The worst-case jamming result, the upper envelope of the family of constant-γ curves, is seen to be "inverse linear" in form, that is, proportional to $(E_b/N_J)^{-1}$:

$$
\max_\gamma \mathrm{P}_e(1; \gamma) = 0.275 \times (E_b/N_J)^{-1} \qquad E_b/N_J > 2\,\mathrm{dB} \tag{4-49a}
$$
$$
= \mathrm{P}_e(1; 1) \qquad E_b/N_J \leq 2\,\mathrm{dB}. \tag{4-49b}
$$

This result is in agreement with the comparable result for equal chip weighting presented in [8], which was computed using a different program. For $L=1$, of course, there is no effect produced by using any kind of weighting, since the bit decision is based on only one chip.

Similar results for $L=1$ are shown in Figures 4-20 and 4-21 for $E_b/N_0 = 15\,\mathrm{dB}$ and 13 dB, respectively. As the value of E_b/N_0 is reduced from 20 dB, the asymptotic error probability for high E_b/N_J rises as shown in these two figures. The fact that the parameters of the worst-case jamming are dependent on the value of E_b/N_0 (that is, on the amount of system noise present) is often overlooked in jamming analyses. These figures illustrate that the results can be quite sensitive to the assumed value of E_b/N_0.

FH/CPFSK in partial-band noise jamming

$L=1$ hop per bit, $E_b/N_0 = 20\,dB$

AGC chip weighting, Differential detection
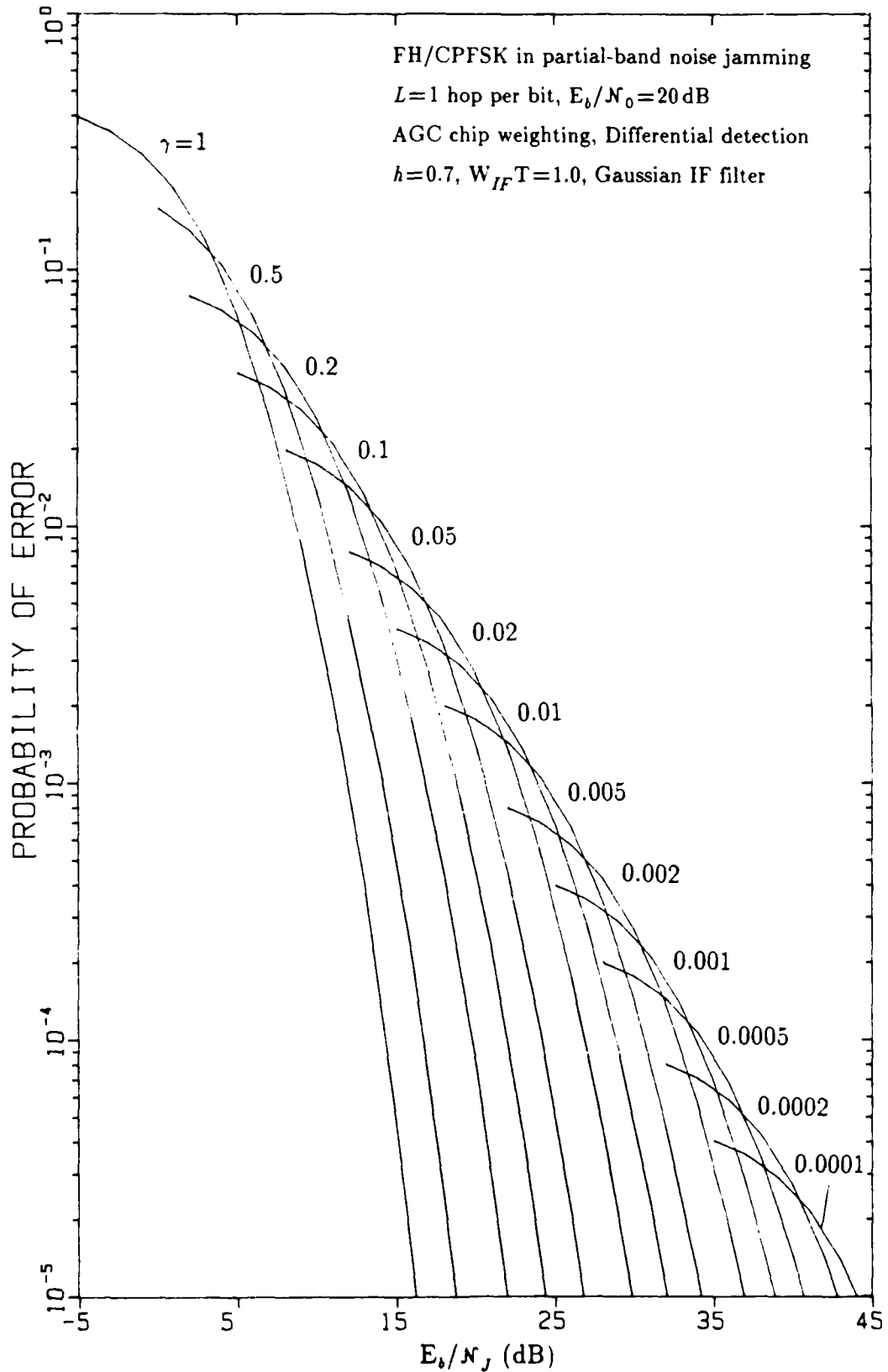
$h=0.7$, $W_{IF}T=1.0$, Gaussian IF filter

FIGURE 4-19 PERFORMANCE OF FH/CPFSK IN PARTIAL-BAND JAMMING
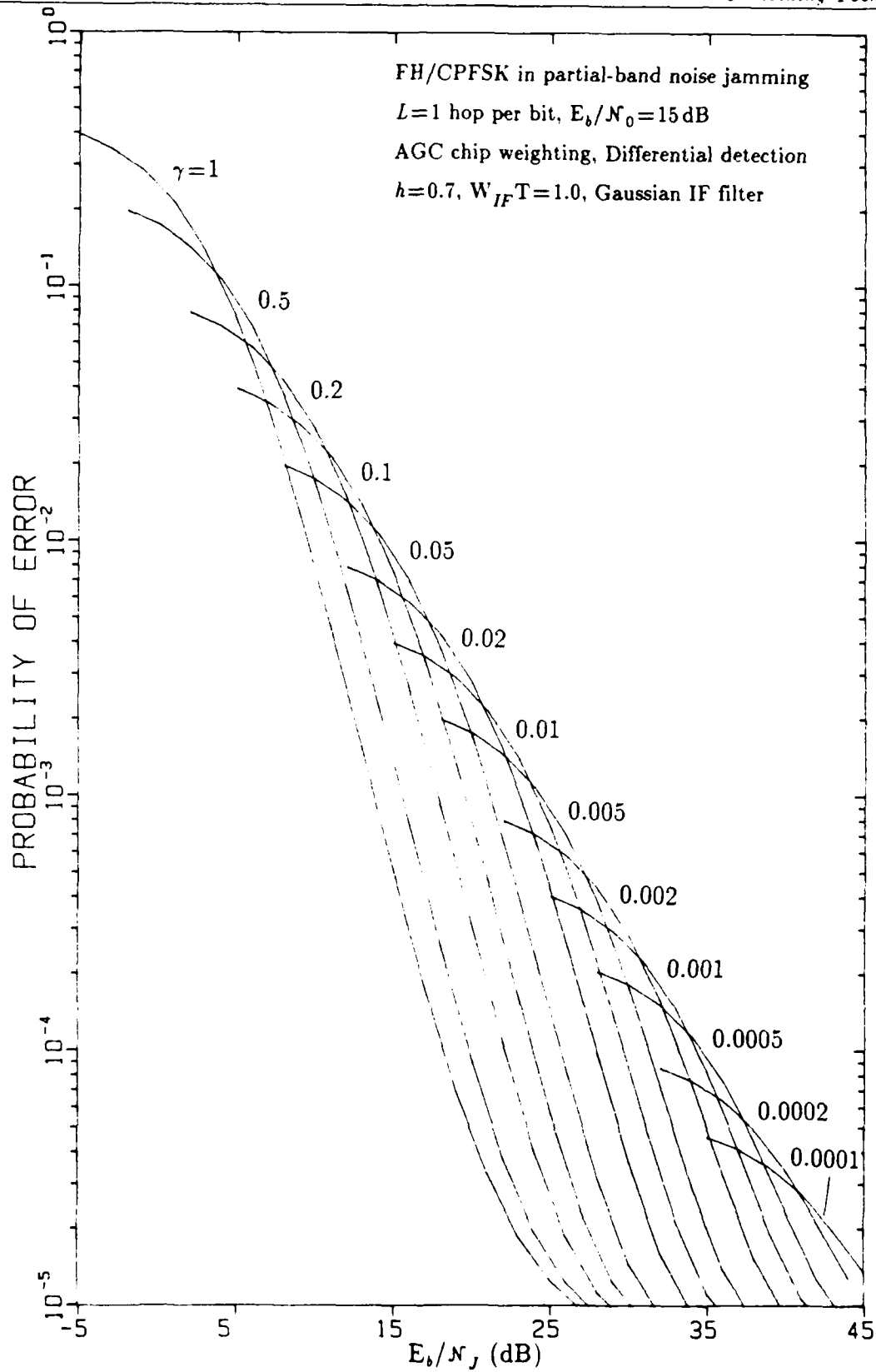FOR $L=1$, DIFFERENTIAL DETECTION, AND AGC WEIGHTING

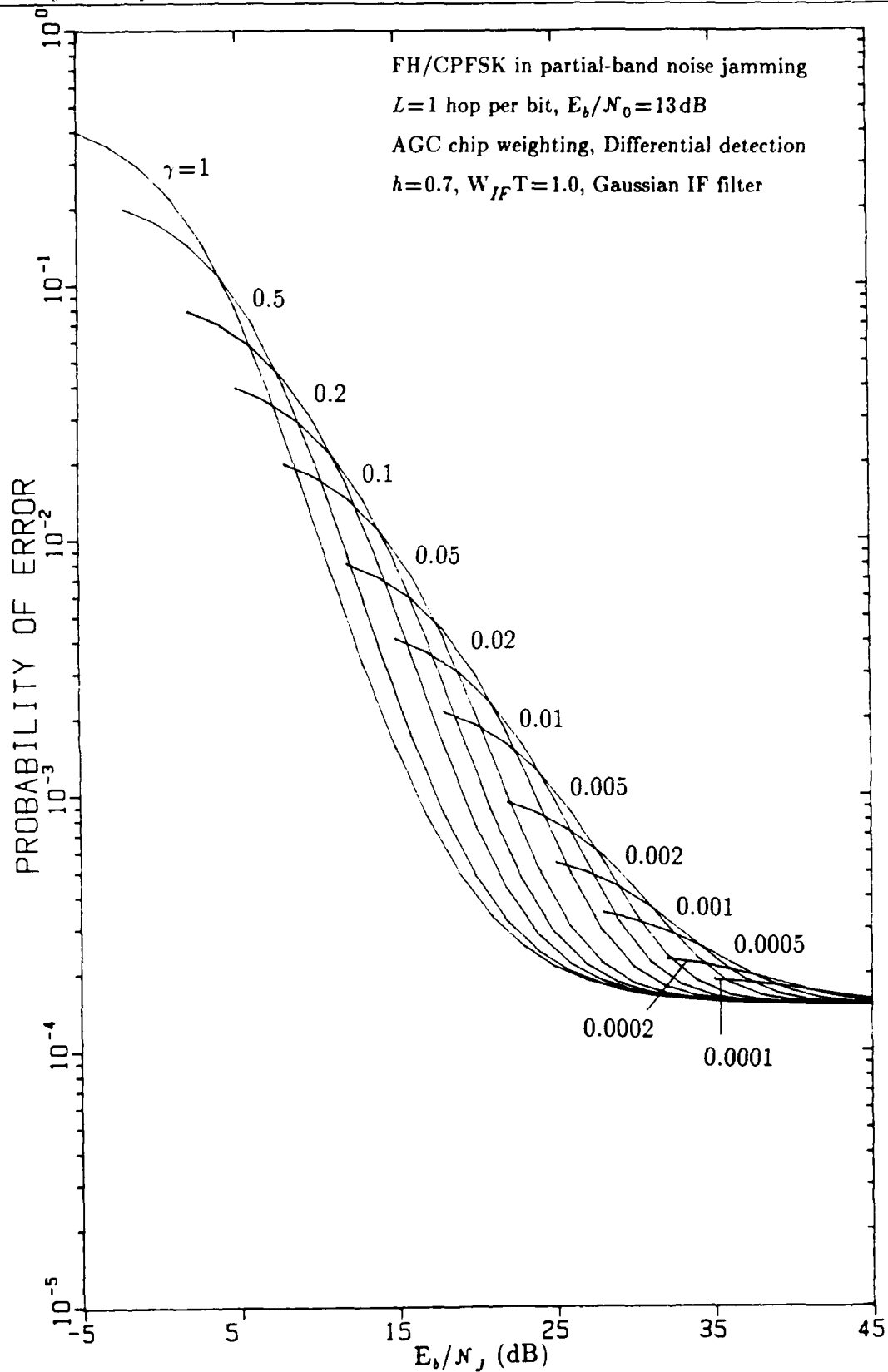FIGURE 4-20 PERFORMANCE OF FH/CPFSK IN PARTIAL-BAND JAMMING FOR $L=1$, DIFFERENTIAL DETECTION, AND $E_b/N_0=15$ dB

FIGURE 4-21 PERFORMANCE OF FH/CPFSK IN PARTIAL-BAND JAMMING
FOR $L=1$. DIFFERENTIAL DETECTION, AND $E_b/N_0=13\,dB$

Results for $L=2$ for $E_b/N_0=20$ dB and 15 dB are presented in Figures 4-22 and 4-23, respectively. In Figure 4-22, for E_b/N_J greater than about 5 dB, the upper envelope of the constant-γ curves has slope equal to -2 on the scale shown, indicating that the worst-case probability of error for $L=2$ using the AGC weighting is proportional to $(E_b/N_J)^{-2}$. This result in itself establishes that the AGC technique works in mitigating the effects of the partial-band jamming. Note, however, from what can be observed in Figure 4-23, that as the amount of thermal or system noise increases, the dependence of the worst-case error on E_b/N_J becomes more complex, since there is a "jamming-noise-dominant region" to the left and a "thermal-noise-dominant region" to the right.

Similar results are shown for $L=3$, 4, 5, and 6 in Figures 4-24 to 4-27. The fact that the increase in diversity produces a deterioration in performance for low values of E_b/N_J can be observed by noting the value of the error probability at $E_b/N_J=-5$ dB in these figures; the steady increase in the error probability is understood to be the effect of noncoherent combining losses, since for strong jamming the worst-case value of γ is $\gamma=1$ (fullband jamming), corresponding to a stationary Gaussian noise channel.

The fact that the increase in diversity tends to produce an improvement in performance for high values of E_b/N_0 and E_b/N_J can be observed in Figures 4-19, 4-22, and 4-24 to 4-27 by noting the worst-case (maximum) value of E_b/N_J required to produce an error probability of 10^{-5}. As L increases to $L=6$, this value is seen to decrease. However, another trend observable from these figures is that the range of E_b/N_J values for which $\gamma=1$ yields the worst-case error probability tends to increase as the order of diversity L is increased. The worst-case value of γ (among those plotted) at $P_e=10^{-5}$ for $E_b/N_0=20$ dB is seen from these figures to be $\gamma=0.0001$, 0.01, 0.1, 0.2, 0.5, and 1.0 for $L=1$, 2, 3, 4, 5, and 6, respectively. Thus for $L>6$ the worst-case value of E_b/N_J needed to produce a 10^{-5} error will begin to increase with L.

A composite of the worst-case error probability performance for FH/CPFSK in partial-band noise jamming using AGC weighting and differential detection is given in Figure 4-28. We observe first that for low values of E_b/N_J (strong jamming) the error probability increases as L increases, due to the fact that for low E_b/N_J the worst-case jamming is fullband jamming ($\gamma=1$), and noncoherent combining losses are proportional to L on the fullband jamming (Gaussian) channel. Next we observe that the value of E_b/N_J required to produce $P_e(L)=10^{-5}$ tends to decrease as L is increased to the value of 6, as previously noted, indicating a "diversity gain" is in effect. Examination of the "under-envelope" of the fixed-L curves revealed that the best value of $L-$in the sense of

FIGURE 4-22 PERFORMANCE OF FH/CPFSK IN PARTIAL-BAND JAMMING
FOR $L=2$, DIFFERENTIAL DETECTION, AND AGC WEIGHTING

FH/CPFSK in partial-band noise jamming
$L=2$ hops per bit, $E_b/\mathcal{N}_0 = 15\,dB$
AGC chip weighting, Differential detection
$h=0.7$, $W_{IF}T=1.0$, Gaussian IF in.

FIGURE 4-23 PERFORMANCE OF FH/CPFSK IN PARTIAL-BAND JAMMING
FOR $L=2$, DIFFERENTIAL DETECTION, AND $E_b/\mathcal{N}_0 = 15\,dB$

FIGURE 4-24 PERFORMANCE OF FH/CPFSK IN PARTIAL-BAND JAMMING
FOR $L=3$, DIFFERENTIAL DETECTION, AND AGC WEIGHTING

84

FH/CPFSK in partial-band noise jamming

$L = 4$ hops per bit, $E_b/N_0 = 20$ dB

AGC chip weighting, Differential detection

$h = 0.7$, $W_{IF}T = 1.0$, Gaussian IF filter

FIGURE 4-25   PERFORMANCE OF FH/CPFSK IN PARTIAL-BAND JAMMING
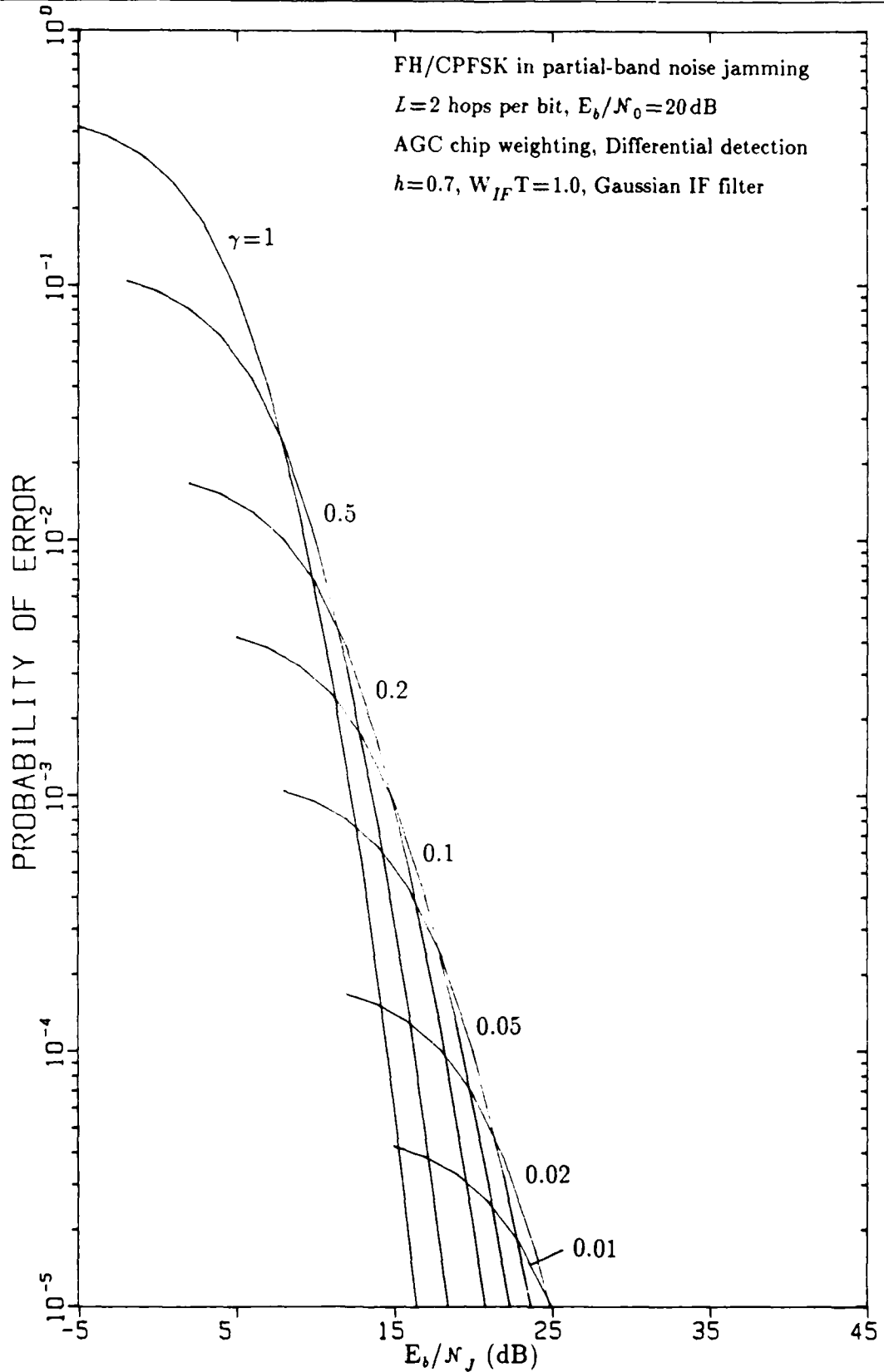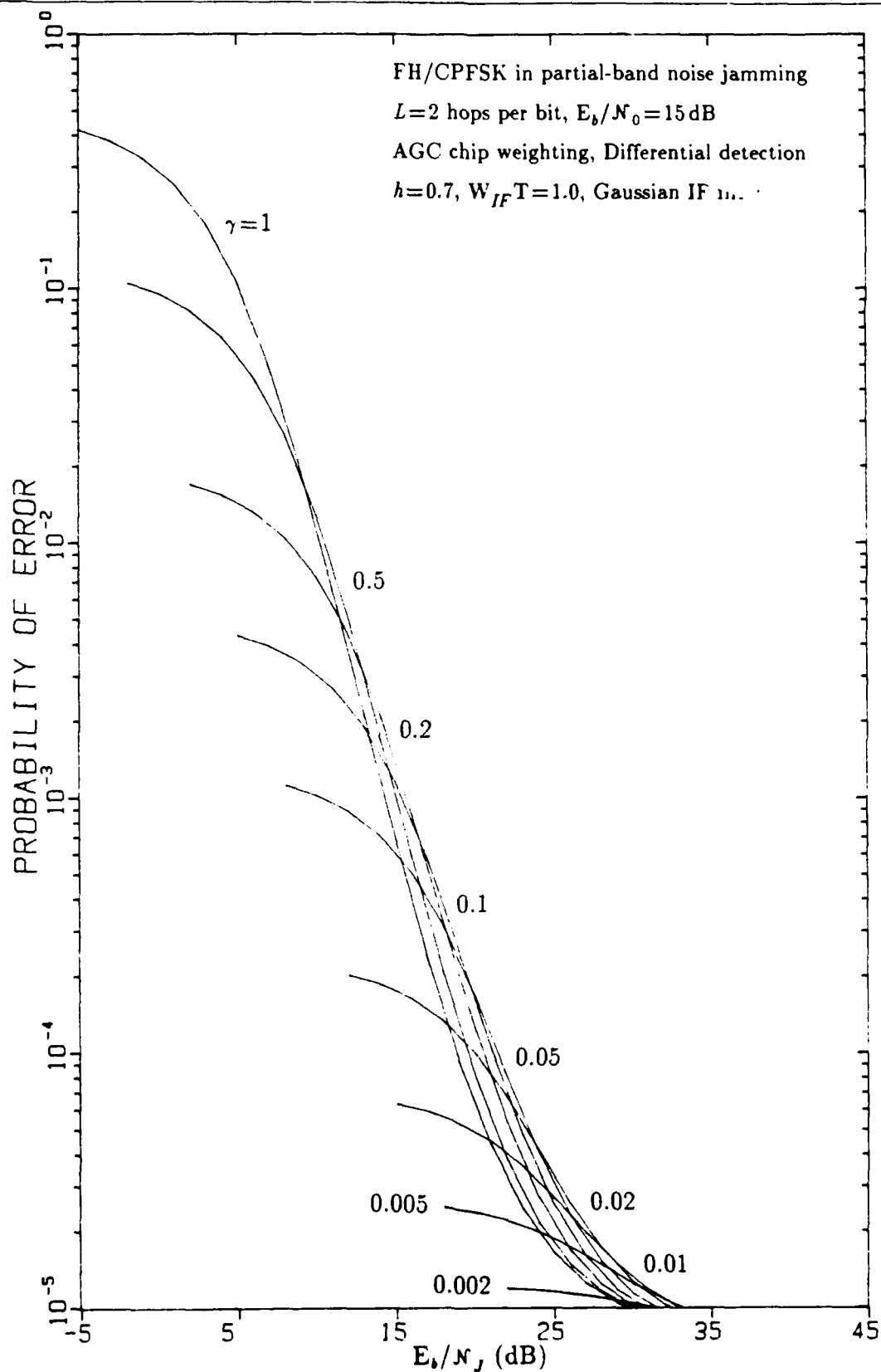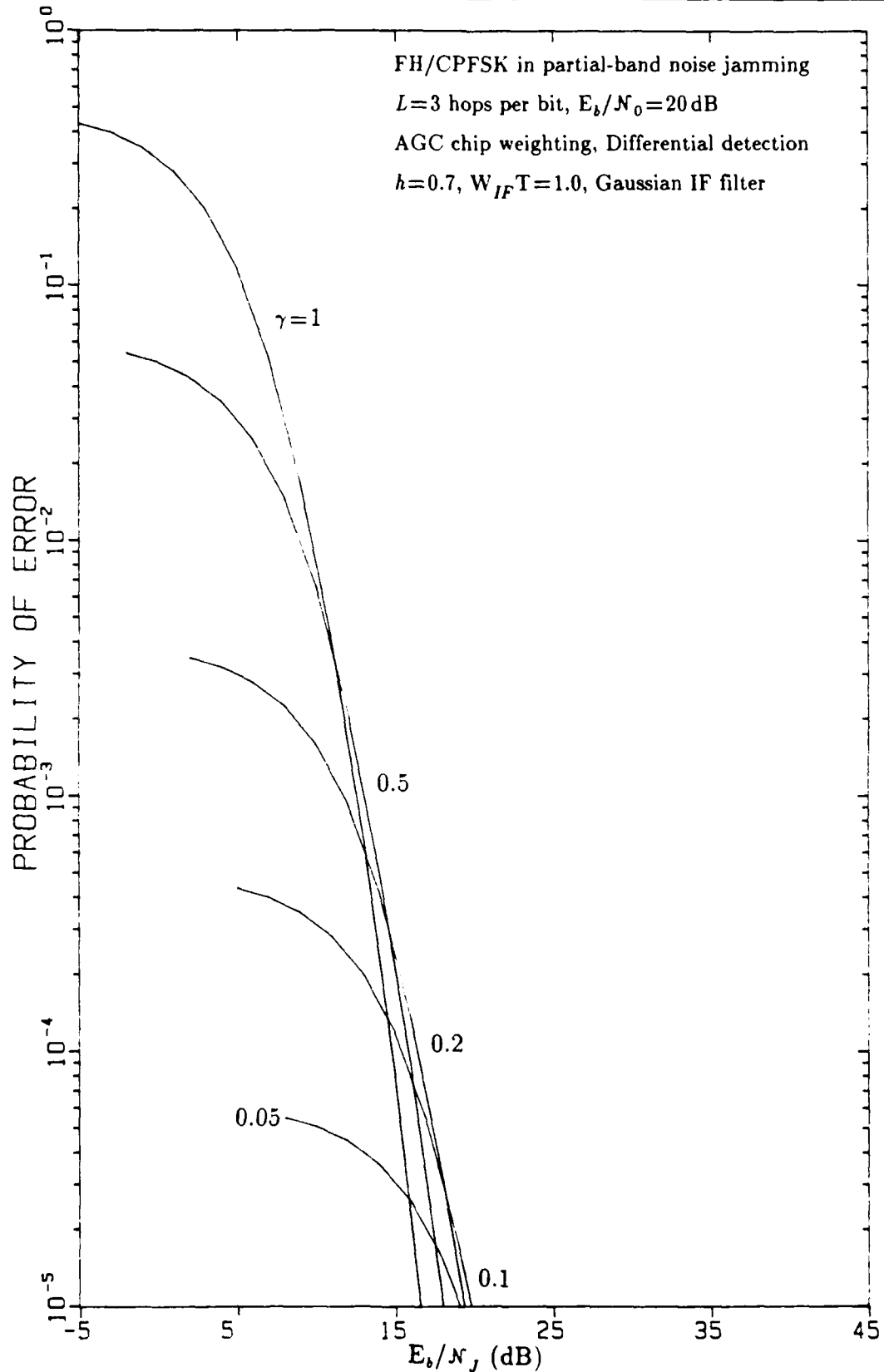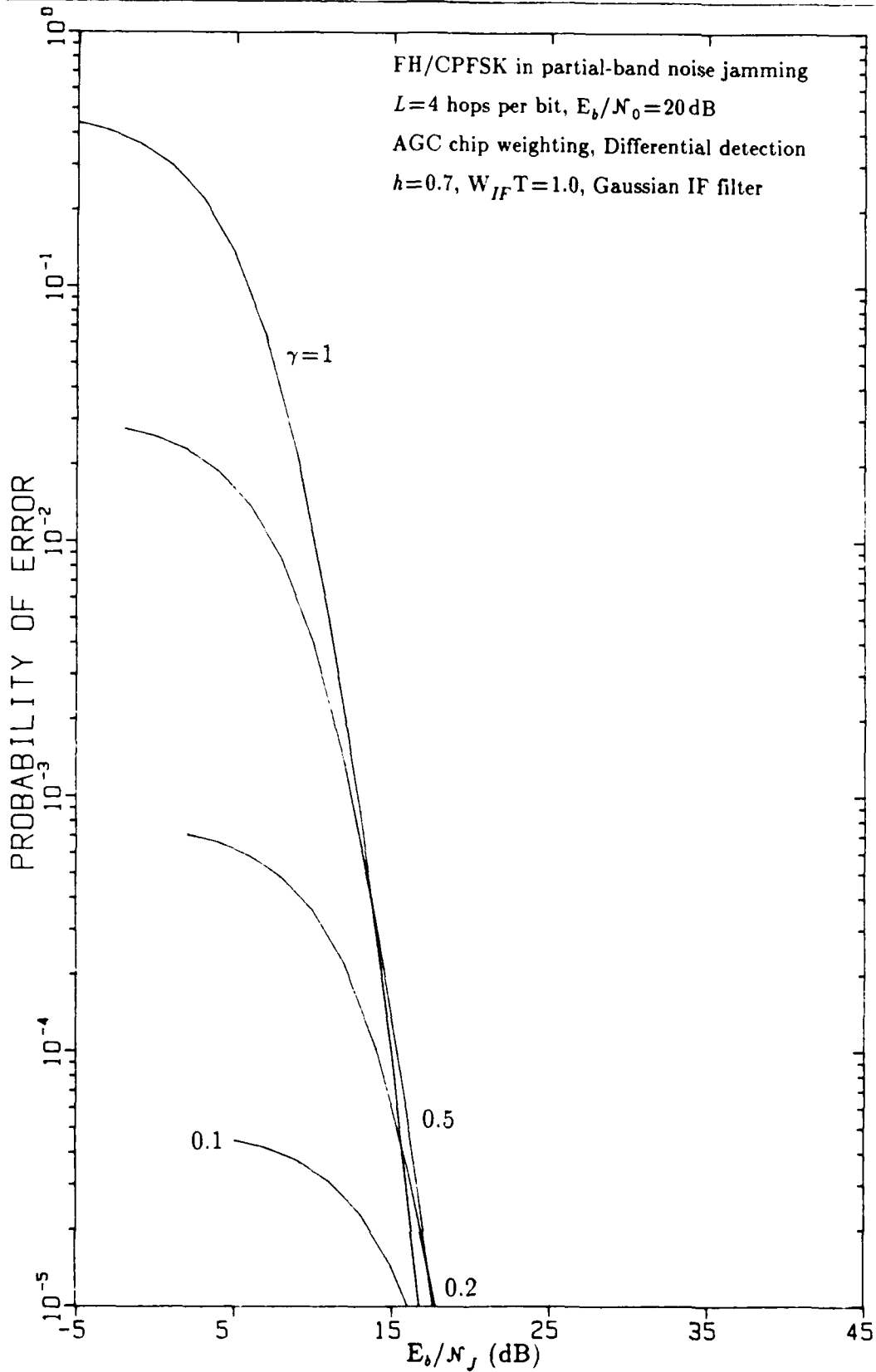FOR $L=4$, DIFFERENTIAL DETECTION, AND AGC WEIGHTING

FIGURE 4-26 PERFORMANCE OF FH/CPFSK IN PARTIAL-BAND JAMMING
FOR $L=5$, DIFFERENTIAL DETECTION, AND AGC WEIGHTING
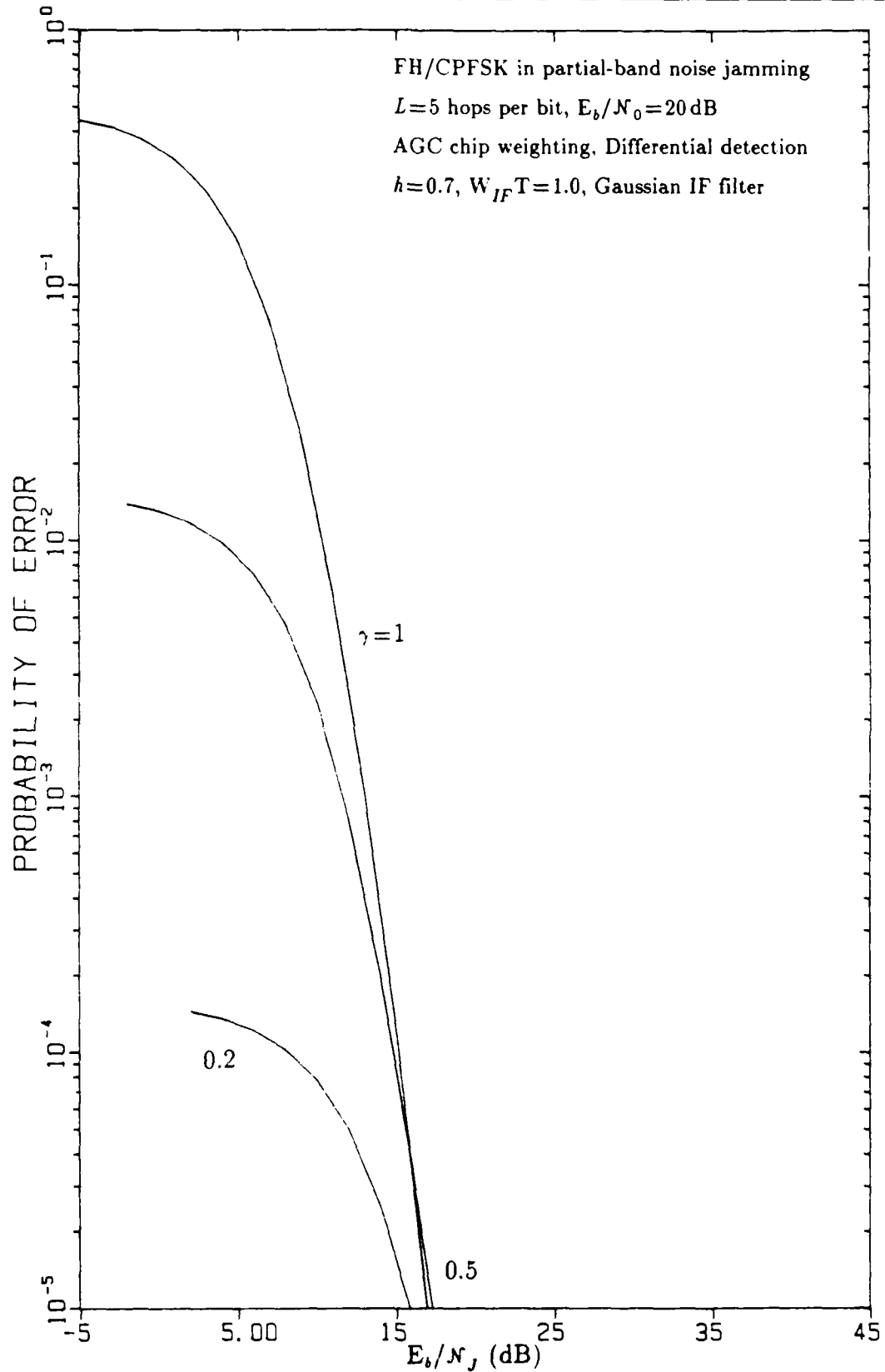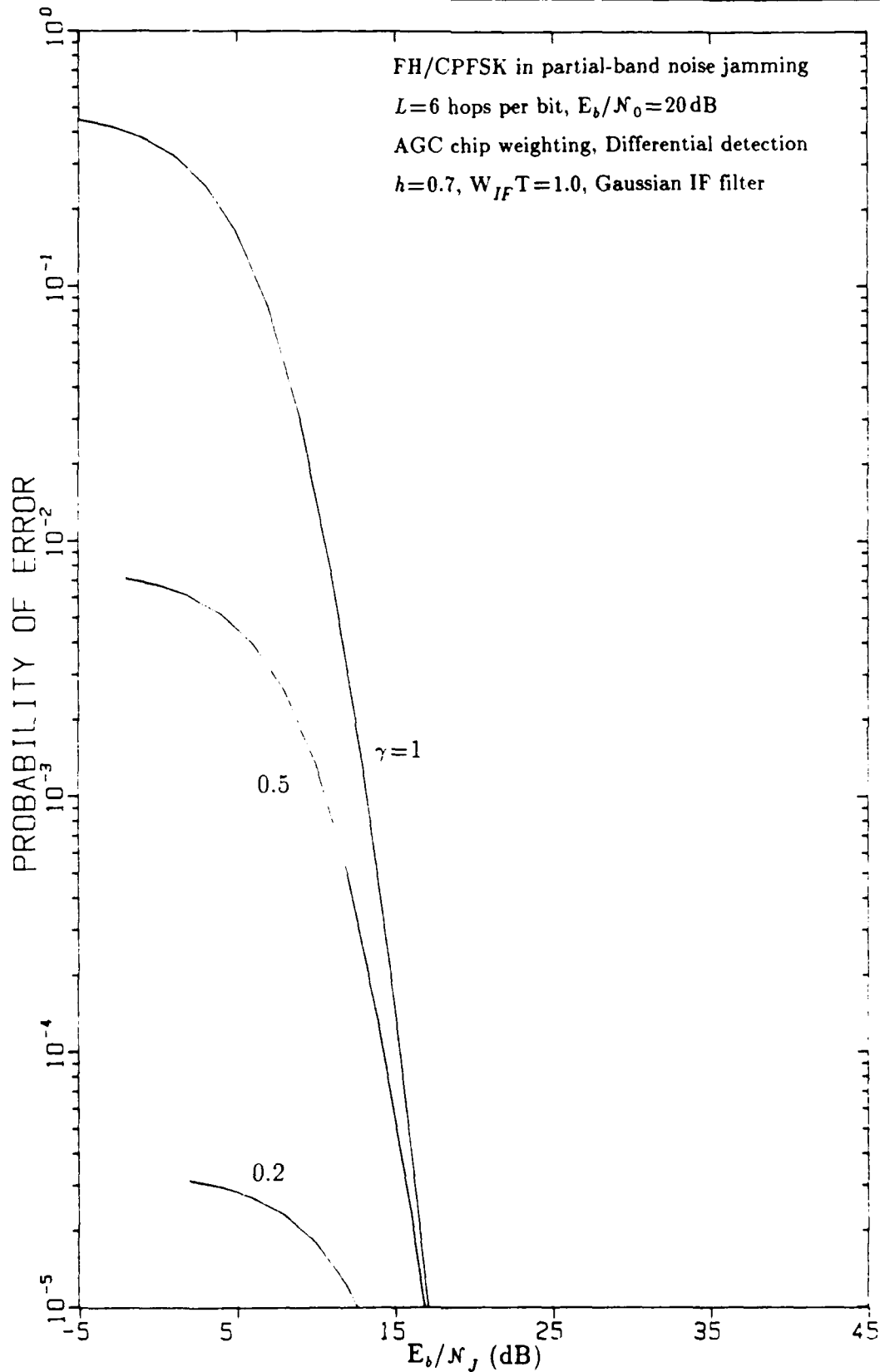
86

FIGURE 4-27 PERFORMANCE OF FH/CPFSK IN PARTIAL-BAND JAMMING
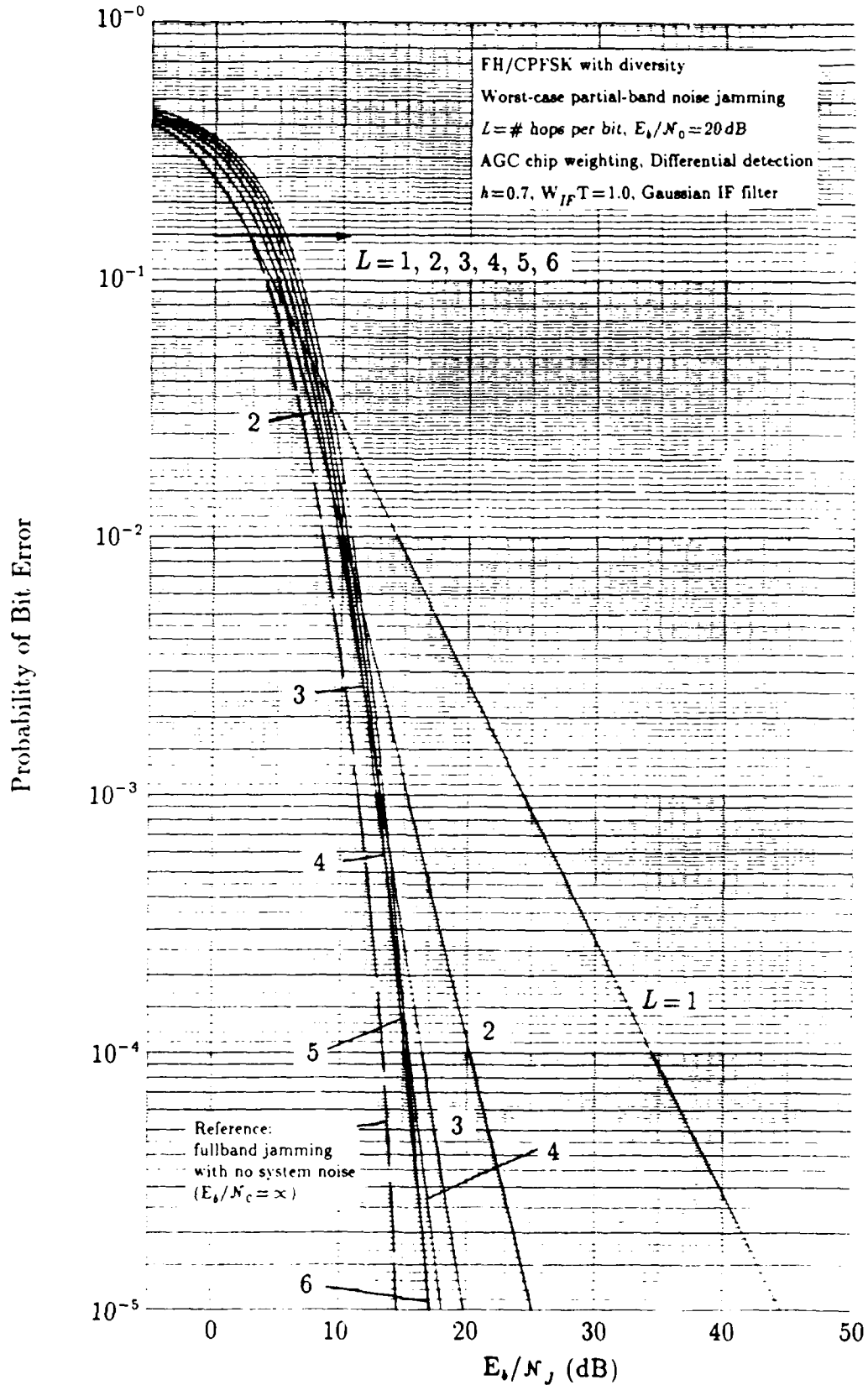FOR $L=6$, DIFFERENTIAL DETECTION, AND AGC WEIGHTING

FIGURE 4-28   DIVERSITY PERFORMANCE OF FH/CPFSK IN PARTIAL-BAND
JAMMING: DIFFERENTIAL DETECTION, AGC WEIGHTING

giving the least value of worst-case P_e—is a function of E_b/N_J (or, looking at it another way, a function of P_e). If the best value of L is always used, the performance of the system against worst-case partial-band noise jamming is improved from the very poor performance of no diversity ($L=1$) to within 3 dB of the system's performance in full-band (non-worst-case) jamming. Thus the use of optimum diversity is capable of limiting to 3 dB the effects of the jammer's efforts to inflict the maximum possible disruption of the system.

It is interesting to compare the set of curves in Figure 4-28 with those for the limiter-discriminator receiver shown previously in Figure 4-18. In doing so we first observe from the "reference" curves in both figures that in fullband jamming the limiter-discriminator FH/CPFSK receiver performs better than the one using differential detection, a well known result. For example, using the values of $h=0.7$ and $W_{IF}T=1.0$ the limiter-discriminator requires about 11.6 dB to produce P_e in the Gaussian channel, compared to 14.7 dB for the differential detector. Yet, in worst-case partial-band noise jamming with both receivers using AGC weighting and optimum diversity, we observe that the differential detector outperforms the limiter-discriminator by requiring a smaller value of E_b/N_J to achieve the same error probability. For example, the optimum diversity for both receivers to achieve $P_e=10^{-5}$ is $L=6$; the differential detector requires $E_b/N_J \approx 17$ dB to accomplish this level of performance, while the limiter-discriminator requires $E_b/N_J \approx 23$ dB.

The clue to understanding the better performance of the differential detector when diversity is employed for FH/CPFSK is to compare the variation in E_b/N_J required to achieve $P_e=0.10$ in both Figures 4-18 and 4-28 as the value of L is increased from $L=1$. The curves in Figure 4-18 are spaced further apart than those in Figure 4-28; this demonstrates that the limiter-discriminator receiver, although it enjoys a "head start" or advantage over the differential detector when $L=1$, is subject to higher noncoherent combining losses (associated with FM click noise as discussed in Section 4.1) than is the differential detector. This point is also brought out by the comparison shown in Figure 4-29, in which we have given both types of receiver the same performance ($P_e=10^{-5}$) for $L=1$ and no jamming. The asymptotic performances of the receivers for high E_b/N_J values is the performance in noise-only for the stated values of E_b/N_0. We observe in Figure 4-29 that the larger noncoherent combining losses prevent the use of $L=2$ from improving the system performance when a limiter-discriminator is employed, for this level of system performance without jamming; however, the differential detector, which has smaller noncoherent combining losses, yields improvement for L as high as $L=3$.

brought out by the comparison shown in Figure 4-29, in which we have given both types of receiver the same performance ($P_e = 10^{-5}$) for $L=1$ and no jamming. The asymptotic performances of the receivers for high $E_b/\mathcal{N}_J$ values is the performance in noise-only for the stated values of $E_b/\mathcal{N}_0$. We observe in Figure 4-29 that the larger noncoherent combining losses prevent the use of $L=2$ from improving the system performance when a limiter-discriminator is employed, for this level of system performance without jamming; however, the differential detector, which has smaller noncoherent combining losses, yields improvement for L as high as $L=3$.

The somewhat poor performance of the limiter-discriminator for $L>1$ can perhaps be improved by adjusting the receiver parameters h and $W_{IF}T$. In [5], for example, it is said that the performance of FH/CPFSK in worst-case partial-band noise jamming is optimized for $h=0.6$ and $W_{IF}T=0.75$. Variation in these parameters to find the best combination under the jamming conditions is outside the scope of the work summarized in this report, however.

Another interesting way to look at what we observe in this comparison is that the differential detector, whose output is proportional to $\sin\Delta\Phi$, performs further processing on the limiter-discriminator output, $\Delta\Phi$: the sine function both *limits* the value of the receiver output, since $|\sin x| \leq 1$, and nullifies the effects of any 2π phase shifts (clicks) superimposed on $\Delta\Phi$ due to the *phase ambiguity* property of the sine function: $\sin(x\pm 2\pi) = \sin x$.

4.5.1.2 Comparison of limiter-discriminator results

We now compare the uncoded receiver performances using diversity combining and limiter-discriminator detection shown in Figure 4-18, for AGC soft-decision combining, and in Figure 4-6, for hard-decision combining. Both figures assume $E_b/\mathcal{N}_0 = 20\,\mathrm{dB}$. It is apparent at once from comparing these two sets of curves that, for limiter-discriminator detection of FH/CPFSK, the hard-decision receiver performs *better* than the soft-decision receiver. For example, using the best value of L, a 10^{-5} error probability is achieved for $E_b/\mathcal{N}_J = 17\,\mathrm{dB}$ for hard-decision combining and for $E_b/\mathcal{N}_J = 23\,\mathrm{dB}$ for soft-decision combining. This is a surprising result, since soft-decision procedures generally outperform hard-decision ones.

The reason for this surprising result is that when diversity is used, the bit or channel symbol energy is split into L chips, with the consequence that the value of the chip energy-to-noise-density ratio is decreased from $E_b/\mathcal{N}_0$ by the factor $1/L$. This decrease in signal energy per observation interval gives rise to a disproportionately
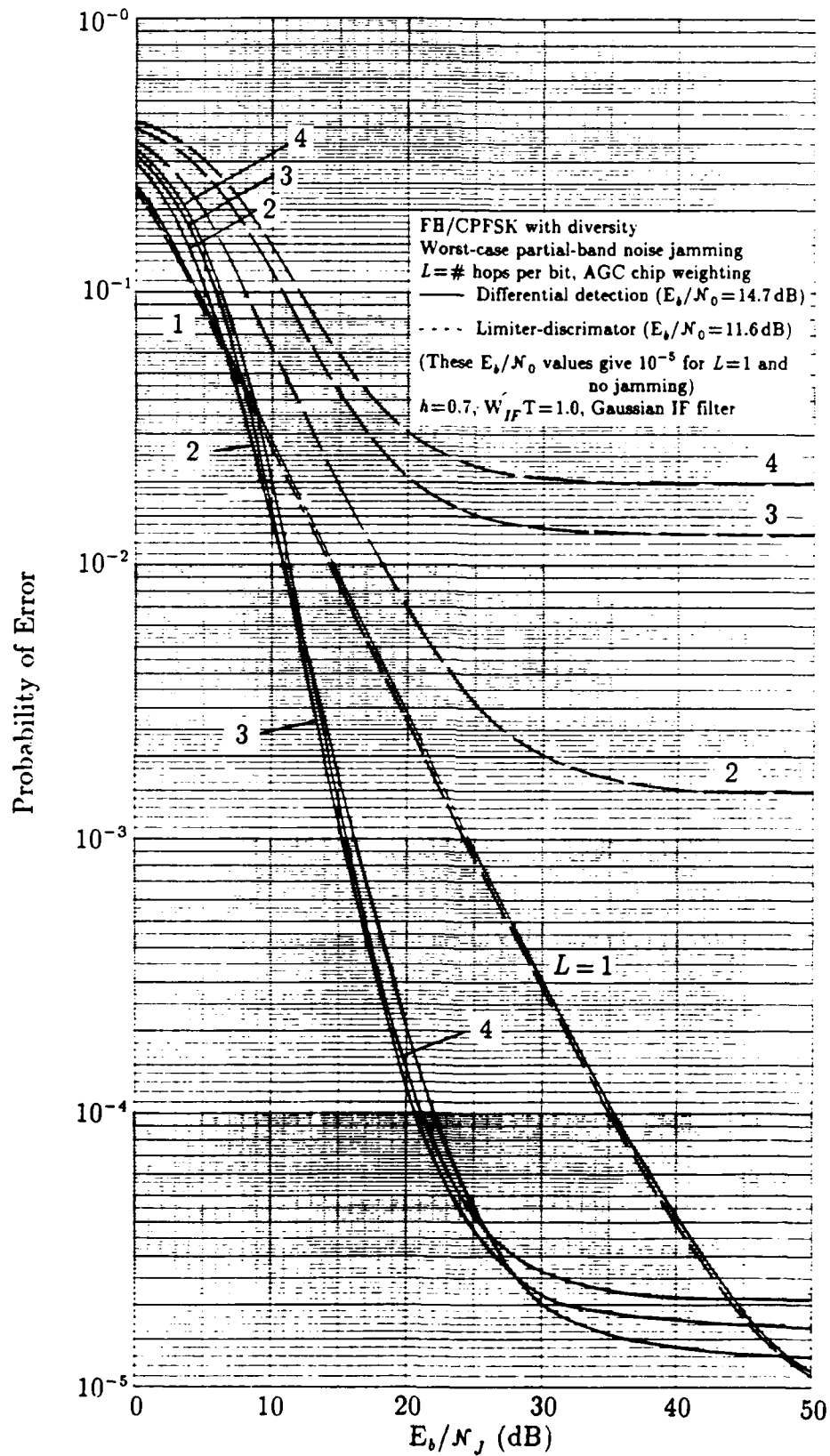
FIGURE 4-29 COMPARISON OF THE DIVERSITY PERFORMANCES OF
FH/CPFSK IN PARTIAL-BAND JAMMING

91

higher risk of FM noise clicks, especially on jammed hops. Now, if soft-decision combining is used, the sum of the differential phase samples can be "contaminated" by the occurrence of a click on any or all of the hops from which the samples are taken. For example, if $L=2$, supposing that one hop is jammed and one is not, the value of the sum of the samples is

$$w_1 \cdot \Delta\Phi_1 + w_0 \cdot \Delta\Phi_2 = \Delta\phi(w_1 + w_0) - 2\pi(w_1 N_1 + w_0 N_2) + w_1 \Delta\eta_1 + w_0 \Delta\eta_2$$

$$= \Delta\phi\left(1 + \frac{1}{\sqrt{\kappa}}\right) - 2\pi\left(\frac{N_1}{\sqrt{\kappa}} + N_2\right) + \frac{\Delta\eta_1}{\sqrt{\kappa}} + \Delta\eta_2 \qquad (4\text{-}50)$$

in which $\Delta\phi$ is the nominal (noiseless) differential phase (assumed positive), the $\Delta\eta$'s are the differential phase noise samples, κ is the ratio of jammed noise power to unjammed noise power, and the N's are click numbers jamming—whose averages are α_1 and α_0 with and without jamming, respectively. Typically, $\Delta\phi$ is between 0.5π and π, and α_0 is very small. Thus while the AGC weighting takes care of the phase noise, in effect equalizing the noise for jammed and unjammed hops, it does not remove the clicks, if and when they occur, although their contributions on jammed hops are attenuated.

Now, when hard decisions on each hop are used, any false decision that is due to jamming or to the occurrence of clicks (which are disproportionately more likely on jammed hops) is automatically "contained" to one "vote" in the overall L-hop decision.

4.5.1.3 General comparison without coding

Comparing now the limiter-discriminator FH/CPFSK receiver with either hard or soft decisions and the differential detector with soft decisions, it would appear from the computed results that the choice of receiver among these three to mitigate the effects of worst-case partial-band noise jamming will depend on the value of $E_b/\mathcal{N}_0$. If there is relatively little thermal noise (high $E_b/\mathcal{N}_0$), the ECCM receiver of choice would be the combination of hard decisions and the limiter-discriminator. If the thermal noise is definitely not negligible ($E_b/\mathcal{N}_0 < 20\,\text{dB}$), the differential detector with AGC-weighted soft decisions should be used.

4.5.2 Coded Performance Results and Comparisons

A number of computations were made of the performance of a coded FH/CPFSK system, assuming that an "outer code" is used in conjunction with an "inner code" consisting of one of the combinations of receiver design and L-hop/code symbol ECCM combining techniques. As discussed in Section 2, the error-correcting outer code selected for the study is a rate-$\frac{1}{2}$, constraint length 7, convolutional code, with either

hard or soft decoding. The comparisons to be made are among the following cases:

A. Limiter-discriminator detection with

    1. Hard-decision diversity combining, hard outer decoding

    2. Soft-decision AGC diversity combining, hard outer decoding

    3. Hard-decision diversity combining, soft outer decoding.

B. Differential detection with

    1. Hard-decision diversity combining, hard outer decoding

    2. Soft-decision AGC diversity combining, hard outer decoding

    3. Hard-decision diversity combining, soft outer decoding.

The methodology for calculating upper bounds on the bit error probability when coding is used was summarized in Section 2.2.2 (pp. 27, 28). Since the rate of the selected code is $r=\frac{1}{2}$, note that numerical values for these bounds as a function of $E_b/\mathcal{N}_J$ can be thought of as being developed in two steps: (1) Find the value of the uncoded error probability for 3 dB less than $E_b/\mathcal{N}_J$ AND 3 dB less for $E_b/\mathcal{N}_0$; and (2) map the value of the uncoded error probability into the value for the coded error probability bound.

For example, equations (2-48) through (2-51) imply that 10^{-7}, 10^{-6}, 10^{-5}, 10^{-4}, 10^{-3}, and 10^{-2} hard-decision decoding error probability bounds result from code symbol error probabilities of 0.007177, 0.01116, 0.01711, 0.02572, 0.03773, and 0.05409, respectively. Thus if we are interested in estimating the region of $E_b/\mathcal{N}_J$ for which the decoded bit error probability is between 10^{-7} and 10^{-2}, then we may look at the curves for the uncoded error probability and find the range of $E_b/\mathcal{N}_J$ for which that quantity is between 0.0072 and 0.054; to these $E_b/\mathcal{N}_J$ values we then add 3 dB. Applying this technique to Figure 4-6 (page 53), we find that for $E_b/\mathcal{N}_0=20$ dB the uncoded error probability is in the range of 0.007 to 0.05 for, approximately, 5.5 dB $\leq E_b/\mathcal{N}_J \leq 14.5$, implying that for hard-decision decoding the coded error probability will be between 10^{-7} and 10^{-2} for $E_b/\mathcal{N}_J$ between 8.5 dB and 17.5 dB. Some approximation is involved because the curves in Figure 4-6 are valid for $E_b/\mathcal{N}_0=20$ dB, not 17 dB.

While this technique is useful for estimating coded results, its primary usefulness is for checking the results for reasonableness. In all of the coded results presented below, the error probabilities were recalculated as functions of $E_b/\mathcal{N}_J$ for fixed values of $E_b/\mathcal{N}_0$ and of γ, the partial-band jamming fraction, and from these parametric curves the worst-case performance was determined.

4.5.2.1   Results for hard-decision diversity combining and hard decoding

In Figure 4-30, the worst-case partial-band noise jamming performance of FH/CPFSK is presented as a function of $E_b/\mathcal{N}_J$ for $E_b/\mathcal{N}_0 = 20\,\text{dB}$, for different values of L, the number of hops per code symbol, and for both limiter-discriminator and differential detection, assuming hard-decision diversity combining and hard decoding. Intersymbol interference has been accounted for in the calculations, using the parameter values $h = 0.7$ and $W_{IF}T = 1.0$, and assuming a Gaussian IF filter.

We first observe, as a check on these results, that the range of $E_b/\mathcal{N}_J$ for which the coded bit error probability falls between 10^{-7} and 10^{-2} is in agreement with that predicted from the relevant uncoded results shown previously in Figure 4-6, for the limiter-discriminator receiver. (Uncoded hard-decision combining performance results were not computed for the differential detector.)

The coded performance of the receiver using limiter-discriminator detection is seen to be uniformly better than that for the receiver using differential detection. While for the unjammed Gaussian channel the limiter-discriminator is about 3.1 dB better compared to the differential detector (using the value of $E_b/\mathcal{N}_0$ required to obtain a 10^{-5} error probability as a basis for comparison), we see from Figure 4-30 that this advantage is reduced to about 1.3 dB in worst-case partial-band noise jamming when coding and diversity are employed.[4] This same margin is observed for no coding and no diversity in worst-case jamming, when the BER curve-fit approximation (4-14) is used to calculate the jammed error probability for the limiter-discriminator receiver.

For both receiver types, the optimum value of L ("optimum diversity") is seen to depend on the value of $E_b/\mathcal{N}_J$. For achieving $P_e = 10^{-5}$, that value is $L = 3$, in contrast to the much higher value (≤ 11) without coding. The reason why a lower value of diversity is optimum with coding than without coding, for achieving the same error probability, is that with coding the symbol error probability at the output of the diversity combining portion of the receiver is much higher (between .007 and .05, as we have seen) and is in the region of the curves parametric in L for which lower values of L tend to be optimum; quite often in this region the worst-case value of γ, the partial-band jamming fraction is close to unity, therefore indicating a nearly Gaussian channel under the noise jamming, so that an increase in L from $L = 1$ tends incurs a noncoherent combining loss in performance for a lower value of L than without coding.

---

[4] A summary comparison of $E_b/\mathcal{N}_J$ requirements to achieve $P_e = 10^{-5}$ with and without diversity and coding will be given below.

$h = 0.7$, $W_{IF}T = 1.0$, Gaussian IF filter
L hops per code symbol (FH/CPFSK)
Hard-decision diversity combining
Outer convolutional coding
(rate 1/2, constraint length 7)
Hard outer decoding
Worst-case partial-band noise jamming

$E_b/N_0 = 20\,\mathrm{dB}$

Differential detection
Limiter-discriminator detection

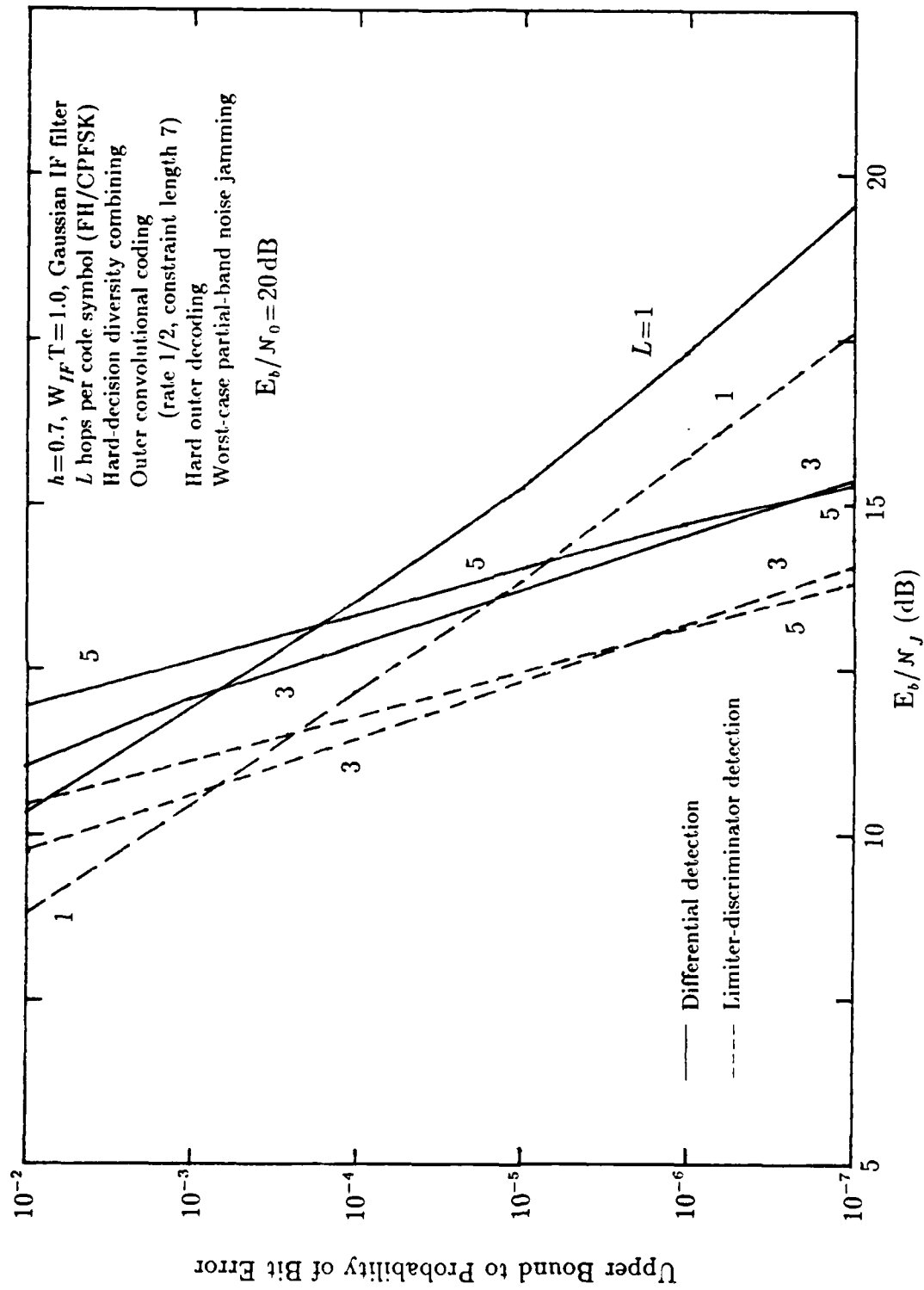E_b/N_J (dB)

Upper Bound to Probability of Bit Error

FIGURE 4-30 CODED PERFORMANCE WITH HARD-DECISION COMBINING AND HARD DECODING

4.5.2.2   Results for soft-decision diversity combining and hard decoding

The worst-case partial-band noise jamming coded performance of limiter-discriminator and differential detection FH/CPFSK receivers is presented in Figure 4-31 for the case of AGC soft-decision diversity combining and hard decoding when $E_b/N_0 =$ 20 dB. It might have been anticipated from the relative performances of these two receivers with AGC combining but without coding that the differential detector would display a better performance with coding. However, the results in Figure 4-31 indicate that the limiter-discriminator consistently achieves a better performance, although for $L > 1$ its advantage is small, on the order of 1 dB or less for a given value of L.

For $L = 1$, the advantage of the limiter-discriminator over the differential detector at the 10^{-5} bit error probability level shown in Figure 4-31 is about 3.7 dB. It should be noted that the same quantity is about 1.4 dB in Figure 4-30, or 2.3 db less, even though in principle the combining and decoding portions of the respective receivers are identical when $L = 1$. This difference is apparently due in part to the use of two different approaches to calculating the probability of error at the output of the combiner (input to the decoder). For hard-decision combining, as noted in connection with Figure 4-30, an approximation (curve fit) was used since it was sufficient for those calculations to utilize a BER curve for $L = 1$. For AGC soft-decision combining, the probability of coded symbol error was computed using a mixture approximation for the characteristic function of the limiter-discriminator output samples. Although as shown in Figure 4-3 (page 50) the curve-fit approximation is very good for the Gaussian channel — the two computational methods agree — evidently for worst-case jamming they disagree slightly, with the difference being magnified when coding is applied.

For the optimum values of AGC diversity combining, the limiter-discriminator receiver achieves a 10^{-5} bit error probability for about a 1.1 dB smaller value of E_b/N_J than does the differential detection receiver.

4.5.2.3   Results for hard-decision diversity combining and soft decoding

Figure 4-32 gives the coded bit error probability for FH/CPFSK in worst-case partial-band noise jamming for both limiter-discriminator and differential detection types of receiver, assuming hard-decision diversity combining, soft-decision decoding, and $E_b/N_0 = 20$ dB. As in Figures 4-30 and 4-32, the limiter-discriminator is seen to achieve a better performance consistently for the range of P_e values shown. At the 10^{-5} level of performance, when optimum diversity is used, the limiter-discriminator's advantage is about 1.5 dB.
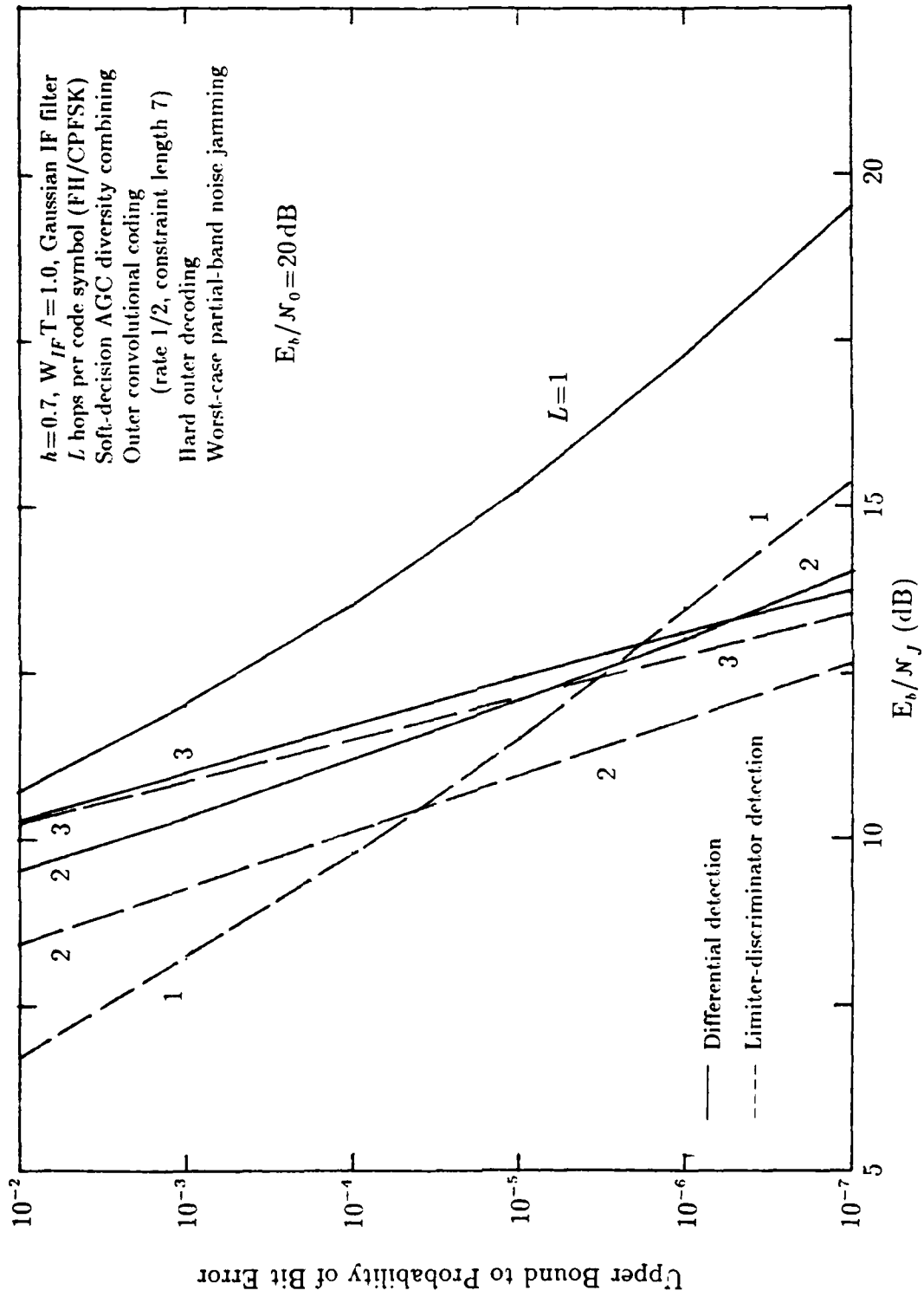
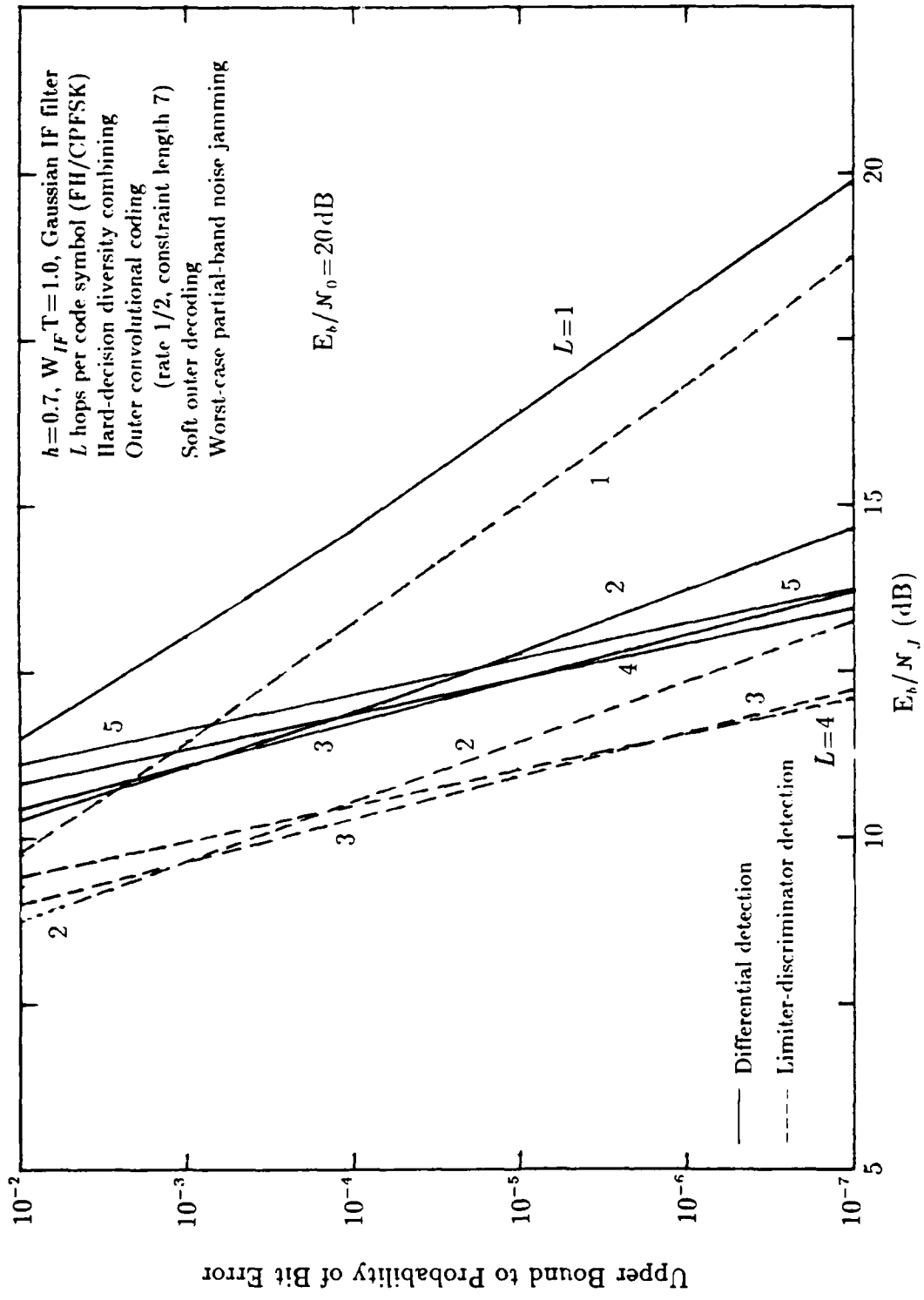FIGURE 4-31 CODED PERFORMANCE WITH AGC SOFT-DECISION COMBINING AND HARD DECODING

FIGURE 4-32 CODED PERFORMANCE WITH HARD-DECISION COMBINING AND SOFT DECODING

In comparing coded results for $L=1$ shown in Figures 4-30, for hard decoding, and 4-32, for soft decoding, we note that there are differences in the values of E_b/N_J required to achieve a particular value of bit error probability, with these values being *higher* for soft-decoding. This draws attention to the fact that both performances are actually upper bounds to the probability of bit error, not the actual bit error probability, and the two bounding techniques give rise to different numbers for the same conditions. When, for example, $L=3$ is considered, it is readily apparent that the soft decoding produces about a 1.4 dB gain over the hard decoding by making use of the additional information made available to it. This number is very close to the 1.5 dB gain predicted in [1].

4.5.2.4 Summary comparison of coded performance results

Supposing that optimum diversity is always used, a kind of lower bound (with respect to the order of diversity) to the error probability upper bounds shown in Figures 4-30 to 4-32 can be constructed as shown in Figure 4-33. It is apparent from this figure that the variation in the value of E_b/N_J required to obtain a bit error of 10^{-5} is relatively slight, being within a range of about 3 dB for different combinations of receiver type, diversity combining technique, and decoding technique.

A consistent pattern (in addition to the advantage of using limiter-discriminator detection instead of differential detection) evident in Figure 4-33 is the following ranking of the combinations of diversity combining and decoding techniques that were studied: generally for P_e values of 10^{-5} or less, best performance is obtained using hard-decision combining and soft decoding. AGC soft-decision combining plus hard decoding is second best, and the combination of hard-decision combining and hard decoding is third best. Some form of soft processing therefore is advantageous.

It is interesting to note that for $10^{-4} < P_e < 10^{-2}$, the ranking of soft decoding and soft combining is reversed. The reason for this behavior seems to be the fact that for these values of the error probability, the optimum diversity is $L=1$ for soft combining and $L=2$ (or 3) for soft decoding. However, as noted before the relative behavior of the two decoding error probability bounds is uncertain for $L=1$, and for these higher values of P_e the tightness of the bounds can be expected to diminish.

A summary of E_b/N_J requirements to achieve $P_e = 10^{-5}$ when $E_b/N_0 = 20$ dB is given in Table 4-1. For reference, the first case shown in the table is the worst-case FH/CPFSK performance for no coding and no diversity, noting the differences obtained
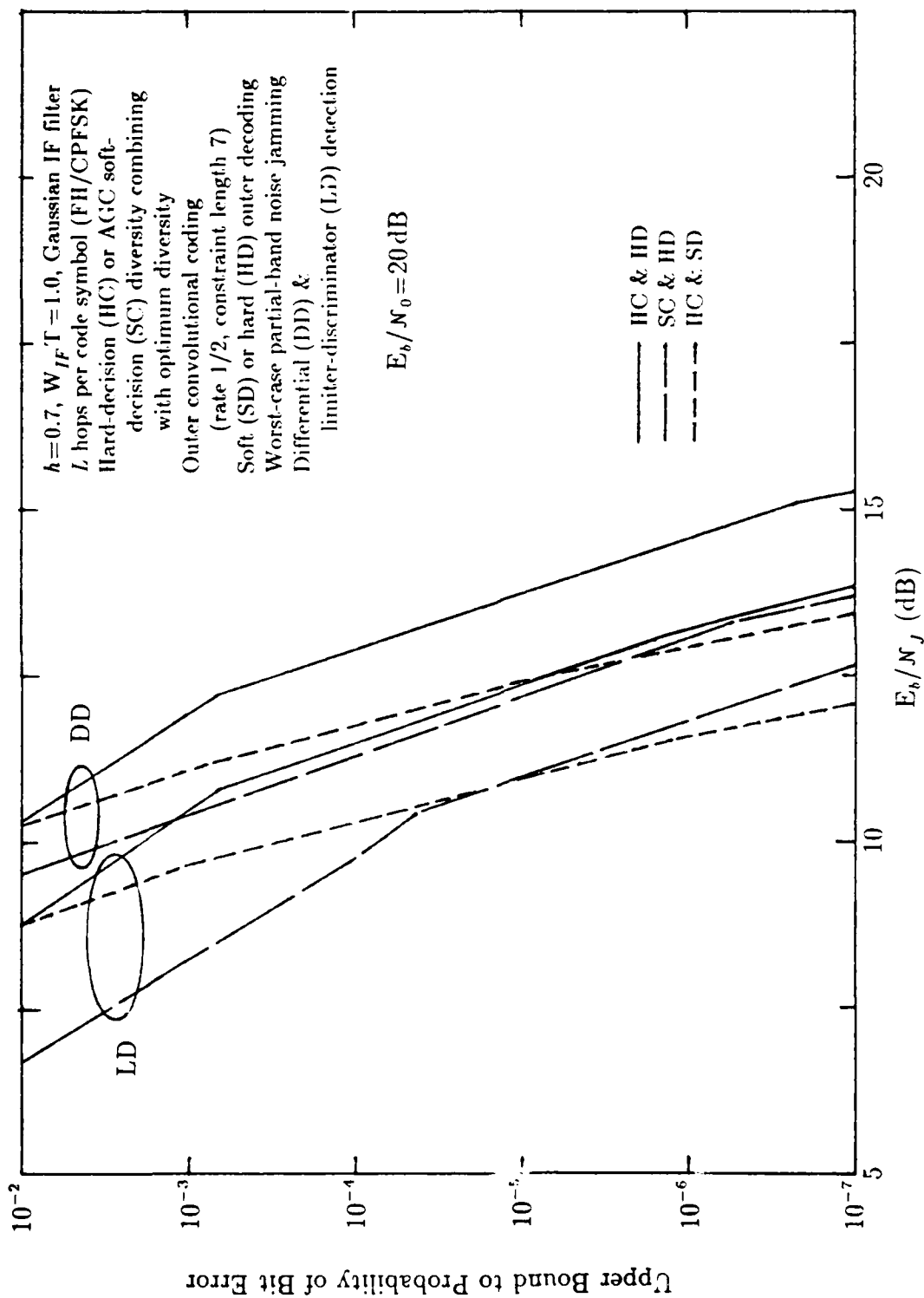
FIGURE 4·33   CODED PERFORMANCE COMPARISON WITH OPTIMUM DIVERSITY

TABLE 4-1

REQUIREMENTS FOR 10^{-5} P_e IN WORST-CASE JAMMING WHEN $E_b/\mathcal{N}_0 = 20$ dB

FH/CPFSK: $h = 0.7$, $W_{IF}T = 1.0$, Gaussian IF filter

Case	Limiter-discriminator $E_b/\mathcal{N}_J$(dB)	Gain	Differential detector $E_b/\mathcal{N}_J$(dB)	Gain
Reference: no coding				
no diversity	43.0^1	---	44.4^3	---
	44.1^2	---		
No coding, optimum diversity				
hard combining	$<16.7^1$ ($L{=}11$)	>26.3	not computed	
AGC combining	$<22.8^2$ (6)	>21.3	17.0 (6)	27.4
Coding only ($L{=}1$)				
hard decoding	13.8^1	29.2	15.2	29.2
	11.5^2	32.6		
soft decoding	15.0^1	28.0	16.4	28.0
Coding, optimum diversity				
hard comb., hard decoding	12.3^1 (3)	30.7	13.7 (3)	30.7
AGC comb., hard decoding	11.0^2 (2)	33.1	12.1 (2)	32.3
hard comb., soft decoding	10.9^1 (3)	32.1	12.4 (3)	32.0

Notes:

1. All hard-decision combining results for the limiter-discriminator were calculated using the curve-fit approximation to the bit error probability.

2. All AGC soft-decision combining results for the limiter-discriminator were calculated using the numerical integration/characteristic function technique.

3. All differential detector results were calculated using the numerical integration/characteristic function technique.

for the limiter-discriminator for the two computational methods used. The second case shown in the table is that of optimum diversity without coding, for which it is evident that diversity alone can produce a gain in performance as high as 26 or 27 dB, in terms of reducing the required E_b/N_J.

The third case shown in Table 4-1 is that of coding alone, without the use of diversity (i.e., $L=1$). Here we observe that coding alone can produce a gain of 28 dB or higher. It is somewhat surprising that the hard-decoding gains are consistently greater (by about 1 dB) than the soft-decoding gains in the cases studied. But on the other hand, for coding alone there is no reason to expect a different performance with soft decoding, since $L=1$. The 1 dB difference therefore is due to the difference in the probability of error upper bounds used.

The fourth and final case shown in Table 4-1 is the combination of optimum diversity, combining method. and decoding technique. Total coding plus diversity gains of about 31-33 dB are seen to be possible. We observe also that the addition of diversity to coding provides an incremental gain in performance of about 2-4 dB, whereas if coding is added to diversity an improvement of about 5 dB is experienced. Thus it would appear that the more influential factor in the improvement in performance is coding. especially when it is considered how much the performance is improved using coding alone.

APPENDIX A
INTERSYMBOL INTERFERENCE ANALYSIS

We have observed that the IF bandpass filter has the effect of distorting the data-modulated phase waveform $\theta_m(t)$, resulting in the distorted phase waveform

$$\phi(t) = \tan^{-1}\left\{\frac{h_0(t)*\sin\theta_m(t)}{h_0(t)*\cos\theta_m(t)}\right\}, \qquad \text{(A-1)}$$

as well as in an amplitude modulation, $a(t)$. For most cases of practical interest, it is sufficient to consider intersymbol interference (ISI) effects (i.e., the overlapping of filter responses from different transmitted symbol or chip intervals) due to immediately adjacent symbols or chips [6]. Therefore, in what follows we consider chip patterns on the FH/CPFSK hops which are the periodic extensions of the patterns

$$
\begin{array}{lll}
1\underline{1}1.\,0\underline{0}0 & \text{(all one's or zeros)}; & \\
0\underline{1}0,\,1\underline{0}1 & \text{(alternating one's and zeros)}; & \text{(A-2)} \\
\text{and} \quad 0\underline{1}10,\,1\underline{0}01,\,1\underline{1}00,\,0\underline{0}11. & &
\end{array}
$$

The "present chip" in each of these sequences is indicated by the underlining. The patterns in (A-2) were selected because they generate the eight possible 3-chip patterns in a very simple manner and can be analyzed easily.

Using the steady-state filtering approach of Tjhung and Wittke [19] and Pawula [11, 12], we recognize that the periodic extension of the in-phase and quadrature signal waveforms for the ith pattern yields the Fourier series

$$\sin\theta_m(t;\,\text{pattern } i) = \sum_{k=1}^{\infty} \alpha_{ki}\cos\left(2\pi k f_{p_i}t + \gamma_{ki}\right) \qquad \text{(A-3a)}$$

and

$$\cos\theta_m(t;\,\text{pattern } i) = \sum_{k=1}^{\infty} \beta_{ki}\cos\left(2\pi k f_{p_i}t + \eta_{ki}\right), \qquad \text{(A-3b)}$$

where f_{p_i} is the appropriate fundamental frequency. Then the responses of the IF filter's lowpass equivalent $h_0(t)$ to these series are

$$u(t;\,\text{pattern } i) \triangleq h_0(t)*\sin\theta_m(t;\,\text{pattern } i)$$

$$= \sum_{k=1}^{\infty} |H_0(k f_{p_i})|\,\alpha_{ki}\cos\left[2\pi k f_{p_i}t + \varphi_{ki} - B(k f_{p_i})\right] \qquad \text{(A-4a)}$$

and

$$v(t;\,\text{pattern } i) \triangleq h_0(t)*\cos\theta_m(t;\,\text{pattern } i)$$

$$= \sum_{k=1}^{\infty} |H_0(k f_{p_i})|\,\beta_{ki}\cos\left[2\pi k f_{p_i}t + \eta_{ki} - B(k f_{p_i})\right]. \qquad \text{(A-4b)}$$

where $|H_0(f)|$ is the magnitude of the lowpass filter's frequency transfer function and $B(f)$ is its phase delay as a function of frequency. The analysis is considerably simplified if we introduce time offsets t_u and t_v such that $\sin[\theta_m(t-t_u)]$ and $\cos[\theta_m(t-t_v)]$, respectively, are even functions. Also, we assume that the filter has a *linear phase delay characteristic*, that is,

$$B(f) = 2\pi f t_d. \tag{A-5}$$

Together, these simplifying factors allow us to rewrite (A-4a) as

$$u(t; \text{pattern } i) \triangleq \sum_{k=1}^{\infty} |H_0(kf_{p_i})|\, \alpha_{ki} \cos[2\pi k f_{p_i}(t + t_u + t_d)] \tag{A-6a}$$

and

$$v(t; \text{pattern } i) \triangleq \sum_{k=1}^{\infty} |H_0(kf_{p_i})|\, \beta_{ki} \cos[2\pi k f_{p_i}(t + t_v + t_d)]. \tag{A-6b}$$

Patterns 1$\underline{1}$1. 0$\underline{0}$0. For the patterns 1$\underline{1}$1 and 0$\underline{0}$0, the undistorted signal is a pure sinusoid, with

$$\theta_m(t; 1\underline{1}1) = -\theta_m(t; 0\underline{0}0)$$

$$= \pi h t/T = 2\pi f_d t. \tag{A-7}$$

Thus for these patterns $\sin\theta_m(t)$ and $\cos\theta_m(t)$ are single-term Fourier series. and their distorted versions are

$$u(t; 1\underline{1}1) = -u(t; 0\underline{0}0) = a_0 \sin[\pi h(t - t_d)/T] \tag{A-8a}$$

and

$$v(t; 1\underline{1}1) = u(t; 0\underline{0}0) = a_0 \cos[\pi h(t - t_d)/T], \tag{A-8b}$$

using the parameter

$$a_0 \triangleq |H_0(f_d)|. \tag{A-9}$$

These quantities in turn give the ISI parameters

$$\Delta\phi(t; 1\underline{1}1) = -\Delta\phi(t; 0\underline{0}0) = \pi h \tag{A-10a}$$

$$a^2(t; 1\underline{1}1) = a^2(t; 0\underline{0}0) = a_0^2 \tag{A-10b}$$

and

$$a^2(t-T; 1\underline{1}1) = a^2(t-T; 0\underline{0}0) = a_0^2. \tag{A-10c}$$

Note that for these patterns the parameter values are independent of the sampling time.

Patterns 0$\underline{1}$0, 1$\underline{0}$1. For the patterns 0$\underline{1}$0 and 1$\underline{0}$1, the original frequency modulation is a $\pm f_d$ squarewave with period $2T$, so that $\theta_m(t)$ is an even, bipolar triangular wave with amplitude $\frac{1}{2}\pi h$ and period $2T$. For pattern 0$\underline{1}$0, the triangular wave's first positive peak occurs at $t = T$, using the convention that the baseband data waveform is such that $d(t) = d_k$ for $(k-1)T < t \leq kT$. We note that pattern 1$\underline{0}$1 is simply the negative of pattern 0$\underline{1}$0. The functions $\sin\theta_m(t; 0\underline{1}0)$ and $\cos\theta_m(t; 0\underline{1}0)$ therefore are even, with

periods 2T and T, respectively. Expansion of these functions in Fourier series yields

$$\sin\theta_m(\text{t}; 0\underline{1}0) = -\sin\theta_m(\text{t}; 1\underline{0}1)$$

$$= -\frac{4h}{\pi}\cos\left(\tfrac{1}{2}\pi h\right)\sum_{k=1}^{\infty}\frac{\cos\left[(2k-1)\pi\text{t}/\text{T}\right]}{(2k-1)^2-h^2} \tag{A-11a}$$

and

$$\cos\theta_m(\text{t}; 0\underline{1}0) = \cos\theta_m(\text{t}+\text{T}; 1\underline{0}1)$$

$$= \frac{2}{\pi h}\sin\left(\tfrac{1}{2}\pi h\right)\left[1-2h^2\sum_{k=1}^{\infty}\frac{\cos\left(2k\pi\text{t}/\text{T}\right)}{4k^2-h^2}\right]. \tag{A-11b}$$

Assuming the filter rejects harmonics with $f>1/\text{T}$, we find that the signal quadrature components for these patterns are

$$\text{u}(\text{t}; 0\underline{1}0) = -\text{u}(\text{t}; 1\underline{0}1)$$

$$= -\frac{4h}{\pi}\cos\left(\tfrac{1}{2}\pi h\right)\left|H_0\left(\tfrac{1}{2\text{T}}\right)\right|\frac{1}{1-h^2}\cos\left[\pi(\text{t}-\text{t}_d)/\text{T}\right] \tag{A-12a}$$

$$= -c_1\cos\left[\pi(\text{t}-\text{t}_d)/\text{T}\right] \tag{A-12b}$$

and

$$\text{v}(\text{t}; 0\underline{1}0) = \text{v}(\text{t}; 1\underline{0}1)$$

$$= \frac{2}{\pi h}\sin\left(\tfrac{1}{2}\pi h\right)\left[1-\frac{2h^2}{4-h^2}\left|H_0\left(\tfrac{1}{\text{T}}\right)\right|\cos\left[2\pi(\text{t}-\text{t}_d)/\text{T}\right]\right] \tag{A-12c}$$

$$= c_2 - c_3\cos\left[2\pi(\text{t}-\text{t}_d)/\text{T}\right]. \tag{A-12d}$$

These quantities at the sampling time $\text{t} = \text{T} + \text{t}_d$ give the ISI parameters

$$\Delta\phi(\text{t}_d+\text{T}; 0\underline{1}0) = -\Delta\phi(\text{t}_d+\text{T}; 1\underline{0}1)$$

$$= 2\tan^{-1}\left(\frac{c_1}{c_2-c_3}\right) \tag{A-13a}$$

$$a^2(\text{t}_d+\text{T}; 0\underline{1}0) = a^2(\text{t}_d+\text{T}; 1\underline{0}1) = c_1^2 + (c_2-c_3)^2 \tag{A-13b}$$

and

$$a^2(\text{t}_d; 0\underline{1}0) = a^2(\text{t}_d; 1\underline{0}1) = c_1^2 + (c_2-c_3)^2. \tag{A-13c}$$

in which the constants are defined as

$$c_1 \triangleq \frac{4h}{\pi(1-h^2)}\cos\left(\tfrac{1}{2}\pi h\right)\left|H_0\left(\tfrac{1}{2\text{T}}\right)\right| \tag{A-14a}$$

$$c_2 \triangleq \frac{2}{\pi h}\sin\left(\tfrac{1}{2}\pi h\right) = \text{sinc}\left(\tfrac{1}{2}h\right) \tag{A-14b}$$

and

$$c_3 \triangleq \frac{4h}{\pi(4-h^2)}\sin\left(\tfrac{1}{2}\pi h\right)\left|H_0\left(\tfrac{1}{\text{T}}\right)\right|. \tag{A-14c}$$

Distorted and undistorted phase-related waveforms for the 010 pattern are illustra-

ted in Figure A-1.

Patterns 0110, 1001. For patterns 0110 and 1001, the original frequency modulation is a $\pm f_d$ squarewave with period 4T, so that $\theta_m(t)$ for these patterns is an even, bipolar triangular wave with amplitude πh and period 4T. For pattern 0110, the triangular wave's first positive peak occurs at $t = 2T$. Pattern 1001 is the negative of pattern 0110. The functions $\sin\theta_m(t; 0110)$ and $\cos\theta_m(t; 0110)$ therefore are even, with periods 4T and 2T, respectively. Their Fourier series expansions are most easily written down as those for pattern 010, but with h replaced by $2h$ and with t replaced by $\frac{1}{2}t$:

$$\sin\theta_m(t; 0110) = -\sin\theta_m(t; 1001)$$

$$= -\frac{8h}{\pi}\cos(\pi h)\sum_{k=1}^{\infty}\frac{\cos[(2k-1)\pi t/2T]}{(2k-1)^2 - 4h^2} \qquad (A-15a)$$

and $\qquad \cos\theta_m(t; 0110) = \cos\theta_m(t; 1001)$

$$= \frac{\sin(\pi h)}{\pi h}\left[1 - 2h^2\sum_{k=1}^{\infty}\frac{\cos(k\pi t/T)}{k^2 - h^2}\right]. \qquad (A-15b)$$

Assuming the filter passes only harmonics of these Fourier series up to $f = 1/T$, we find that the signal quadrature components for these patterns are

$$u(t; 0110) = -u(t; 1001)$$

$$= -\frac{8h}{\pi}\cos(\pi h)\left\{\frac{1}{1-4h^2}|H_0(\tfrac{1}{4T})|\cos[\pi(t-t_d)/2T]\right.$$

$$\left. + \frac{1}{9-4h^2}|H_0(\tfrac{3}{4T})|\cos[3\pi(t-t_d)/2T]\right\} \qquad (A-16a)$$

$$= -c_4\cos[\pi(t-t_d)/2T] - c_5\cos[3\pi(t-t_d)/2T] \qquad (A-16b)$$

and $\qquad v(t; 0110) = v(t; 1001)$

$$= \frac{\sin(\pi h)}{\pi h}\left\{1 - \frac{2h^2}{1-h^2}|H_0(\tfrac{1}{2T})|\cos[\pi(t-t_d)/T]\right.$$

$$\left. - \frac{2h^2}{4-h^2}|H_0(\tfrac{1}{T})|\cos[2\pi(t-t_d)/T]\right\} \qquad (A-16c)$$

$$= c_6 - c_7\cos[\pi(t-t_d)/T] - c_8\cos[2\pi(t-t_d)/T]. \qquad (A-16d)$$

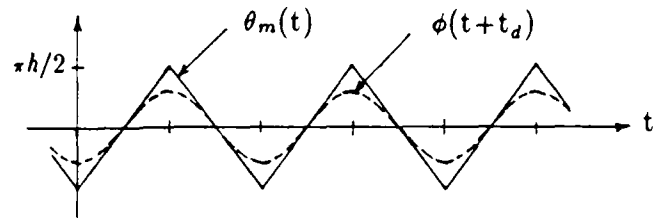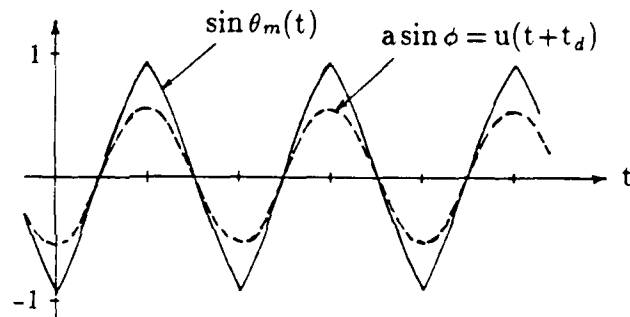At the sampling time $t = t_d + T$, these functions give rise to the ISI parameters
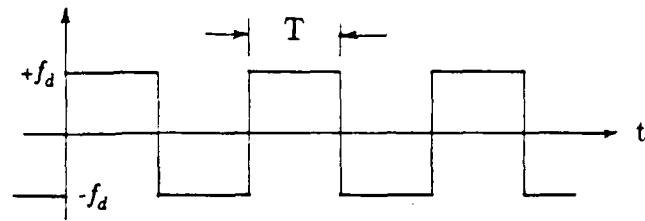
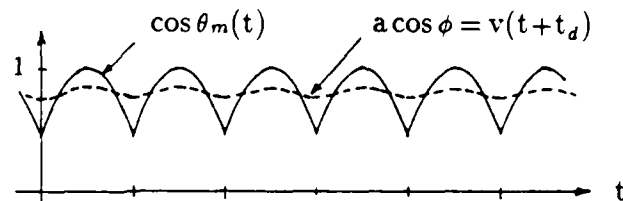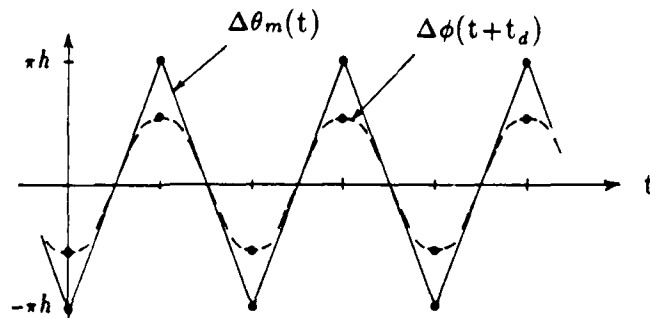FIGURE A-1 WAVEFORMS ASSOCIATED WITH THE PATTERN 010

107

$$\Delta\phi(t_d+T;\ 0\underline{1}10) = -\Delta\phi(t_d+T;\ 1\underline{0}01) \qquad \text{(A-17a)}$$

$$= \tan^{-1}\left(\frac{c_4+c_5}{c_6-c_7-c_8}\right) \qquad \text{(A-17b)}$$

$$a^2(t_d+T;\ 0\underline{1}10) = a^2(t_d+T;\ 1\underline{0}01) = (c_6+c_7-c_8)^2 \qquad \text{(A-17c)}$$

and
$$a^2(t_d;\ 0\underline{1}10) = a^2(t_d;\ 1\underline{0}01) \qquad \text{(A-17d)}$$

$$= (c_4+c_5)^2 + (c_6-c_7-c_8)^2 \qquad \text{(A-17d)}$$

in which the constants are defined as

$$c_4 \triangleq \frac{8h}{\pi(1-4h^2)}\cos(\pi h)\,|H_0(\tfrac{1}{4T})| \qquad \text{(A-18a)}$$

$$c_5 \triangleq \frac{8h}{\pi(9-4h^2)}\cos(\pi h)\,|H_0(\tfrac{3}{4T})| \qquad \text{(A-18b)}$$

$$c_6 \triangleq \frac{\sin(\pi h)}{\pi h} = \mathrm{sinc}(h) \qquad \text{(A-18c)}$$

$$c_7 \triangleq \frac{2h^2}{1-h^2}c_6\cdot|H_0(\tfrac{1}{2T})| \qquad \text{(A-18d)}$$

and
$$c_8 \triangleq \frac{2h^2}{4-h^2}c_6\cdot|H_0(\tfrac{1}{T})|. \qquad \text{(A-18e)}$$

Figure A-2 illustrates the various phase-related quantities for pattern $0\underline{1}10$.

Patterns $1\underline{1}00$, $0\underline{0}11$. Since pattern $1\underline{1}00$ and its negative, pattern $0\underline{0}11$, are time-shifted versions of patterns $0\underline{1}10$ and $1\underline{0}01$, we can immediately write that

$$u(t;\ 1\underline{1}00) = -u(t;\ 0\underline{0}11) \qquad \text{(A-19a)}$$

$$= u(t+T;\ 0\underline{1}10)$$

$$= c_4\sin[\pi(t-t_d)/2T] - c_5\sin[3\pi(t-t_d)/2T] \qquad \text{(A-19b)}$$

and
$$v(t;\ 1\underline{1}00) = v(t;\ 0\underline{0}11) \qquad \text{(A-19c)}$$

$$= v(t+T;\ 0\underline{1}10)$$

$$= c_6 + c_7\cos[\pi(t-t_d)/T] - c_8\cos[2\pi(t-t_d)/T]. \qquad \text{(A-19d)}$$

The corresponding ISI parameters at the sampling time are

$$\Delta\phi(t_d+T;\ 1\underline{1}00) = -\Delta\phi(t_d+T;\ 0\underline{0}11) \qquad \text{(A-20a)}$$

$$= \tan^{-1}\left(\frac{c_4+c_5}{c_6-c_7-c_8}\right) \qquad \text{(A-20b)}$$

$$a^2(t_d+T;\ 1\underline{1}00) = a^2(t_d+T;\ 0\underline{0}11) \qquad \text{(A-20c)}$$

$$= (c_4+c_5)^2 + (c_6-c_7-c_8)^2 \qquad \text{(A-20d)}$$
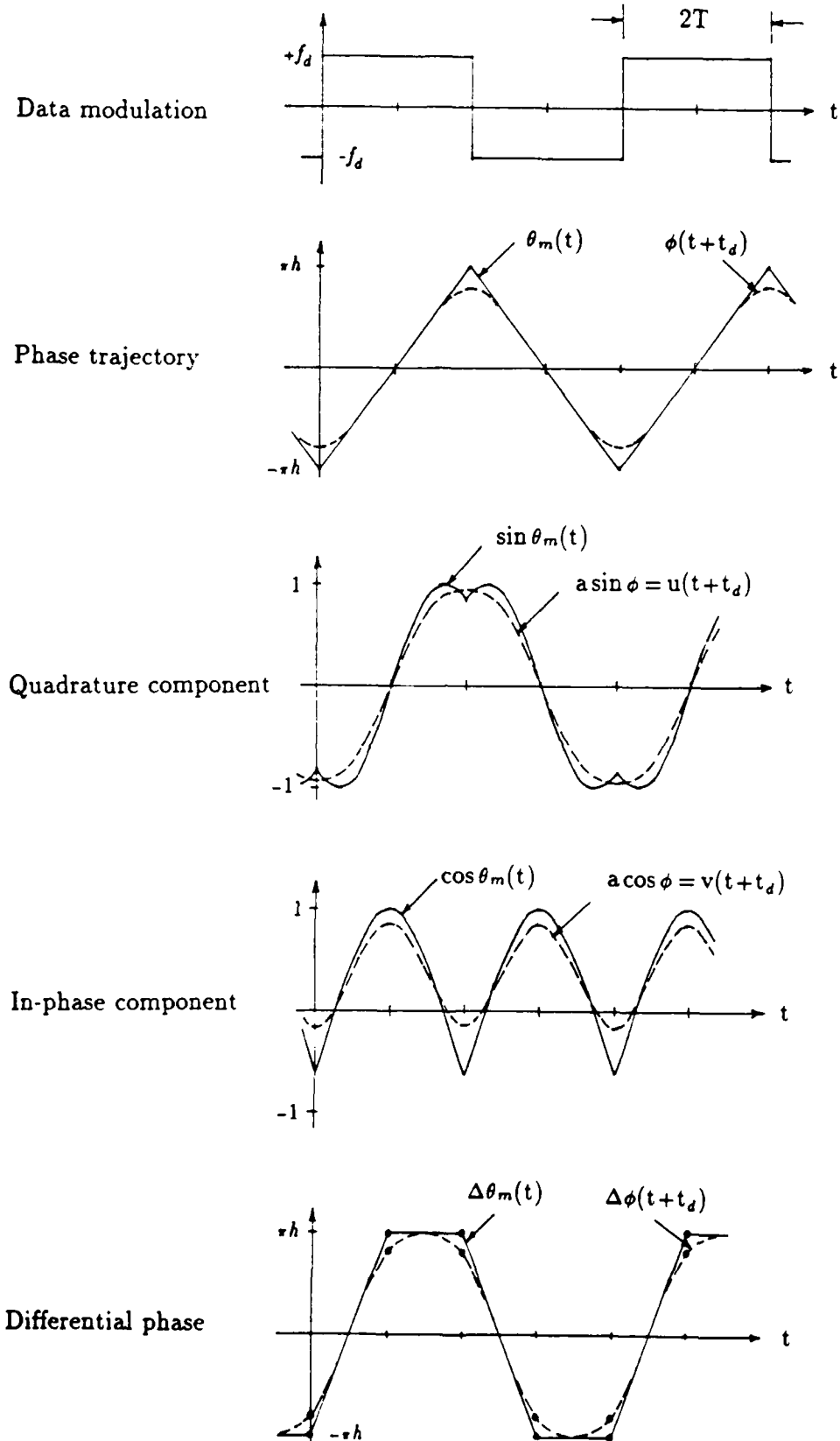
FIGURE A-2 WAVEFORMS ASSOCIATED WITH THE PATTERN 0110

109

and
$$a^2(t_d; 0\underline{1}10) = a^2(t_d; 1\underline{0}01) \qquad \text{(A-20d)}$$

$$= (c_6 + c_7 - c_8)^2 \qquad \text{(A-20d)}$$

Example values of the ISI pattern waveform parameters are given in Table A-1. A composite plot of all the differential phase waveforms $\Delta\phi(t)$ for the eight patterns is presented in Figure A-3 for example values of the input parameters h and $W_{IF}T$.

TABLE A-1
ISI PATTERN PARAMETER VALUES

Conditions: $h = 2f_d T = 0.7$, $D = W_{IF}T = 1.0$, Gaussian IF filter
CNR = carrier-to-noise power ratio

Data Patterns	$\Delta\phi$(rad.)	U/CNR	V/CNR	W/CNR
111, 000	±2.1991	0.6806	0.0000	0.6806
011, 100	±1.7108	0.7784	−0.0997	0.7719
010, 101	±1.2239	0.8696	0.0000	0.8696
110, 001	±1.7108	0.7784	0.0997	0.7719
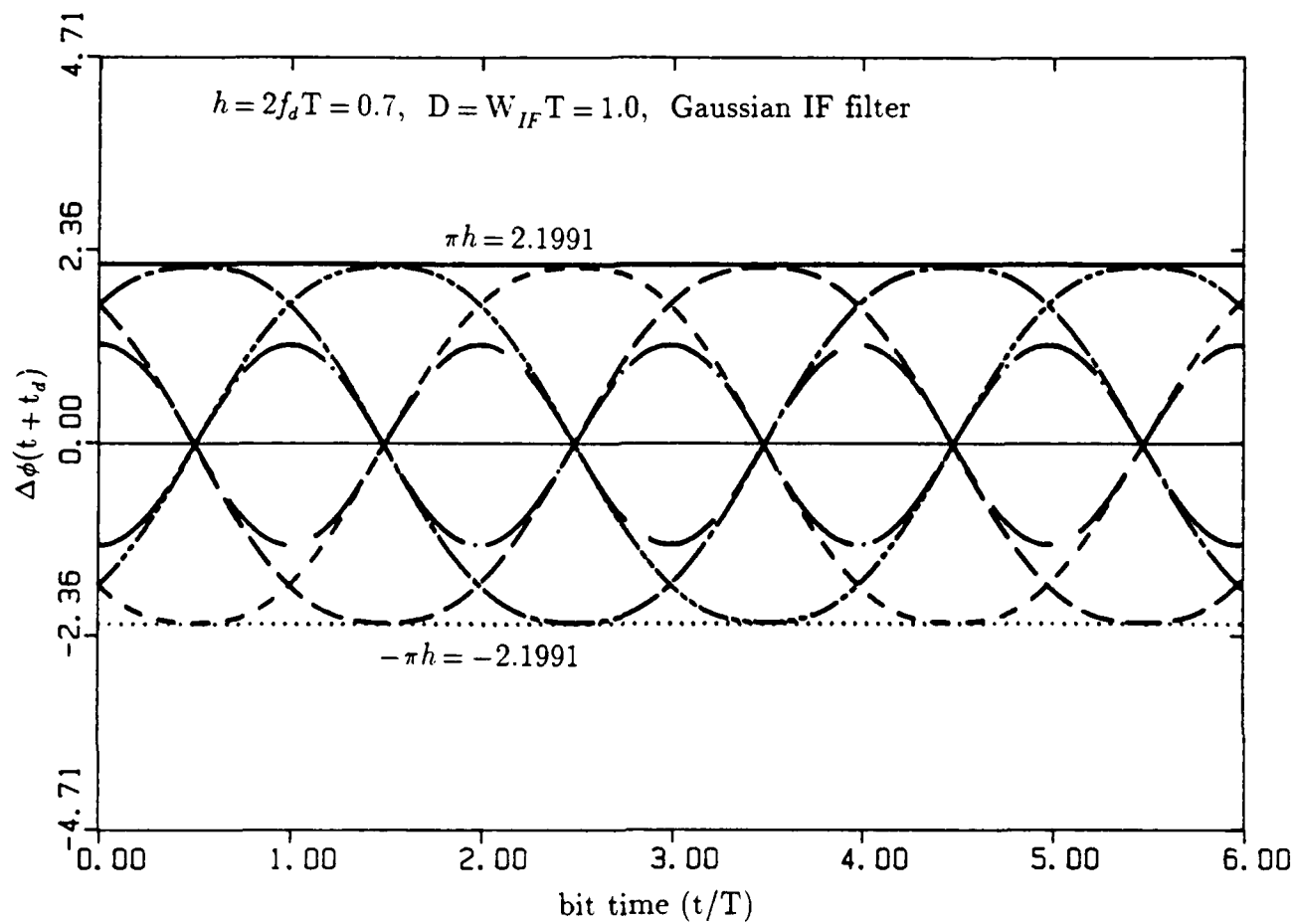
FIGURE A-3 EXAMPLE CALCULATED DIFFERENTIAL PHASE WAVEFORMS

APPENDIX B
PROPERTIES OF THE TRUNCATED GAUSSIAN DISTRIBUTION

B.1 DEFINITION

Let a truncated Gaussian probability density function (PDF) be defined as

$$p_{TG}(x) \triangleq \begin{cases} K e^{-x^2/2\sigma_0^2}, & |x| \leq a \\ 0, & \text{otherwise.} \end{cases} \qquad \text{(B-1)}$$

In the text, this PDF is used as a point of departure for development of an approximation to the modulo-2π differential phase PDF $p_\psi(x)$, with $a = \pi$.

B.2 NORMALIZATION FACTOR

The integral of the PDF (B-1) must equal unity. Therefore we have

$$1 = \int_{-a}^{a} dx \, p_{TG}(x) = 2K \int_{0}^{a} dx \, e^{-x^2/2\sigma_0^2}$$

$$= 2K\sigma_0\sqrt{2} \int_{0}^{umax} du \, e^{-u^2}, \quad umax \triangleq a/\sigma_0\sqrt{2}$$

$$= K\sigma_0\sqrt{2\pi} \, \text{erf}(a/\sigma_0\sqrt{2}), \qquad \text{(B-2a)}$$

or
$$K^{-1} = \sigma_0\sqrt{2\pi} \, \text{erf}(a/\sigma_0\sqrt{2}). \qquad \text{(B-2b)}$$

Note that

$$\lim_{\sigma_0 \to \infty} K = \frac{1}{2a}. \qquad \text{(B-2c)}$$

B.2 VARIANCE

Since the mean value is zero, the variance of the distribution whose PDF is given by (B-1) is calculated as

$$\sigma_{TG}^2 = 2K \int_{0}^{a} dx \, x^2 e^{-x^2/2\sigma_0^2}$$

$$= 2\sqrt{2} K\sigma_0^3 \int_{0}^{a^2/2\sigma_0^2} du \, \sqrt{u} \, e^{-u}$$

$$= 2\sqrt{2} K\sigma_0^3 \, \gamma(\tfrac{3}{2}; \, a^2/2\sigma_0^2) \qquad \text{(B-3a)}$$

$$= \sigma_0^2 \cdot \frac{P(\tfrac{3}{2}; \, a^2/2\sigma_0^2)}{\text{erf}(a/\sigma_0\sqrt{2})}, \qquad \text{(B-3b)}$$

112

in which $\gamma(\nu; x)$ is the incomplete gamma function and [17]

$$P(\nu; x) \triangleq \frac{\gamma(\nu;x)}{\Gamma(\nu)} \tag{B-4a}$$

$$= \frac{x^{\nu}e^{-x}}{\Gamma(\nu+1)} \, {}_1F_1(1; \nu+1; x) \tag{B-4b}$$

is the cumulative probability distribution function (CDF) for a chi-squared random variable with 2ν degrees of freedom [17, chapter 26]. In (B-4b), the ${}_1F_1$ function is the confluent hypergeometric function. Now, since [17]

$$P(\tfrac{3}{2}; x) = P(\tfrac{1}{2}; x) - \frac{\sqrt{x}e^{-x}}{\Gamma(\tfrac{3}{2})} \tag{B-5a}$$

$$= \operatorname{erf}(\sqrt{x}) - \frac{\sqrt{x}e^{-x}}{\Gamma(\tfrac{3}{2})}, \tag{B-5b}$$

it follows that

$$P(\tfrac{3}{2}; a^2/2\sigma_0^2) = \operatorname{erf}(a/\sigma_0\sqrt{2}) - \frac{a}{\sigma_0}\sqrt{\tfrac{2}{\pi}}\,e^{-a^2/2\sigma_0^2}. \tag{B-5c}$$

Substituting this result in (B-3b) gives

$$\sigma_{TG}^2 = \sigma_0^2\left[1 - \frac{\frac{a}{\sigma_0}\sqrt{\frac{2}{\pi}}\,e^{-a^2/2\sigma_0^2}}{\operatorname{erf}(a/\sigma_0\sqrt{2})}\right]. \tag{B-6}$$

An empirical inversion of this formula which we have developed for $a = \pi$ is

$$\sigma_0^2 = \sigma_{TG}^2. \qquad\qquad\qquad \sigma_{TG}^2 \le 1 \tag{B-7a}$$

$$= \exp\left\{\frac{\ln\sigma_{TG}^4}{[1-\ln\sigma_{TG}^2/\ln(\pi^2/3)]^{0.4}}\right\}. \quad \sigma_{TG}^2 > 1. \tag{B-7b}$$

An alternate expression to (B-6) is obtained by substituting (B-4b) into (B-3) twice, making use of the fact that $\operatorname{erf}(\sqrt{x}) = P(\tfrac{1}{2}; x)$ in the denominator, which results in

$$\sigma_{TG}^2 = \frac{a^2}{3} \cdot \frac{{}_1F_1(1; \tfrac{5}{2}; \zeta)}{{}_1F_1(1; \tfrac{3}{2}; \zeta)}, \quad \zeta \equiv \frac{a^2}{2\sigma_0^2}, \tag{B-8a}$$

$$= \frac{a^2}{3} \cdot \frac{1+\frac{2}{5}\zeta+\frac{2}{5}\cdot\frac{2}{7}\zeta^2+\frac{2}{5}\cdot\frac{2}{7}\cdot\frac{2}{9}\zeta^3+\cdots}{1+\frac{2}{3}\zeta+\frac{2}{3}\cdot\frac{2}{5}\zeta^2+\frac{2}{3}\cdot\frac{2}{5}\cdot\frac{2}{7}\zeta^3+\cdots}$$

$$= \frac{a^2}{3}\left\{1 - \tfrac{4}{15}\zeta + \tfrac{8}{315}\zeta^2 + \tfrac{16}{4725}\zeta^3 - \tfrac{1184}{779625}\zeta^4 + \cdots\right\}$$

$$\approx \frac{a^2}{3}\left\{1 - \tfrac{4}{15}\zeta + \tfrac{8}{315}\zeta^2\right\}. \tag{B-8b}$$

Solving for σ_0^2 gives the approximation

$$\sigma_0^2 \approx \frac{2a^2}{21}\left(1 - \sqrt{1-\frac{10}{7}\left(1-\frac{3\sigma_{TG}^2}{a^2}\right)}\right)^{-1}; \tag{B-9}$$

113

this approximation is satisfactory for $\sigma^2_{TG} > 2$ when $a = \pi$, or when $\dfrac{3\sigma^2_{TG}}{a^2} \geq .5$. For smaller values of σ^2_{TG}, we have the empirical relations given in (B-7).

B.3 CHARACTERISTIC FUNCTION

The characteristic function for the truncated Gaussian distribution is found from

$$C_{TG}(\nu) = K \int_{-a}^{a} dx\, e^{j\nu x} e^{-x^2/2\sigma_0^2} \tag{B-10a}$$

$$= \frac{\operatorname{erf}\left(\dfrac{a}{\sigma_0\sqrt{2}} - \dfrac{j\nu\sigma_0}{\sqrt{2}}\right) - \operatorname{erf}\left(-\dfrac{a}{\sigma_0\sqrt{2}} - \dfrac{j\nu\sigma_0}{\sqrt{2}}\right)}{2\operatorname{erf}(a/\sigma_0\sqrt{2})} \tag{B-10b}$$

$$= \frac{\operatorname{Re}\left\{\operatorname{erf}\left(\dfrac{a}{\sigma_0\sqrt{2}} - \dfrac{j\nu\sigma_0}{\sqrt{2}}\right)\right\}}{\operatorname{erf}(a/\sigma_0\sqrt{2})}. \tag{B-10c}$$

This exact form is not suitable for computation. Alternate forms for the characteristic function can be developed, however. The first one makes use of the symmetry of the integral in (B-10a) to write

$$C_{TG}(\nu) = 2K \int_{0}^{a} dx\, e^{-x^2/2\sigma_0^2} \cos\nu x \tag{B-10a}$$

$$= 2K \sum_{n=0}^{\infty} \frac{(-1)^n \nu^{2n}}{(2n)!} \int_{0}^{a} dx\, x^{2n}\, e^{-x^2/2\sigma_0^2},$$

using a power series for the cosine function. Next, making use of the fact that $(2n)!$ equals $2^{2n}\Gamma(n+\tfrac{1}{2})\,n!/\sqrt{\pi}$, and transforming the integral by $y = x^2/2\sigma_0^2$ results in

$$C_{TG}(\nu) = K\sigma_0\sqrt{2\pi} \sum_{n=0}^{\infty} \frac{(-1)^n(\tfrac{1}{2}\nu)^{2n}}{n!\,\Gamma(n+\tfrac{1}{2})} (\sigma_0\sqrt{2})^{2n} \int_{0}^{a^2/2\sigma_0^2} dy\, y^{n-1/2}\, e^{-y}$$

$$= K\sigma_0\sqrt{2\pi} \sum_{n=0}^{\infty} \frac{(-\tfrac{1}{2}\nu^2\sigma_0^2)^n}{n!} \frac{\gamma(n+\tfrac{1}{2};\ a^2/2\sigma_0^2)}{\Gamma(n+\tfrac{1}{2})} \tag{B-10b}$$

$$= K\sigma_0\sqrt{2\pi} \sum_{n=0}^{\infty} \frac{(-\tfrac{1}{2}\nu^2\sigma_0^2)^n}{n!} P(n+\tfrac{1}{2};\ a^2/2\sigma_0^2). \tag{B-10c}$$

Another development from (B-10a) uses integration by parts to obtain

$$C_{TG}(\nu) = 2K \frac{\sin\nu x}{\nu} e^{-x^2/2\sigma_0^2}\Big|_{0}^{a} + \frac{2K}{\nu\sigma_0^2} \int_{0}^{a} dx\, e^{-x^2/2\sigma_0^2} \sin\nu x$$

114

$$= 2\mathrm{K}ae^{-a^2/2\sigma_0^2}\frac{\sin a\nu}{a\nu} + \mathrm{K}\sigma_0\sqrt{2\pi}\sum_{n=0}^{\infty}\frac{(-\frac{1}{2}\nu^2\sigma_0^2)^n}{n!}\,\mathrm{P}(n+\tfrac{3}{2};\ a^2/2\sigma_0^2), \qquad \text{(B-11a)}$$

after undergoing a development similar to that used to obtain (B-10c). After noting that

$$\mathrm{P}(n+\tfrac{3}{2};\ x^2) = \mathrm{P}(\tfrac{3}{2};\ x^2) - e^{-x^2}\sum_{k=1}^{n}\frac{x^{2k+1}}{\Gamma(k+\frac{3}{2})} \le \mathrm{P}(\tfrac{3}{2};\ x^2), \qquad \text{(B-11b)}$$

and substituting this bound into (B-11a), we find the bound

$$C_{TG}(\nu) < 2\mathrm{K}ae^{-a^2/2\sigma_0^2}\frac{\sin a\nu}{a\nu} + \mathrm{K}\sigma_0\sqrt{2\pi}\,\mathrm{P}(\tfrac{3}{2};\ a^2/2\sigma_0^2)\sum_{n=0}^{\infty}\frac{(-\frac{1}{2}\nu^2\sigma_0^2)^n}{n!}$$

$$= 2\mathrm{K}ae^{-a^2/2\sigma_0^2}\frac{\sin a\nu}{a\nu} + \mathrm{K}\sigma_0\sqrt{2\pi}\,\mathrm{P}(\tfrac{3}{2};\ a^2/2\sigma_0^2)e^{-\nu^2\sigma_0^2/2}$$

$$= \xi\cdot\frac{\sin a\nu}{a\nu} + (1-\xi)\cdot e^{-\nu^2\sigma_0^2/2} \qquad \text{(B-11c)}$$

where

$$\xi \triangleq \frac{a}{\sigma_0}\sqrt{\tfrac{2}{\pi}}\,e^{-a^2/2\sigma_0^2}[\mathrm{erf}(a/\sigma_0\sqrt{2})]^{-1}. \qquad \text{(B-11d)}$$

This second, mixture expression for the truncated Gaussian CHF is preferred because, using the bound as an approximation, it is readily discerned from it that the CHF has the form

$$C_{TG}(\nu) \approx \xi\cdot C_U(\nu;\ a) + (1-\xi)\cdot C_G(\nu;\ \sigma_0^2), \qquad \text{(B-12)}$$

in which $C_U(\nu;\ a)$ is the CHF for a random variable uniformly distributed on $(-a,\ a)$ and $C_G(\nu;\ \sigma_0^2)$ is the CHF for a zero-mean Gaussian random variable with variance σ_0^2. Further, the mixture parameter ξ is seen to approach the value $\xi = 1$ as $\sigma_0 \to \infty$, that is, as the SNR$\to$0, and approaches zero as SNR$\to\infty$.

115

APPENDIX C
FUNCTIONS RELATED TO THE GAUSSIAN FILTER

In the analysis of CPFSK systems, it is con on to assume an IF bandpass filter with noise bandwidth W_{IF} and a "Gaussian-shaped" spectral transfer function:

$$H_{IF}(f) = H_0(f - f_{IF}) + H_0(f + f_{IF}) \tag{C-1a}$$

where

$$H_0(f) = e^{-\pi (f/W_{IF})^2/2 - j2\pi f t_d}. \tag{C-1b}$$

C.1 FILTER IMPULSE RESPONSE

The equations above imply that the impulse response of the bandpass filter is modelled by

$$h_{IF}(t) = 2 h_0(t) \cos(2\pi f_{IF} t). \tag{C-2a}$$

with the "equivalent lowpass filter" impulse response being

$$h_0(t) = \int_{-\infty}^{\infty} df H_0(f) e^{j2\pi f t}$$

$$= W_{IF} \sqrt{2} e^{-2\pi W_{IF}^2 (t - t_d)^2} \tag{C-2b}$$

$$= \frac{1}{\sigma_h \sqrt{2\pi}} e^{-(t - t_d)^2/2\sigma_h^2}, \tag{C-2c}$$

where

$$\sigma_h \triangleq (2 W_{IF} \sqrt{\pi})^{-1}. \tag{C-2d}$$

This lowpass filter response is nonrealizable in that it is nonzero for $t < 0$. However, if the filter phase delay t_d is sufficiently long, the integral over positive values of the argument is very close to unity, indicating that the filter response for $t < 0$ can be neglected:

$$\int_0^{\infty} dt h_0(t) = Q_G(-2 W_{IF} t_d \sqrt{\pi}) \approx 1, \ W_{IF} t_d > 1 \tag{C-3a}$$

where

$$Q_G(x) = \frac{1}{\sqrt{2\pi}} \int_x^{\infty} dy \, e^{-y^2/2} \tag{C-3b}$$

$$= \tfrac{1}{2}[1 - \mathrm{erf}(\tfrac{x}{\sqrt{2}})]. \tag{C-3c}$$

is the complementary cumulative probability distribution function for a Gaussian random variable and $\mathrm{erf}(\cdot)$ is the error function.

116

C.2 RESPONSE TO NARROWBAND WAVEFORMS

The response $y(t)$ of the bandpass filter to a general narrowband waveform $x(t)$ with in-phase and quadrate components $I(t)$ and $Q(t)$,

$$x(t) = I(t)\cos\omega_{IF}t - Q(t)\sin\omega_{IF}t \tag{C-4}$$

using $\omega_{IF} = 2\pi f_{IF}$, can be developed as follows:

$$y(t) = \int_{-\infty}^{t} du\,[I(u)\cos\omega_{IF}u - Q(u)\sin\omega_{IF}u]\cdot 2h_0(t-u)\cos\omega_{IF}(t-u)$$

$$= \int_{-\infty}^{t} du\, I(u)h_0(t-u)\left\{\cos\omega_{IF}t + \cos\omega_{IF}(2u-t)\right\}$$

$$- \int_{-\infty}^{t} du\, Q(u)h_0(t-u)\left\{\sin\omega_{IF}t + \sin\omega_{IF}(2u-t)\right\}$$

$$\approx \cos\omega_{IF}t\int_{-\infty}^{t} du\, I(u)h_0(t-u) -\sin\omega_{IF}t\int_{-\infty}^{t} du\, Q(u)h_0(t-u) \tag{C-5a}$$

$$= u(t)\cos\omega_{IF}t - v(t)\sin\omega_{IF}t \tag{C-5b}$$

with $u(t)$ and $v(t)$ being the in-phase and quadrature components of the filter output, respectively.

The same result can be obtained using the "complex envelope" notation to write

$$x(t) = \mathrm{Re}\left\{[I(t)+jQ(t)]e^{j\omega_{IF}t}\right\} = \mathrm{Re}\left\{X(t)e^{j\omega_{IF}t}\right\} \tag{C-6a}$$

and

$$y(t) = \mathrm{Re}\left\{[u(t)+jv(t)]e^{j\omega_{IF}t}\right\} = \mathrm{Re}\left\{Y(t)e^{j\omega_{IF}t}\right\}, \tag{C-6b}$$

with the understanding that the effect of the bandpass filter in terms of its equivalent lowpass filter can be expressed by the convolution

$$Y(t) = \int_{-\infty}^{t} du\, X(u)h_0(t-u). \tag{C-7}$$

C.3 INTEGRALS RELATED TO FILTERING OF THE TRANSIENT PHASE

The following integrals are used in Section 3 of the text in connection with the effect of a Gaussian IF bandpass filter on the transient phase difference due to imperfect synchronism between transmitter and receiver hopping synthesizers. The integrals proceed from the desire to calculate

$$\mathfrak{I}(t_1,\, t_2;\, \nu,\, \sigma,\, \gamma) \triangleq (\sigma\sqrt{2\pi})^{-1}\int_{t_1}^{t_2} dx\cos 2\pi\nu x\; e^{-(x-\gamma)^2/2\sigma^2}. \tag{C-8}$$

The solution begins with a simple translation to obtain

$$\sigma\sqrt{2\pi}\,\mathfrak{I}(t_1,\,t_2;\,\nu,\,\sigma,\,\gamma) = \cos 2\pi\nu\gamma \int_{t_1-\gamma}^{t_2-\gamma} dx\cos 2\pi\nu x\, e^{-x^2/2\sigma^2}$$

$$- \sin 2\pi\nu\gamma \int_{t_1-\gamma}^{t_2-\gamma} dx\sin 2\pi\nu x\, e^{-x^2/2\sigma^2}$$

$$= \cos 2\pi\nu\gamma \cdot \sigma\sqrt{2\pi}\,\mathfrak{I}_c(t_1-\gamma,\,t_2-\gamma;\,\nu,\,\sigma)$$

$$- \sin 2\pi\nu\gamma \cdot \sigma\sqrt{2\pi}\,\mathfrak{I}_s(t_1-\gamma,\,t_2-\gamma;\,\nu,\,\sigma). \tag{C-9}$$

The first integral defined in (C-9) is

$$\mathfrak{I}_c(A,\,B;\,\nu,\,\sigma) \triangleq (\sigma\sqrt{2\pi})^{-1}\int_A^B dx\cos 2\pi\nu x\, e^{-x^2/2\sigma^2} \tag{C-10a}$$

$$= (\sigma\sqrt{2\pi})^{-1} \sum_{n=0}^{\infty} \frac{(-1)^n(2\pi\nu)^{2n}}{(2n)!} \int_A^B dx\, x^{2n} e^{-x^2/2\sigma^2}$$

$$= \frac{1}{2}\sum_{n=0}^{\infty} \frac{(-2\pi^2\nu^2\sigma^2)^n}{n!\,\Gamma(n+\frac{1}{2})} \left\{ \gamma(n+\tfrac{1}{2};\,B^2/2\sigma^2) - \gamma(n+\tfrac{1}{2};\,A^2/2\sigma^2) \right\} \tag{C-10b}$$

in which $\gamma(a;\,x)$ is the incomplete gamma function, a series expansion of the cosine function was used, and the fact that $(2n)! = \Gamma(n+\frac{1}{2})\,n!\,2^{2n}/\sqrt{\pi}$ was also used. Now, recognizing that [17]

$$\frac{\gamma(n+\frac{1}{2};\,x^2)}{\Gamma(n+\frac{1}{2})} < \frac{\gamma(\frac{1}{2};\,x^2)}{\Gamma(\frac{1}{2})} = \mathrm{erf}\,x, \tag{C-11}$$

we replace the gamma functions in (C-10b) with their values for $n=0$ to obtain the approximation

$$\mathfrak{I}_c(A,\,B;\,\nu,\,\sigma) \approx e^{-2(\pi\nu\sigma)^2} \cdot \tfrac{1}{2}\left\{ \mathrm{erf}(B/\sigma\sqrt{2}) - \mathrm{erf}(A/\sigma\sqrt{2}) \right\}. \tag{C-12a}$$

In the text, we have $\nu = kf_{\Delta\theta}$, harmonics of the fundamental frequency of the transient phase difference waveform, and $\sigma = \sigma_h$ is given by (C-2d). Therefore, since the factor involving the error functions in (C-12) is a most unity, the value of $\mathfrak{I}_c$ is governed by the exponential factor, which equals

$$e^{-2(\pi\nu\sigma)^2} = e^{-\pi(kf_{\Delta\theta}/W_{IF})^2/2} = |H_0(kf_{\Delta\theta})|. \tag{C-12b}$$

The second integral defined in (C-9) is

$$\mathfrak{I}_s(A,\,B;\,\nu,\,\sigma) \triangleq (\sigma\sqrt{2\pi})^{-1}\int_A^B dx\sin 2\pi\nu x\, e^{-x^2/2\sigma^2} \tag{C-13a}$$

118

$$= (\sigma\sqrt{2\pi})^{-1} \sum_{n=0}^{\infty} \frac{(-1)^n (2\pi\nu)^{2n+1}}{(2n+1)!} \int_A^B \mathrm{d}x\, x^{2n+1} e^{-x^2/2\sigma^2}$$

$$= \frac{\pi\nu\sigma}{\sqrt{2}} \sum_{n=0}^{\infty} \frac{(-2\pi^2\nu^2\sigma^2)^n}{n!\,\Gamma(n+\frac{3}{2})} \left\{ \gamma(n+1;\ B^2/2\sigma^2) - \gamma(n+1;\ A^2/2\sigma^2) \right\} \qquad \text{(C-13b)}$$

using the same analytical techniques as were used to obtain (C-10b). Recognizing that the incomplete gamma function for integer first arguments can be expressed by [17]

$$\frac{\gamma(n+1;\ x^2)}{\Gamma(n+1)} = 1 - e^{-x^2} \sum_{k=0}^{n} \frac{x^{2k}}{k!} < 1 - e^{-x^2}, \qquad \text{(C-14)}$$

we replace the gamma functions in (C-13b) with their values for $n=0$ to obtain the approximation

$$\mathfrak{I}_s(A,\ B;\ \nu,\ \sigma) \approx \frac{\pi\nu\sigma}{\sqrt{2}} \left(e^{-A^2/2\sigma^2} - e^{-B^2/2\sigma^2} \right) \sum_{n=0}^{\infty} \frac{(-2\pi^2\nu^2\sigma^2)^n}{\Gamma(n+\frac{3}{2})}, \qquad \text{(C-15)}$$

in which the series is the confluent hypergeometric function:

$$\sum_{n=0}^{\infty} \frac{(-2\pi^2\nu^2\sigma^2)^n}{\Gamma(n+\frac{3}{2})} = \frac{2}{\sqrt{\pi}}\,{}_1F_1(1;\ \tfrac{3}{2};\ -2\pi^2\nu^2\sigma^2) \qquad \text{(C-16a)}$$

$$= \frac{2}{\sqrt{\pi}}\,e^{-2(\pi\nu\sigma)^2}\,{}_1F_1(\tfrac{1}{2};\ \tfrac{3}{2};\ 2\pi^2\nu^2\sigma^2) \qquad \text{(C-16b)}$$

$$\approx \frac{1}{2(\pi\nu\sigma)^2\sqrt{\pi}},\ \text{for}\ \nu\sigma \gg 1. \qquad \text{(C-16c)}$$

Thus we have the asymptotic approximation

$$\mathfrak{I}_s(A,\ B;\ \nu,\ \sigma) \approx \frac{1}{2\pi\nu\sigma\sqrt{2\pi}} \left(e^{-A^2/2\sigma^2} - e^{-B^2/2\sigma^2} \right). \qquad \text{(C-17)}$$

Clearly, the factor involving the exponentials can at most equal ± 1. Therefore, the magnitude of (C-17) is controlled by the first factor. Substituting for ν and σ, we find that this factor equals

$$\frac{1}{2\pi\nu\sigma\sqrt{2\pi}} = \frac{1}{2\pi\sqrt{2}(kf_{\Delta\theta}/W_{IF})}. \qquad \text{(C-18)}$$

REFERENCES

1. D. J. Torrieri, "Frequency Hopping with Multiple Frequency-Shift Keying and Hard Decisions," *IEEE Trans. on Commun.*, vol. COM-32, pp. 574-582 (May 1984).

2. F. deJager and C. B. Dekker, "Tamed Frequency Modulation—A Novel Approach to Achieve Spectral Economy in Digital Transmission," *IEEE Trans. on Commun.*, vol. COM-26, pp. 534-542 (May 1978).

3. K.-S. Chung, "Generalized Tamed Frequency Modulation and its Application for Mobile Radio Communications," *IEEE Trans. on Vehicular Tech.*, vol. VT-33, pp. 103-113 (August 1984).

4. K. J. P. Fonseka and N. Ekanayake, "Differential Detection of Narrow-Band Bi nary FM," *IEEE Trans. on Commun.*, vol. COM-33, pp. 725-729 (July 1985).

5. M. K. Simon and C. C. Wang, "Differential versus Limiter-Discriminator Detec tion of Narrow-band FM," *IEEE Trans. on Commun.*, vol. COM-31, pp. 1227-1234 (November 1983).

6. D. E. Cartier, "Limiter-Discriminator Detection Performance of Manchester and NRZ Coded FSK," *IEEE Trans. on Aerospace and Elec. Syst.*, vol. AES-13, pp. 62-70 (January 1977).

7. L. L. Campbell, P. H. Wittke, and G. D. Swanson, "The Distribution of the Amp litude and Continuous Phase of a Sinusoid in Noise," *IEEE Trans. on Info. Thy.*, vol. IT-34, pp. 1388-1395 (November 1988).

8. J. S. Lee Associates, Inc., "The Diversity ECCM Performance of Frequency-Hop ping CPFSK in Partial-Band Noise Jamming," final report under contract DAAL03-87-C-0006 with the Army Research Office, 25 May 1988 (DTIC ac cession number AD-A 197 738).

9. J. H. Roberts, *Angle Modulation: The Theory of Systems Assessment.* Stevenage, Herts.: Peregrinus Ltd., 1977.

10. D. Middleton, *An Introduction to Statistical Communication Theory.* New York: McGraw-Hill, 1960.

11. R. F. Pawula, "On the Theory of Error Rates for Narrow-band Digital FM," *IEEE Trans. on Commun.*, vol. COM-29, pp. 1634-1643 (November 1981).

12. R. F. Pawula, "Refinements to the Theory of Error Rates for Narrow-band Digital FM," *IEEE Trans. on Commun.*, vol. COM-36, pp. 509-513 (April 1988).

13. R. F. Pawula, S. O. Rice, and J. H. Roberts, "Distribution of the Phase Angle Be tween Two Vectors Perturbed by Gaussian Noise," *IEEE Trans. on Commun.*, vol. COM-30, pp. 1828-1841 (August 1982).

14. L. E. Miller and J. S. Lee, "Bandpass Correlator Analysis for General Input As sumptions," *IEEE Trans. on Info. Thy.*, vol. IT-28, pp. 973-977 (Nov. 1982).

15. L. E. Miller, R. H. French, J. S. Lee, and H. M. Kwon, "Uncoded Diversity Sum Performance of FH/CPFSK in Partial-Band Jamming," *Proc. IEEE 1988 Military Commun. Conf.*, San Diego, pp. 625-629.

16. A. H. Nuttall, "Alternate Forms for Numerical Evaluation of Cumulative Probability Distributions Directly from Characteristic Functions," *Proc. IEEE*, vol. 58, pp. 1872-1873 (November 1970).

17. M. Abramowitz and I. A. Stegun (eds.), *Handbook of Mathematical Functions*, National Bureau of Standards Applied Mathematics Series 55. Washington, DC: Government Printing Office, June 1964, Ninth printing, Nov. 1970.

18. N. M. Blachman, "Gaussian Noise—Part II: Distribution of Phase Change of Narrow-Band Noise Plus Sinusoid," *IEEE Trans. on Info. Thy.*, vol. IT-34, pp. 1401-1405 (November 1988).

19. T. T. Tjhung and P. M. Wittke, "Carrier Transmission of Binary Data in a Restricted Band," *IEEE Trans. on Commun. Tech.*, vol. COM-18, pp. 295-304 (August 1970).

20. J. S. Lee Associates, Inc., "Optimum Jamming Studies," final report under contract DAAK21-85-C-0047 with the Army Signals Warfare Center, March 1986 (DTIC accession number AD-C 038 732L).

21. L. E. Miller, R. H. French, and J. S. Lee, "Comparison of Parametric and Nonparametric Nonlinear Diversity Combining Schemes for Frequency-Hopping FSK Systems in Partial-Band Noise Jamming," *Proc. IEEE 1987 Military Commun. Conf.*, Washington, pp. 718-723.

22. J. S. Lee, L. E. Miller, and R. H. French, "The Analyses of Uncoded Performances for Certain ECCM Receiver Design Strategies for Multi-hops/symbol FH/MFSK Waveforms," *IEEE J. Selected Areas in Commun.*, vol. SAC-3, pp.611-621 (September 1985).

23. L. E. Miller, J. S. Lee, and A. P. Kadrichu, "Probability of Error Analyses of a BFSK Frequency-Hopping System with Diversity Under Partial-Band Jamming Interference—Part III: Performance of a Square-Law Self-Normalizing Soft Decision Receiver," *IEEE Trans. on Commun.*, vol. COM-34, pp. 669-675 (July 1986).

24. J. S. Lee Associates, Inc., "The Effectiveness of Frequency-Hopping Random MFSK Against Worst-Case Partial-Band Noise Jamming," final report under contract DAAG29-85-C-0021 with the Army Research Office, August 1986 (DTIC accession number AD-A 172 929).

25. D. J. Torrieri, *Principles of Secure Communication Systems*. Dedham, MA: Artech House, 1985.

26. B. Flerchinger and T. Higgins, "Dynamic Testing of Frequency Agile Radios," Hewlett-Packard Company RF & Microwave Measurement Symposium and Exhibition, April 1988.

27. C. Conticello, "ECCM in VHF Tactical Communications," *Signal*, October 1986, pp. 67-75.

28. D. M. Russell, "Tactical Radios Designed to Elude Enemy Jammers," *Defense Electronics*, June 1983, pp. 110-130.

29. D. J. Torrieri, "Fundamental Limitations on Repeater Jamming of Frequency-Hopping Communications," *IEEE J. Selected Areas in Commun.*, vol. SAC-4, pp. 569-575 (May 1989).

30. J. R. Alexovich and R. M. Gagliardi, "Effect of PLL Frequency Synthesizer in FSK Frequency-Hopped Communications," *IEEE Trans. on Commun.*, vol. COM-37, pp. 268-276 (March 1989).

31. C.-M. Su and L. B. Milstein, "The Analysis of a Coherent Frequency Hopped Spread Spectrum System," *Proc. IEEE 1988 Military Commun. Conf.*, San Diego, pp. 611-615.

32. Hughes Aircraft Company, Ground Systems Group, "Enhanced Position Location Reporting System (EPLRS) Technical Description," document produced under contract DAAB07-82-C-J096, 25 May 1988.

33. The Singer Company, Kearfott Division, "Prime Item Development Specification for JTIDS Class 2M Terminal Full Scale Engineering Development," document Y201P851A100 (rev. 2) produced under contract F19628-86-C-0035, 31 October 1986.

34. Racal-Tacticom Limited, "Jaguar Radio BCC 66H Technical Manual," undated.

35. J. R. Klauder, A. C. Price, S. Darlington, and W. J. Albersheim, "The Theory and Design of Chirp Radars," Monograph 3660, Bell Telephone System Technical Publications (reprint from *Bell System Technical J.*, 1960).